Efficiency Boosting of Surfactants with Poly(ethylene oxide)-Poly(alkyl glycidyl ether)s – A New Class of Amphiphilic Polymers

*Kristina Schneider[§,a], Patrick Verkoyen[§,b], Maximilian Krappel[a], Christina Gardiner[a], R. Schweins[c], Holger Frey[b], Thomas Sottmann[a]**

a. Institute of Physical Chemistry, University of Stuttgart, Pfaffenwaldring 55, 70569 Stuttgart, Germany

b. Department of Chemistry, Johannes Gutenberg University Mainz, Duesbergweg 10-14, 55128 Mainz, Germany.

c. Institut Laue-Langevin, DS/LSS, 71 avenue des Martyrs, CS 20156, 38042 Grenoble CEDEX 9, France

*Corresponding author: thomas.sottmann@ipc.uni-stuttgart.de, Tel. +49(0)711-685-64494, Fax. +49(0)711-685-64443

[§]These authors have contributed equally: Kristina Schneider and Patrick Verkoyen.

KEYWORDS: microemulsions, phase behavior, microstructure, SANS, amphiphilic diblock copolymers, polyethers, anionic ring opening polymerization (AROP), efficiency boosting effect, long-chain *n*-alkanes.

ABSTRACT

Twenty years ago it was found that adding small amounts of amphiphilic block copolymers like poly(ethylene propylene)-*co*-poly(ethylene oxide) (PEP-*b*-PEO) to microemulsion systems strongly increases the efficiency of medium-chain surfactants to solubilize water and oil. Although being predestined to serve as a milestone in microemulsion research, the effect has only scarcely found its way into applications. In this work, we propose a new type of efficiency boosters, namely poly(ethylene oxide)-poly(alkyl glycidyl ether)s (PEO-*b*-PAlkGE) and their "carbonated" poly(ethylene oxide)-poly(carbonate alkyl glycidyl ether) analogs. Their synthesis via anionic ring opening polymerization (AROP) from commercially available long-chain alkyl glycidyl ethers (AlkGE) and mono methoxy poly(ethylene glycol)s as macroinitiators can be performed at low cost and on a large scale. We demonstrate that these new PEO-*b*-PAlkGE copolymers with dodecyl and hexadecyl side chains in the nonpolar block strongly increase the efficiency of both pure and technical-grade *n*-alkyl polyglycol ether surfactants to form microemulsions containing pure *n*-alkanes or even technical-grade waxes. A result which could be of interest for industrial applications where reduced surfactant needs would have significant economic and ecological implications. For *n*-decane microemulsions, the boosting effect of PEO-*b*-PAlkGE and PEP-*b*-PEO polymers can be scaled on top of each other, when plotting the efficiency semi-logarithmically versus the polymeric coverage of the amphiphilic film. Interestingly, a somewhat different scaling behavior was observed for *n*-octacosane microemulsions at elevated temperatures, suggesting that the polymers show less self-avoidance and rather behave as almost ideal chains. A similar trend was found for the increase of the bending rigidity κ upon polymeric coverage of the amphiphilic film, which was obtained from the analysis of small-angle neutron scattering (SANS) measurements.

INTRODUCTION

Microemulsions. Microemulsions consist of at least three different components, with two of them being immiscible under standard conditions. The miscibility of these two immiscible components, namely a hydrophilic/polar component (e.g. water) (A) and a hydrophobic/nonpolar component (e.g. oil) (B), can be facilitated by an amphiphilic component (e.g. surfactant) (C). Such mixtures are referred to as microemulsions[1] if they are thermodynamically stable, macroscopically homogeneous albeit nanostructured mixtures containing an amphiphilic film. Microemulsions are characterized by their multifarious nanostructures[2], as well as their enormous interface and they excel at reducing the oil/water interfacial tension to low and ultra-low values.[3–6] More than half a century of extensive research has shown that these properties can easily be tuned and adjusted by parameters like temperature, pressure, or the addition of components such as cosurfactants and salt.[7] The properties themselves, but also their adjustability, enable numerous technical applications of microemulsions, for instance in washing processes[8,9], enhanced oil recovery[10,11] or in cosmetic and pharmaceutic applications[12–14]. However, compared to emulsions, which are only kinetically stable, high amounts of surfactant required to formulate microemulsions pose significant economic and ecological drawbacks. The latter may arise from surfactants' potential hazards for humans (e.g. damaged skin from surfactants in cosmetics) and the ecosystem in general (e.g. non-biodegradable surfactants).

The Efficiency Boosting Effect. A milestone in microemulsion research was the observation that the addition of small amounts of amphiphilic diblock copolymers can lead to a strong reduction of the amount of surfactant needed to formulate microemulsions.[15,16] By means of ternary nonionic microemulsions of the type H_2O – *n*-decane – tetraethylene glycol monodecyl ether ($C_{10}E_4$)[16,17], it was shown that amphiphilic diblock copolymers of the type poly(ethylene propylene)-*co*-poly(ethylene

oxide) (PEP-*b*-PEO)[18,19] act as a kind of macro-surfactant forced into the amphiphilic film, since water and *n*-decane are good solvents for the PEO and PEP block, respectively. In systematic phase behavior and microstructure studies, it was found that in addition to the efficiency boosting, the addition of PEP-*b*-PEO polymers also results in water and oil domains with larger length scales as well as a further decrease of the already ultra-low oil/water interfacial tension.[15] Additionally, the formation of liquid crystalline phases, e.g. the lamellar phase (L_α), which are a prominent feature of microemulsion systems stabilized by long chain surfactants (alkyl chain length longer than C_{10}), can partly be controlled by adjusting the alkyl chain length of the surfactants as well as the concentration and block size of the amphiphilic copolymers.[16,17,20] *Endo et al*. proved by elaborate neutron scattering experiments employing a high-precision two-dimensional contrast variation technique that the PEP-*b*-PEO polymers are indeed anchored in the amphiphilic film, with the PEP and PEO blocks forming mushroom-like structures in the oil and water domains, respectively.[21] *Gompper et al*.[22] explained the enormous efficiency boosting effect in terms of the bending elastic energy[23] of fluctuating polymer-decorated surfactant membranes by taking into account the effect of the membrane-anchored copolymers onto the spontaneous curvature and the bending moduli $\varkappa$ and $\bar{\kappa}$[24,25]. Based on these theoretical considerations, it was found that the efficiency boosting effect scales with the number density of block copolymers anchored into the membrane as well as the end-to-end distances of hydrophilic and hydrophobic blocks.[21,26] Over the last two decades, several research groups have investigated the role of the copolymers' molecular structure on their efficiency boosting effect in mostly balanced bicontinuously structured microemulsions[21,26–31], whereas *Foster et al.* utilized the boosting effect of PEP-*b*-PEO diblock copolymers to enable the formation of giant water-in-oil microemulsion droplets[32]. *Johannson et. al* studied the effect of poly(ethylene oxide)-*b*-poly(dodecene oxide), poly(ethylene oxide)-*b*-poly(butylene oxide), and

the Ketjenlube comb-polymer on quaternary microemulsion systems of the type D_2O – *n*-octane – *n*-octyl-β-D-glucoside – 1-octanol.[27] *Frank et al.*[33] and *Brodeck et al*. used different types of sticker polymers (hydrophilic alcohol ethoxylates) and Y-shaped polymers (PEO-*b*-PEP-*b*-PEO) in ternary microemulsion systems of the type D_2O – *n*-decane – $C_{10}E_4$[34], while *Klemmer et al*. used poly(ethylene oxide)-*b*-poly(butylene oxide) (PEO-*b*-PBO) to increase the efficiency of pseudo-ternary H_2O/NaCl – *n*-decane – $C_{10}E_4$ microemulsions[30]. Recently, some of us studied the efficiency boosting effect of a new type of poly(ethylene oxide)-*b*-poly(butylene carbonate) block copolymers (PEO-*b*-PBC) in microemulsion systems containing technically relevant polar oils.[31] Furthermore, the impact of triblock (ABA or ABC) copolymers such as poloxamers (PEO-*b*-PPO-*b*-PEO)[30,35], amphiphilic random copolymers[36] as well as charged diblock copolymers consisting of poly(ethylene-*co*-propylene) and sodium poly(styrene sulfonate) (PEP-*b*-PSS)[37] as efficiency boosters has been investigated. While all these amphiphilic copolymers were found to increase the efficiency of surfactants to solubilize water and oil into each other, the boosting strength strongly depends on their amphiphilicity as well as the structure and size of their hydrophilic and hydrophobic blocks. On the contrary, a so-called "anti-boosting" effect was found for non-amphiphilic homopolymers[28] and for some special kinds of poloxamers of the type PEO-*b*-PPO-*b*-PEO, where the PPO unit is significantly larger than the PEO units[38]. Although the boosting effect of amphiphilic diblock copolymers seems to be predestined to eradicate the disadvantage of the need for high surfactant amounts to stabilize microemulsions, it has only scarcely found its way into applications.[39] Some prominent reasons for this are a difficult and expensive large-scale polymer synthesis[17] as well as the weakening of the boosting effect with increasing dispersity of the polymer blocks, especially in the case of remaining homopolymers.

Poly(ethylene oxide)-*b*-Poly(alkyl glycidyl ether)s (PEO-*b*-PAlkGEs) -- A Promising New Type of Efficiency Boosters. Long-chain alkyl glycidyl ethers (AlkGEs) are highly hydrophobic epoxide monomers that can be polymerized by the conventional anionic ring opening polymerization (AROP) approach adding crown ethers[40], via catalysts[41,42] or adding phosphazene bases[43]. Using the established AROP approach, the molar masses of the polyethers can be adjusted by the initiator to monomer ratio. Due to the absence of catalysts or other toxic components, a one-step purification protocol yields pure polyethers on a multi-gram scale. In this work, we report the synthesis of well-defined amphiphilic diblock polyethers with narrow dispersities from $Đ$ = 1.03 to 1.09. Using different macroinitiators and long-chain AlkGE monomers, different block copolymers have been synthesized under systematic variation of the hydrophilic/lipophilic balance (*HLB*). We emphasize that due to the commercial availability of the macroinitiator (Me-PEO, also called mPEG) and the availability of epoxy monomers in pure and technical grades, the synthesis of these diblock copolymers can be performed at low cost and on multi-gram scale via the synthesis route shown in Scheme 1.

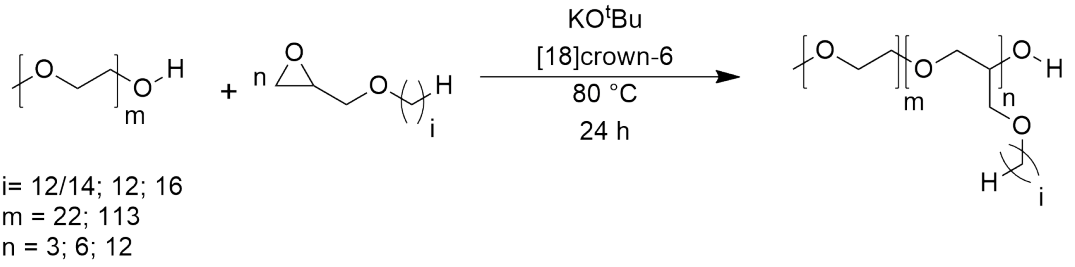

Scheme 1. Synthesis of AB diblock copolymers using Me-PEO macroinitiators and the long-chain alkyl glycidyl ethers C_{12}GE, C_{16}GE and the technical grade $C_{12/14}$GE.

Having this new type of easy-to-synthesize poly(ethylene oxide)-*b*-poly(alkyl glycidyl ether) (PEO-*b*-PAlkGE) polymers with narrow dispersities at hand (cf. Table 1), the objective of this work was to investigate their influence on both model-type and technically relevant

microemulsions. Thus, in a first step, we studied the effect of Me-P(EO)$_{113}$-*b*-P(C$_{12}$GE)$_7$ on the phase behavior and microstructure of the model microemulsion system H_2O/NaCl – *n*-decane – $C_{10}E_4$. For technical applications, such as enhanced oil recovery, efficient solubilization of long chain *n*-alkanes is of interest, which is why we investigated the extent of boosting of PEO-*b*-PAlkGE polymers in H_2O/NaCl – *n*-octacosane – $C_{16}E_6$ microemulsions[44] in the next step. By means of this microemulsion system, the effect of varying both the alkyl chain length and the number of repeating units of the alkyl glycidyl ether block was studied. With respect to their technical application, the influence of technical-grade "carbonated" poly(ethylene oxide)-poly(carbonate alkyl glycidyl ether) copolymers was investigated in the *n*-octacosane microemulsion and in the technical-grade system consisting of H_2O/NaCl – Sasolwax 5805 – Genapol O 050/O 080. In all microemulsion systems studied, the size of both the PEO and the PAlkGE block was chosen to be considerably smaller than the diameter of the water and oil domains to suppress the formation of liquid crystalline phases. With the analysis of the recorded phase diagrams and small angle neutron scattering (SANS) curves, we finally not only quantified the effect of the polymers on the bending rigidity $\varkappa$ but also used the scaling relation suggested by *Gompper et al.*[22,26,29] in order to compare the boosting of the PEO-*b*-PAlkGE polymers with the extensively investigated PEP-*b*-PEO polymers.

EXPERIMENTAL PART

Reagents. Solvents, reagents and surfactants were purchased from Acros Organics, Bachem, Clariant, Deutero, Eurisotop, Fluka, Sasol Germany GmbH, Sigma-Aldrich and TCI and used as received, unless otherwise stated.

For the synthesis of the diblock polyethers, the two different alkyl glycidyl ethers C_{12}GE and C_{16}GE were synthesized to ensure high purity of the epoxide monomers. Additionally, the

synthesized $C_{12}GE$ was copolymerized with CO_2 to generate hydrophobic polycarbonate blocks. Since the living anionic ring-opening polymerization (AROP) is limited to epoxide monomers with high purity, additional copolymerization reactions of CO_2 with a commercially available alkyl glycidyl ether mixture ($C_{12/14}GE$, technical-grade) were carried out. All epoxide monomers were dissolved in benzene and dried overnight under reduced pressure before polymerization to remove water residues. The dispersities of the purchased macroinitiator Me-P(EO)$_{113}$ (5 kg mol^{-1}, $Đ$ = 1.04) were determined by size-exclusion chromatography (SEC) (eluent: dimethylformamide (= DMF), calibration: PEO, M_n = 238 – 44000 g mol^{-1}). The deuterated solvent (chloroform-*d*) used for nuclear magnetic resonance (NMR) measurements was received from Deutero GmbH.

For the phase behavior studies, double-distilled H_2O, *n*-decane ($C_{10}H_{22}$, Sigma-Aldrich, purity of >99%) and *n*-octacosane ($C_{28}H_{58}$, Acros Organics, purity of 99%) were used. Sasolwax 5805 (Sasol Germany GmbH) was used as a technical-grade mixture of linear (*n*) and branched (*iso*) alkanes ranging from C_{19} to C_{46} with an average carbon number of 30.5 (see gas chromatography (GC) spectrum in [44]). As pure surfactants, tetraethylene glycol monodecyl ether (= $C_{10}E_4$, $C_{18}H_{38}O_5$, Bachem AG, purity of >99%) and hexaethylene glycol monohexadecyl ether (= $C_{16}E_6$, $C_{28}H_{58}O_7$, Fluka, purity of >98%) were used. Technical-grade nonionic surfactants of the Genapol O series (Clariant (Frankfurt, Germany)), which consist of ethoxylated oleyl alcohols with a broad distribution of their ethoxylation degrees, were utilized. For Genapol O 050 and Genapol O 080, the mean ethoxylation degrees are 5 and 8, respectively. For the SANS measurements, H_2O was replaced with D_2O (Eurisotop, purity of 99% D) to adjust bulk-contrast.

Synthesis. The synthesis and purification of the commercial monomers as well as the pure $C_{12}GE$ and $C_{16}GE$ epoxide monomers was carried out as reported before. Additionally, the synthesis of the

homopolymers was performed as reported in [40]. The synthesis of the novel diblock copolymers employed in the current study is described in the following.

Diblock copolymer synthesis. In the following, the general reaction procedure for the synthesis of the PEO-*b*-AlkGEs is described by means of Me-P(EO)$_{113}$-*b*-P(C$_{12}$GE)$_6$. In a 50 mL Schlenk flask, 1 g (0.2 mmol, 1 equiv.) of Me-P(EO)$_{113}$ (M_n = 5.000 g mol^{-1}), 17.9 mg (0.16 mmol, 0.8 equiv.) of potassium *tert*-butoxide (KO^{t}Bu), and 84.6 mg (0.3 mmol, 1.6 equiv.) of 18-Crown-6 were dissolved in 5 mL of a benzene/methanol mixture (4.5 mL benzene / 0.5 mL methanol). Subsequently, the mixture was dried overnight under reduced pressure at 60 °C to yield the partly deprotonated initiator. The reaction mixture was heated to 80 °C and 290 mg (1.2 mmol, 6 equiv.) of the dried C$_{12}$GE were added with a syringe under argon (1 atm). The reaction mixture was then stirred for 24 h at 80 °C. After completion of the reaction, 1 mL of methanol, and 3 mL of dichloromethane (DCM) were added at room temperature. The product was precipitated in diethyl ether at room temperature, centrifuged, and the precipitated product was dried under reduced pressure at 40 °C. Subsequently, the polymer was dialyzed in methanol to fully remove salts and crown ether residues. ^{1}H NMR (300 MHz, chloroform-*d*) δ (ppm) = 3.93 - 3.39 (m, 588 H, backbone), 3.37 (s, 3 H, C*H*$_3$-O), 1.60 – 1.46 (m, 12 H, O CH$_2$ C*H*$_2$), 1.37 - 1.18 (m, 108 H, O CH$_2$ CH$_2$ (C*H*$_2$)$_9$ CH$_3$), 0.86 (t, 18 H, *J* = 7.0 Hz, C*H*$_3$).

The "carbonate" polymers used in this work contain a CO$_2$ group within the hydrophobic alkyl glycidyl ether block of the polymer. The general reaction procedure is described for Me-P(EO)$_{113}$-P(CO$_2$C$_{12/14}$GE)$_7$. An autoclave equipped with a stirring-bar was filled with 1 g (0.2 mmol, 1 equiv.) of Me-P(EO)$_{113}$ (M_n = 5000 g mol^{-1}), 1.95 g (8 mmol, 20 equiv.) of the dried C$_{12/14}$GE (technical-grade), 15.3 mg (0.024 mmol, 0.6 equiv.) of Co(Salen)Cl and 13.7 mg (0.024 mmol, 0.6 equiv.) of [PPN]Cl under argon atmosphere. The reaction mixture was stirred under carbon dioxide

pressure of 50 bar at room temperature for 20 h. The crude product was dissolved in DCM and the catalyst was deactivated with 0.5 mL of a solution of 5 vol% HCl in methanol. A neutral aluminum oxide column and 400 mL tetrahydrofuran (THF) as eluent were used for further purification of the product to eliminate the catalyst. The solvent was evaporated under reduced pressure and the product was dissolved again and precipitated in ice-cold diethyl ether. The colorless solid was then dried under reduced pressure for 24 h. ^{1}H NMR (300 MHz, chloroform-*d*) δ (ppm) = 5.04 (s, 7 H, carbonyl backbone), 4.43 - 4.21 (m, 14 H, carbonyl backbone), 3.96 - 3.75 (m, 14 H, O C*H*$_2$ CH), 3.75 - 3.60 (m, 538 H, polyether backbone and -O-C*H*$_2$-CH$_2$-), 3.41 (s, 3 H, C*H*$_3$-O), 1.65 - 1.48 (m, 14 H, O CH$_2$ C*H*$_2$), 1.39 - 1.15 (m, 246 H, O CH$_2$ CH$_2$ (C*H*$_2$)$_9$ CH$_3$), 0.92 - 0.87 (m, 21 H, C*H*$_3$). The synthesis protocol for the diblock copolymers with the general structure Me-P(EO)$_{113}$-P(CO$_2$C$_{12}$GE)$_n$ that contain the pure C_{12}GE in combination with carbon dioxide, follows the same procedure as with the use of the $C_{12/14}$GE mixture (technical-grade), but with decreased amounts of the catalyst system (0.06 equivalents).

While the poly(ethylene oxide)-poly(alkyl glycidyl ether)s (PEO-*b*-PAlkGE) were synthesized with a high yield between 70 and 98 %, the yield of the "carbonated" poly(ethylene oxide)-poly(carbonate alkyl glycidyl ether) analogs was moderate (30 to 60 %, Table S1).

Phase Behavior Studies. The procedure for the investigation of the phase behavior of nonionic microemulsion systems can be found elsewhere.[44] Here, we will only focus on the most important procedures for the water/NaCl (A) – oil (B) – nonionic surfactant (C)/amphiphilic diblock copolymer (D) systems studied in this work. For sample preparation, all components are weighed out in test tubes with an accuracy of $\Delta m = \pm 0.001$ g, starting with the amphiphilic diblock copolymer (smallest amount) and the surfactant(s) followed by the respective oil, which are known

to be good solvents for nonionic surfactants. To avoid the formation of liquid crystals, water/NaCl ("brine", with $\varepsilon = 0.001$) was added in the last step. Before the test tubes were sealed with a polyethylene stopper, a stirring bar was added to the sample. After homogenization at low and high temperatures, the samples' phase behavior was studied as a function of temperature with the help of a temperature-controlled water bath (Thermo-Haake DC30, with a temperature control up to $\Delta T = 0.02$ K). For this, the samples were stirred until the temperature equilibrium was reached. The stirring was then stopped and the numbers and types of coexisting phases were determined by visual inspection of both transmitted and scattered light using crossed polarizers to recognize anisotropic phases. After the phase transition temperatures were determined with a precision of $\Delta T = \pm 0.05$ K for a given composition, the sample was diluted with brine and oil to repeat the process for lower values of γ.

In order to characterize the phase behavior of a microemulsion system in general and the efficiency boosting effect of amphiphilic block copolymers in particular, it has been proven useful to perform so-called $T(\gamma)$-sections through the Gibbs phase prism.[44–46] To be more precise, the phase behavior was studied as a function of temperature and mass fraction

$$\gamma = \frac{m_C + m_D}{m_A + m_B + m_C + m_D} \tag{1}$$

of amphiphiles, which comprises both, surfactant(s) (C) and block copolymer (D). The mass fraction α of oil (B) in the brine (A)/oil (B) mixture was adjusted to a value that corresponds to a volume fraction

$$\phi = \frac{V_B}{V_A + V_B} = 0.500 \tag{2}$$

using the respective components' densities. Note that for these symmetric systems, using equal volumes of oil and water results in a zero mean curvature of the amphiphilic film at the phase inversion temperature (*PIT* or $\tilde{T}$).[2] Traces of sodium chloride (= NaCl) were added to water (mass fraction $\varepsilon = 0.001$) to screen possible electrostatic interactions of ionic impurities.

The amount of polymer (D) within the overall amphiphilic mixture is defined as follows

$$\delta = \frac{m_D}{m_C + m_D}. \tag{3}$$

For the analysis of the recorded phase diagrams and scattering curves with respect to the scaling of the efficiency boosting effect[22,26], the respective volume fractions $\phi_{C,i}$ of the surfactant in the amphiphilic film is needed. $\phi_{C,i}$ can be calculated from the volume fraction

$$\phi_C = \frac{V_C}{V_A + V_B + V_C + V_D} = \frac{V_C}{V_{total}} \tag{4}$$

of surfactant in the overall mixture taking into account the monomeric solubility

$$\phi_{C,monb} = \frac{V_{C,monb}}{V_{C,monb} + V_B} \tag{5}$$

of the nonionic surfactants in the oil according to

$$\phi_{C,i} = \phi_C - \frac{\phi_{C,monb}(1 - \phi_C)\phi}{V_{tot}}. \tag{6}$$

Here, $V_{C,monb}$ is the surfactant volume monomerically solubilized in the oil volume V_B. For the studied systems, monomeric solubilities of $\phi_{C10E4,monb} = 0.016$ in *n*-decane[47] and $\phi_{C16E6,monb} = 0.014$ in *n*-octacosane were used for the respective phase inversion temperatures (PIT). Both values were determined from measurements of the microemulsion (middle) phase volume as a function of γ at the PIT. Note that the monomeric solubility of $C_{10}E_4$ and $C_{16}E_6$ as well as of the technical-grade Genapol O

050 and Genapol O 080 in water (cmc) can be neglected.[47] For the sake of completeness, the volume fraction of copolymer

$$\phi_D = \frac{V_D}{V_A + V_B + V_C + V_D} \quad (7)$$

can be estimated assuming a polymer density of 1 g cm^{-3}.

Instrumentation. *^{1}H NMR (300 MHz)* spectra were recorded on a Bruker Avance III HD (300 MHz, 5 mm BBFO-head with z-gradient and ATM, BACS 60 sample changer) and referenced internally to the proton signal of the deuterated solvent (here: Chloroform-*d*).

Size exclusion chromatography (SEC) was performed in DMF with 1 g/L lithium bromide as eluent and *MZ-Analysetechnik HEMA 300/100/40* columns at 50 °C, using an RI detector at a flow rate of 1 mL/min. Calibration was carried out using poly(ethylene glycol) (PEO) standards provided by *PSS*. Additional SEC measurements were performed in THF using an *MZ-Gel SD plus e5/e3/100* column at 30 °C. Calibration was carried out using polystyrene standards provided by *PSS*.

Differential scanning calorimetry (DSC) measurements were carried out under nitrogen atmosphere using a *PerkinElmer DSC 8500* in the temperature range of -50 to 70 °C, with heating rates of 20 K min^{-1}, and 10 K min^{-1} for the first and second heating cycle, respectively. A temperature plateau at 70 °C for one minute was used after the first heating, followed by a cooling run with a rate of 10 K min^{-1}.

Small-angle neutron scattering (SANS) measurements were performed to study the influence of the new PEO-*b*-PAlkGE copolymers on the microstructure of the respective microemulsions and to determine the end-to-end distances of some of the homopolymers in the respective solvents.

All scattering curves were recorded by adjusting the so-called bulk-contrast. Therefore, H_2O was replaced with D_2O while keeping the sample composition constant with respect to their volume ratios. Note that for D_2O, the phase boundaries are about 2 K lower than with H_2O.[48] For the determination of the end-to-end distances of the PAlkGE homopolymers, deuterated *n*-alkanes were used.

All scattering experiments on microemulsion systems were performed at the D11 spectrometer of the *Institut Laue-Langevin* (ILL) in Grenoble (France), where a neutron wavelength of $\lambda = 5.5$ Å with a wavelength spread of $\Delta\lambda/\lambda = 9\%$ (fwhm, specified by the ILL) was adjusted. Three different detector/collimation distances, namely 39 m/40.5 m, 8 m/20.5 m and 1.5 m/8 m, were used to obtain a scattering vector

$$q = \frac{4\pi}{\lambda} \cdot \sin(\frac{\theta}{2}) \tag{8}$$

ranging from 0.0016 $Å^{-1}$ to 0.4695 $Å^{-1}$. The SANS experiments on homopolymers in their respective solvents were performed at the instrument NG7 30m SANS at the *National Institute of Standards and Technology* (NIST) in Gaithersburg, Maryland (USA) and the KWS-1 instrument operated by the *Jülich Centre for Neutron Science* (*JCNS*) at the *Heinz Maier-Leibnitz Zentrum* (MLZ), Garching (Germany). While at NIST, the following settings were used: wavelength $\lambda = 6$ Å and detector/collimation distances 1.33 m/5.42 m, 4 m/8.52 m, 13.17 m/14.72 m resulting in a *q*-range from 0.0126 $Å^{-1}$ to 0.4450 $Å^{-1}$; at the MLZ, $\lambda = 5$ Å and *det./coll.* = 1.5 m/8 m, 8 m/8 m, 20 m/20 m were adjusted resulting in a *q*-range from 0.0097 $Å^{-1}$ to 0.5835 $Å^{-1}$. The wavelength distribution was $\Delta\lambda/\lambda = 13.8\%$ (fwhm) at the NG7 30m SANS and 10% at KWS-1.

The measured scattering intensities were normalized to absolute scale using the incoherent scattering of H_2O (optical path length 1 mm) at ILL, the empty beam measurements at NIST, and

Plexiglas (optical path length 1.5 mm) at MLZ. The software packages *LAMP* (ILL), *IGOR Pro* (NIST), and *QtiSAS* (MLZ) were used to perform the reduction of the raw data. To obtain the differential cross section $d\sigma(q)/d\Omega = I(q)$, the data were radially averaged masking defective detector pixels and taking into account dark current and empty cell scattering as well as the detector dead time.

Prior to the SANS measurements, the phase behavior of the microemulsion samples was checked in a water bath at the desired temperatures. All samples were then filled into Hellma quartz QS glass cells with an optical path length of 1 mm. Afterwards, the samples were transferred into our home-built 5 position cell holder, which allows temperature adjustments with an accuracy of ± 0.1 K. Note that this cell holder can be shaken manually to ensure the mixing and homogeneity of the microemulsion samples. Before and after each measurement, the homogeneity of the samples was checked visually after several minutes of waiting time. Note that at NIST, where only homopolymer samples were studied, the onsite cell holder was used.

RESULTS AND DISCUSSION

This section starts with the characterization of the Me-P(EO)$_{113}$-*b*-P(C$_i$GE)$_n$, Me-P(EO)$_{113}$-*b*-P(CO$_2$C$_i$GE)$_n$ and the Me-P(EO)$_{113}$-P(CO$_2$C$_{12/14}$GE)$_n$ copolymers. Subsequently, the influence of this new type of amphiphilic copolymers on the solubilization efficiency and microstructure of microemulsions containing *n*-decane or *n*-octacosane is demonstrated by varying the copolymer concentration (δ) as well as the alkyl side chain length (i) and the number of repeating units of the alkyl glycidyl ether block (n). To suppress the formation of liquid crystalline phases, the size of the PEO block was set to 113 EO, while the PAlkGE block was chosen to not be larger than $i = 16$

and $n = 9$, ensuring that the end-to-end distances of the two blocks are considerably smaller than the diameter of the water and oil domains in the microemulsion (see Tables 2 and S4).[20,30] To prove that the efficiency boosting effect can be successfully transferred to technical applications, the technical-grade Me-P(EO)$_{113}$-P(CO$_2$C$_{12/14}$GE)$_7$ polymer was used to boost the efficiency of technical-grade Genapol O surfactants to solubilize Sasolwax 5805 in brine. The last part of this section deals with the quantification of the copolymers' effect on the bending rigidity $\varkappa$ as well as the comparison of the boosting strength of this new copolymer type with the extensively investigated PEP-*b*-PEO polymers by applying the scaling relation of *Gompper et al.*.[22,26]

Synthesis and Characterization. The polymerization of hydrophobic long-chain alkyl glycidyl ethers (here: C_{12}GE and C_{16}GE) with commercially available monofunctional Me-PEO macroinitiators ($M_n = 5000$ g mol^{-1}) leads to amphiphilic diblock copolymers with tailorable hydrophobic/hydrophilic ratios on multi-gram scale. Due to the underlying mechanism of the anionic ring opening polymerization (AROP), the different polymerizations yield diblock polyethers with monomodal and narrow molar mass distributions ranging from $Đ = 1.03$ to 1.08 (see Figure 1).

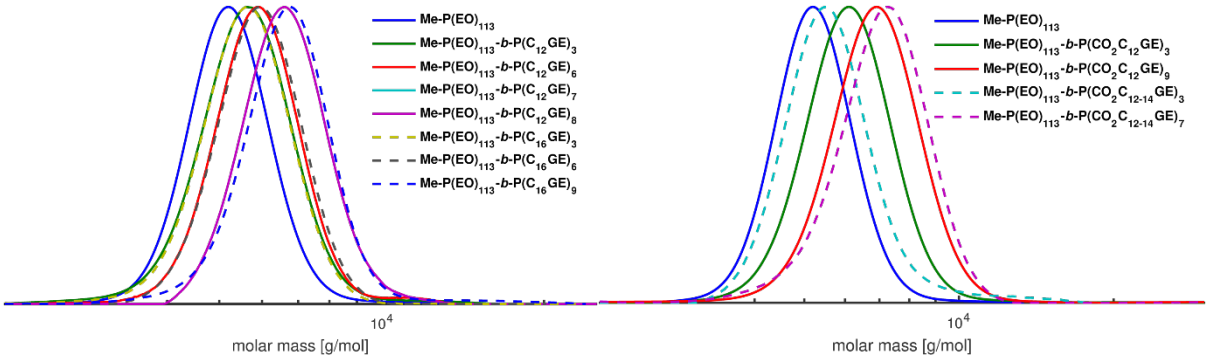

Figure 1. SEC traces of the synthesized diblock copolymers using Me-P(EO)$_{113}$ as a macroinitiator in combination with pure C_{12}GE, pure C_{16}GE, and technical-grade $CO_2C_{12/14}$GE, respectively (eluent: DMF, calibration: PEO standards).

Table 1. Synthesized Amphiphilic Diblock Copolymers, their Experimentally Determined Molar Masses Obtained from ^{1}H NMR[a], Molar Mass Distribution $Đ$ Obtained from SEC[b] and Melting Temperatures (T_m) of the Two Polymer Blocks within the Diblock Copolymer.

Polymer sample	$M_{n,theo}$/ g mol^{-1}	$M_{n,exp}$/ g mol^{-1} [a]	$Đ$ [b]	T_m/°C [c]
Me-P(EO)$_{113}$-*b*-P(C_{12}GE)$_3$	5699	5700	1.05	-4; 55
Me-P(EO)$_{113}$-*b*-P(C_{12}GE)$_6$	6426	6400	1.08	1; 53
Me-P(EO)$_{113}$-*b*-P(C_{12}GE)$_7$	6668	6670	1.06	-
Me-P(EO)$_{113}$-*b*-P(C_{12}GE)$_8$*	6911	6910	1.06	3; 53
Me-P(EO)$_{113}$-*b*-P(C_{16}GE)$_3$	5866	5870	1.04	56
Me-P(EO)$_{113}$-*b*-P(C_{16}GE)$_6$	6760	6760	1.06	35; 53
Me-P(EO)$_{113}$-*b*-P(C_{16}GE)$_9$*	7654	7650	1.05	38; 52
Me-P(EO)$_{113}$-*b*-P(CO_2C_{12}GE)$_3$	5831	5830	1.04	-3; 54
Me-P(EO)$_{113}$-*b*-P(CO_2C_{12}GE)$_9$	7549	7550	1.05	-2; 54
Me-P(EO)$_{113}$-*b*-P($CO_2C_{12/14}$GE)$_3$	5872	5870	1.06	3; 55
Me-P(EO)$_{113}$-*b*-P($CO_2C_{12/14}$GE)$_7$	7072	7070	1.05	-3; 53

[a] Determined by ^{1}H NMR (300 MHz, $CDCl_3$); [b] determined by SEC (eluent: DMF, calibration: PEO standards); [c] measured by DSC, the first listed melting temperature (T_m) can be assigned to the alkyl glycidyl ether block and the second T_m can be assigned to the PEO block. [d] more repeating units were targeted.

The experimentally determined molar masses ($M_{n,exp}$) (Table 1 and Table S1) are in good agreement with the theoretically calculated molar masses ($M_{n,theo}$). However, it should be noted that for Me-P(EO)$_{113}$-*b*-P(C$_{12}$GE)$_8$ and Me-P(EO)$_{113}$-*b*-P(C$_{16}$GE)$_9$, a higher degree of polymerization of $n = 12$ was targeted. The lower values could be explained by impurities in the epoxide monomers or the reaction mixture (e.g. water) leading to termination of the polymerization reaction or to the formation of additional living chain ends and the formation of homopolymers with increasing amount of monomer. However, narrow molar mass distributions for all synthesized diblock copolymers were obtained, indicating a controlled polymerization.

Differential scanning calorimetry (DSC) measurements of the synthesized amphiphilic diblock copolymers reveal the presence of two different melting temperatures T_m that can be assigned to the melting points of the PAlkGE and the PEO block, respectively. These results are in good agreement with previous investigations of ABA triblock copolymers and similar systems, indicating a phase segregation of the respective blocks driven by crystallization of both PEO and the long alkyl chains (Figures S2 to S11, Table S1).[40,49–51]

Efficiency Boosting of Me-P(EO)$_{113}$-*b*-P(C$_{12}$GE)$_7$ in H$_2$O/NaCl – *n*-Decane – C$_{10}$E$_4$. It was 20 years ago that *Jakobs et al*. discovered the efficiency boosting effect by adding small amounts of amphiphilic block copolymers of the type PEP-*b*-PEO to the symmetric (equal volumes of water and *n*-decane; $\phi = 0.500$) model microemulsion system H$_2$O – *n*-decane – C$_{10}$E$_4$.[16] By considering these studies as a kind of benchmark, we systematically studied the influence of the new type of

poly(ethylene oxide)-*b*-poly(alkyl glycidyl ether) copolymers on the phase behavior and microstructure of the same microemulsion system. Note that we added traces of NaCl to water (mass fraction $\varepsilon = 0.001$) to screen possible electrostatic interactions of ionic impurities. Besides the facile synthesis, the adjustability of the molecular structure of the PEO-*b*-PAlkGE copolymers is an outstanding property. By deliberately varying *m*, *n* and *i*, the number of repeating units of the two blocks but also the length of the alkyl side chain within the AlkGE block can be adjusted.

As a starting point, similar to *Jakobs et al*. in their 1999 paper[16], we demonstrate the boosting effect of the new Me-P(EO)$_{113}$-*b*-P(C$_{12}$GE)$_7$ copolymer by preparing four different samples of the symmetric microemulsion H$_2$O/NaCl – *n*-decane – C$_{10}$E$_4$/ Me-P(EO)$_{113}$-*b*-P(C$_{12}$GE)$_7$. When using the same overall volume, equal volumes of oil and water ($\phi = 0.500$), and a constant surfactant plus copolymer mass fraction $\gamma = 0.050$ (☆), all samples form three phases at the phase inversion temperature $T = 30.7$ °C of the system without polymer. The photos in Figure 2 impressively show that the volume of the microemulsion (middle) phase strongly increases when the mass fraction δ of Me-P(EO)$_{113}$-*b*-P(C$_{12}$GE)$_7$ in the C$_{10}$E$_4$/Me-P(EO)$_{113}$-*b*-P(C$_{12}$GE)$_7$ mixture is increased from $\delta = 0$ to $\delta = 0.075$. Thus, much more water and oil can be solubilized by the same amount of amphiphile. This emphasizes a strong increase of efficiency, which is also reflected by the changing visual appearance of the microemulsion phase from opalescent to whitish. The increasing length scale of the water and oil domains obviously leads to a stronger light scattering. Furthermore, the water and oil excess phase exhibit almost identical volumes, which strongly indicates that the hydrophilic-lipophilic balance seems to be unaffected by the addition of copolymer.

As a next step, the influence of the Me-P(EO)$_{113}$-*b*-P(C$_{12}$GE)$_7$ copolymer upon the phase behavior of the H$_2$O/NaCl – *n*-decane – C$_{10}$E$_4$ system was quantitatively studied as a function of temperature and mass fraction of amphiphile (surfactant and copolymer) at a constant $\phi = 0.500$ and $\varepsilon = 0.001$.

The recorded phase diagrams are shown on the left side of Figure 2. In general, the phase behavior of all systems resembles the well-known phase behavior of nonionic microemulsion systems.[46] A fishtail-shaped one-phase region occurs at intermediate temperatures between two phase boundaries. While at lower temperatures, an oil-in-water microemulsion co-exists with an oil-excess phase ($\underline{2}$), a water-in-oil microemulsion co-exists with a water-excess phase ($\overline{2}$) at higher temperatures. With decreasing mass fraction γ of amphiphile, the phase boundaries converge and eventually coincide in the so-called optimum point $\tilde{X}$, defined by the minimum amount $\tilde{\gamma}$ of surfactant plus polymer needed to form a microemulsion at the phase inversion temperature PIT ($\tilde{T}$). At mass fractions below $\tilde{\gamma}$, a three-phase region (3) can be found between the two-phase regions. Note that in this study, we primarily focus on the influence of the new amphiphilic block copolymers on the so-called optimum point $\tilde{X}$. Therefore, mainly the phase boundaries limiting the one phase region at $\gamma \geq \tilde{\gamma}$ were determined.

Starting with the phase diagram of the pseudo-ternary microemulsion system, the $\tilde{X}$ point can be found at $\tilde{\gamma} = 0.135$ and $\tilde{T} = 30.6$ °C, which is in almost quantitative agreement with literature.[16] Upon replacing only a small fraction of $C_{10}E_4$ with Me-P(EO)$_{113}$-*b*-P(C_{12}GE)$_7$ ($\delta = 0.025$), $\tilde{\gamma}$ decreases to $\tilde{\gamma} = 0.114$, i.e. the efficiency to formulate a microemulsion increases. At the same time, the PIT increases to $\tilde{T} = 31.1$ °C because the hydrophilic Me-P(EO)$_{113}$-block is larger than the hydrophobic P(C_{12}GE)$_7$-block.[52] A further increase of δ shifts the minimum amount of $C_{10}E_4$ and Me-P(EO)$_{113}$-*b*-P(C_{12}GE)$_7$ needed to formulate a microemulsion to even lower values. For $\delta = 0.075$, a value of $\tilde{\gamma} = 0.077$ is found. Thus, both the phase diagrams as well as the swelling of the volume of the microemulsion phase prove the strong efficiency boosting of the PEO-*b*-PAlkGE copolymers. Whether the boosting effect of the new type of copolymers is comparable to the extensively investigated PEP-*b*-PEO polymers will be discussed at the end of this section by applying the

scaling relation of *Gompper et al.*.[22,26] Note that the $\tilde{X}$-points are compiled in Table S2 of the SI in form of $\tilde{\gamma}$ and $\tilde{T}$ values.

Subsequently, the influence of the Me-P(EO)$_{113}$-*b*-P(C$_{12}$GE)$_7$ copolymer on the microstructure of the D$_2$O/NaCl – *n*-decane – C$_{10}$E$_4$ systems was studied by two sets of systematic SANS experiments. The scattering curves recorded in bulk contrast are shown on the right hand side of Figure 2. All curves resemble the typical shape found for bicontinuous microemulsions[53]: Starting from low q-values, where the curves show a plateau, a scattering peak is found at middle $q = q_{max}$, after which the intensity decreases proportional to q^{-4} before the incoherent background is reached. However, due to the strong scattering and the neutron path length of 1 mm, contributions of multiple scattering can be observed especially around $q \approx 2q_{max}$.

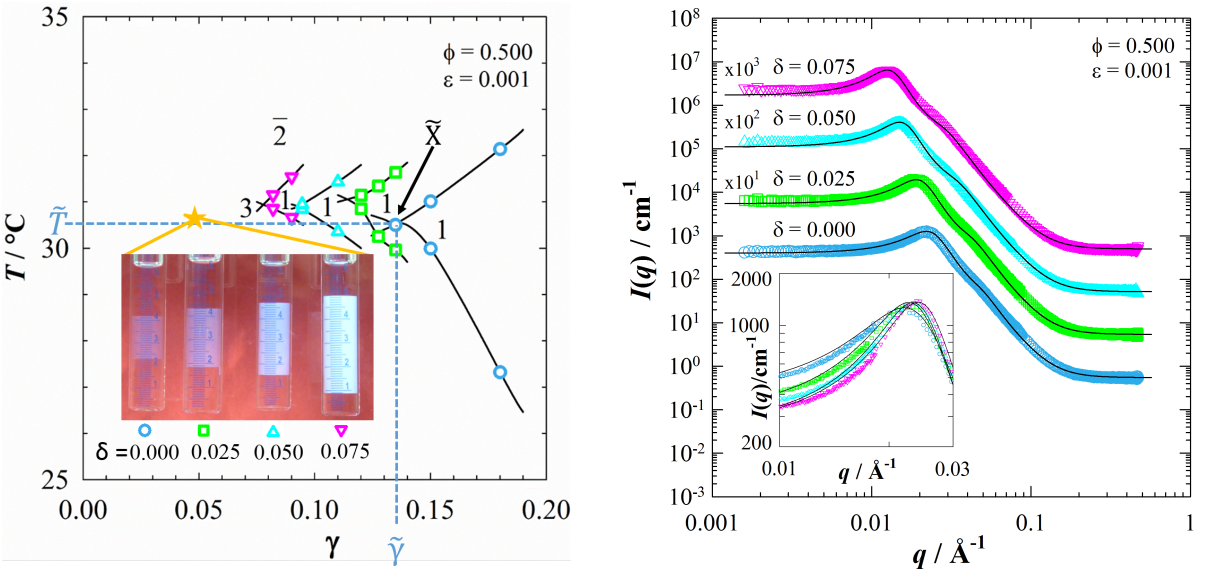

Figure 2. Left: $T(\gamma)$ diagrams of the system H$_2$O/NaCl – *n*-decane – C$_{10}$E$_4$/Me-P(EO)$_{113}$-*b*-P(C$_{12}$GE)$_7$, recorded at $\delta = 0$ (○), 0.025 (□), 0.050 (△) and 0.075 (▽) with $\phi = 0.500$ and $\varepsilon = 0.001$. 1, $\underline{2}$, $\overline{2}$ and 3 denote the regions where a one-phase microemulsion (1), or coexistences of an o/w-microemulsion with an oil excess phase ($\underline{2}$), a w/o microemulsion with water excess phase ($\overline{2}$), and a bicontinuous microemulsion with water and oil excess phases (3) can be observed. The shift of the $\tilde{X}$ points toward lower values of γ upon increasing δ clearly proves the strong efficiency boosting, which is also visible by the growth of the

microemulsion phase shown in the photos of samples prepared at $T = 30.7$ °C and $\gamma = 0.050$ (☆) with varying δ-values. **Right:** Bulk contrast SANS curves of samples recorded along two pathways: Close to the respective $\tilde{X}$ points the scattering peak shifts to smaller q-values and higher intensities with increasing polymer content. Note that the curves are displaced by a factor of 10. Inset: Scattering curves of samples at $\phi_c = 0.144$ exhibit an increasing sharpness of the scattering peak with increasing δ. All curves are analyzed using the *TS* model[53] taking into account double scattering[54,55].

In the main part of Figure 2 (right), the scattering curves of the first set of experiments, which were performed to determine the length scale and the ordering of the efficiency-boosted microemulsions, are shown. These samples were prepared near the $\tilde{X}$ point of the respective system, i.e. in the one phase region at $\phi_{c+D} \approx \tilde{\phi}_{C+D} + 0.02$. Here, the surfactant/copolymer volume fraction ϕ_{c+D} is used instead of the mass fraction γ (taking into account the higher density of D_2O) in order to adjust the same composition of phase behavior and SANS samples. Considering the trend of the scattering curves with increasing Me-P(EO)$_{113}$-*b*-P(C$_{12}$GE)$_7$ content, a strong shift of the scattering peak to lower q and higher I can be observed when δ is increased from $\delta = 0$ to 0.075. This shift is a clear indication of increasing water and oil domain sizes in the bicontinuous microstructure, which is in agreement with the shift of the $\tilde{X}$ point to lower surfactant mass fractions $\tilde{\gamma}$ induced by the efficiency boosting of Me-P(EO)$_{113}$-*b*-P(C$_{12}$GE)$_7$ copolymers. Furthermore, the sharpness of the scattering peak increases slightly, indicating that the copolymer induces a better structural ordering of the bicontinuous microemulsion.

The scattering curves are analyzed using the model by *Teubner and Strey*[53] taking into account double scattering contributions[54,55] according to

$$I(q) = \frac{I_{0,1}}{\left(1 - \frac{I_{0,1}}{I_{\max,1}}\right)\left(\frac{q^2}{q_{\max}^2} - 1\right)^2 + \frac{I_{0,1}}{I_{\max,1}}} + \frac{I_{0,2}}{\left(1 - \frac{I_{0,2}}{I_{\max,2}}\right)\left(\frac{q^2}{4q_{\max}^2} - 1\right)^2 + \frac{I_{0,2}}{I_{\max,2}}} + I_{\text{incoh.}} \qquad (9)$$

where $I_{0,1} = I_0 \cdot (1 - f \cdot x)$ and $I_{0,2} = I_0 \cdot f \cdot x$ are the single and double scattering contributions of the scattering intensity at $q = 0$, respectively. Thereby, f specifies the fraction of double scattering and x the additional broadening due to higher order multiple scattering contributions and the wavelength spread of the neutrons. Similarly, $I_{max,1} = I_{max}\ (1 - f)$ and $I_{max,2} = I_{max} \cdot f$ are the single and double scattering contributions of the scattering at $q = q_{max}$ and $q = 2q_{max}$, respectively.

Relating $I_{0,1}$, $I_{max,1}$ and q_{max} with the coefficients of the order parameter expansion via $a_2 = 1/I_{0,1}$, $c_2 = (1/I_{0,1} - 1/I_{max,1})/q_{max}^4$ and $c_1 = -2c_2q_{max}^2$, the periodicity d_{TS}, the correlation length ξ_{TS}, and the amphiphilicity factor f_a can be determined

$$\xi_{TS} = \left[\frac{1}{2}\left(\frac{a_2}{c_2}\right)^{1/2} + \frac{1}{4}\frac{c_1}{c_2}\right]^{-1/2}, \tag{10}$$

$$d_{TS} = 2\pi\left[\frac{1}{2}\left(\frac{a_2}{c_2}\right)^{1/2} - \frac{1}{4}\frac{c_1}{c_2}\right]^{-1/2} \text{ and} \tag{11}$$

$$f_a = \frac{a_1}{\sqrt{4a_2c_2}}. \tag{12}$$

f_a is an important parameter to quantify the amphiphilic strength of an amphiphile and the structural order of a microemulsion system. While positive values are found for uncorrelated interfaces in disordered systems, negative f_a values are observed for systems with correlated interfaces.[56–58] By crossing the Lifshitz line, located at $f_a = 0$, toward negative f_a values, a peak develops in the scattering curve.[56,57] Typically, for microemulsions the f_a value ranges between -0.6 and -0.9. The more negative the amphiphilicity factor, the better the structuring of the microemulsion. Note that a perfectly structured lamellar phase exhibits an amphiphilicity factor of $f_a = -1$.[56–58]

Additionally, the parameter d_{TS} and ξ_{TS} can be used to determine the bending rigidity

$$\frac{\varkappa_{\mathrm{SANS}}}{k_{\mathrm{B}}T} = \frac{10\sqrt{3}\pi}{64}\frac{\xi_{\mathrm{TS}}}{d_{\mathrm{TS}}}, \tag{13}$$

using the model of random interfaces derived by *Safran et al.*[59] with k_B being the *Boltzmann* constant. Note that recent simulations on triangulated surfaces[60] as well as elaborate experimental studies, including phase behavior, SANS and neutron spin echo (NSE) experiments[61], indicate that $\varkappa_{\mathrm{SANS}}$ determined this way (eq. (13)) is rather a mixture of the bending rigidity κ and the saddle splay modulus $\bar{\kappa}$. Nevertheless, in this study we used the model of random interfaces to analyze the SANS curves because of the following reasons: Firstly, in order to separate the contributions of κ and $\bar{\kappa}$ to $\varkappa_{\mathrm{SANS}}$, one of two parameters has to be determined using independent methods. NSE, which is a reliable but elaborate method to determine the bare bending rigidity κ_0, was not available. Secondly, the bar saddle splay modulus $\bar{\kappa}_0$ can in principle be determined from the location of the so-called optimum point $\tilde{X}$, i.e. the instability of the bicontinuously structured micoemulsion.[62–64] However, the exact value of $\bar{\kappa}$ at $\tilde{X}$ is not exactly defined. While usually $\bar{\kappa}_0$ is set to 0 at the $\tilde{X}$ point,[62–64] *Holderer et al.* had to use $\bar{\kappa}_0$=0.28 k_BT[61] in order to achieve agreement with both the predicted relative contributions of κ and $\bar{\kappa}$ (0.15 and -0.85, respectively[60]) as well as the values of the bare bending rigidity κ_0 determined by NSE.

The fit of the experimental scattering data by eq. (9) is shown as black solid lines in Figure 2, right. It not only describes the peak but the entire scattering curve almost quantitatively. The sample composition, measuring temperature, d_{TS}, ξ_{TS}, f_a and $\varkappa_{\mathrm{SANS}}$ (according to eq. (13)) are summarized in Table 2. In accordance with the shift of the scattering peak to lower q, the periodicity d_{TS} increases by almost a factor two from 272 Å to 484 Å when δ is increased from $\delta = 0$ to 0.075. Simultaneously, the amphiphilicity factor f_a becomes slightly more negative and the bending rigidity $\varkappa_{\mathrm{SANS}}$ increases somewhat. Both trends indicate a slightly better structural

ordering, which is most probably caused by an increasing relative distance of the SANS samples from the $\tilde{X}$ point.

In the second set of SANS experiments, the influence of the Me-P(EO)$_{113}$-*b*-P(C$_{12}$GE)$_7$ copolymer on the microstructure was studied at constant surfactant volume fraction $\phi_c = \tilde{\phi}_{c,0} + 0.02 = 0.144$. Note that $\tilde{\phi}_{c,0}$ defines the surfactant volume fraction at the $\tilde{X}$ point of the polymer-free system ($\delta = 0$). The inset in Figure 2 (right) shows the respective scattering curves with focus on the region around the scattering peak. As can be seen, the peak, which stays almost at the same q_{max}, becomes significantly sharper when δ is increased from $\delta = 0$ to 0.075, indicating a considerably better ordering of the bicontinuous structure. Indeed, the analysis of the scattering data by the extended *TS* model (eq. (9)) provides an almost constant periodicity (as expected for $\phi_c = 0.144$ = constant), but an increasingly negative f_a value, decreasing from f_a = -0.83 to f_a = -0.91, proving the presence of very well-structured bicontinuous microemulsions.[57,58] Simultaneously, the addition of Me-P(EO)$_{113}$-*b*-P(C$_{12}$GE)$_7$ leads to a considerable increase of the amphiphilic film's bending rigidity $\varkappa_{SANS}$, which increases from 0.44 k_BT to 0.61 k_BT.

Efficiency Boosting of Me-P(EO)$_{113}$-*b*-P(C$_{12}$GE)$_7$ in H$_2$O/NaCl – *n*-Octacosane – C$_{16}$E$_6$. For some technical applications, as for instance enhanced oil recovery (EOR) but also cleaning and washing processes, the efficient solubilization of long-chain oils and waxes in microemulsions is of great interest, because it is closely related to ultra-low values of the oil/water interfacial tension and excellent wetting properties.[2,3,65] Very recently, it was shown that symmetric microemulsions containing pure long-chain oils (e.g. *n*-octacosane) or even technical-grade waxes (e.g. Sasolwax 5805) can be formulated using on the order of 15wt% of pure and technical-grade non-ionic *n*-alkyl polyglycol ether type surfactants.[44,66] However, in order to decrease the environmental

impact of surfactants and the overall costs, a considerable reduction of the amount of surfactant needed to form microemulsions is highly desirable.

This was our motivation to study whether the new PEO-*b*-PAlkGE copolymers can also be used to increase the efficiency of long-chain surfactants to formulate microemulsions containing long-chain oils or even technical-grade waxes. Thus, the influence of Me-P(EO)$_{113}$-*b*-P(C$_{12}$GE)$_7$ on the phase behavior of the H_2O/NaCl – *n*-octacosane – hexaethylene glycol monohexadecyl ether ($C_{16}E_6$) system was quantitatively studied by recording a $T(\gamma)$-section at a constant $\phi = 0.500$ and $\varepsilon = 0.001$. The phase diagrams for different polymer contents are shown on the left side of Figure 3. As can be seen, strong efficiency boosting was also found in this microemulsion system, which exhibits a relatively high phase inversion temperature of $\tilde{T} = 66.8$ °C. Upon replacing only a small fraction of $C_{16}E_6$ with Me-P(EO)$_{113}$-*b*-P(C$_{12}$GE)$_7$ ($\delta = 0.050$), the one phase region extends into lower mass fractions of amphiphile, with the $\tilde{X}$ point decreasing from $\tilde{\gamma} = 0.144$ to $\tilde{\gamma} = 0.105$. Further increasing δ to $\delta = 0.100$ shifts the $\tilde{X}$ point to an even lower value of $\tilde{\gamma} = 0.071$. Note that the PIT stays almost constant at $\tilde{T} \approx 66.8$ °C, whereas it slightly increases in the *n*-decane microemulsions with increasing δ. Furthermore, a two-phase coexistence of a lamellar (L_α) and a microemulsion phase can be found at relatively large γ values. This behavior is in agreement with the results obtained for the efficiency boosting in *n*-decane microemulsions with PEP-*b*-PEO copolymers. At low values of δ, a suppression of the liquid crystal formation, e.g. the L_α phase, was observed, while the opposite effect, i.e. a stabilization of liquid crystal phases, was found for $\delta \geq 0.10$.[16,20] Note that the appearance of liquid crystal phases, such as the lamellar phase, is ambiguous. While they are preferentially used e.g. in food applications[67] or as templates for the synthesis of mesoporous silica[68], the formation of these often highly viscous phases is undesirable in applications[69], where microemulsions should be highly dilutable with water or oil.

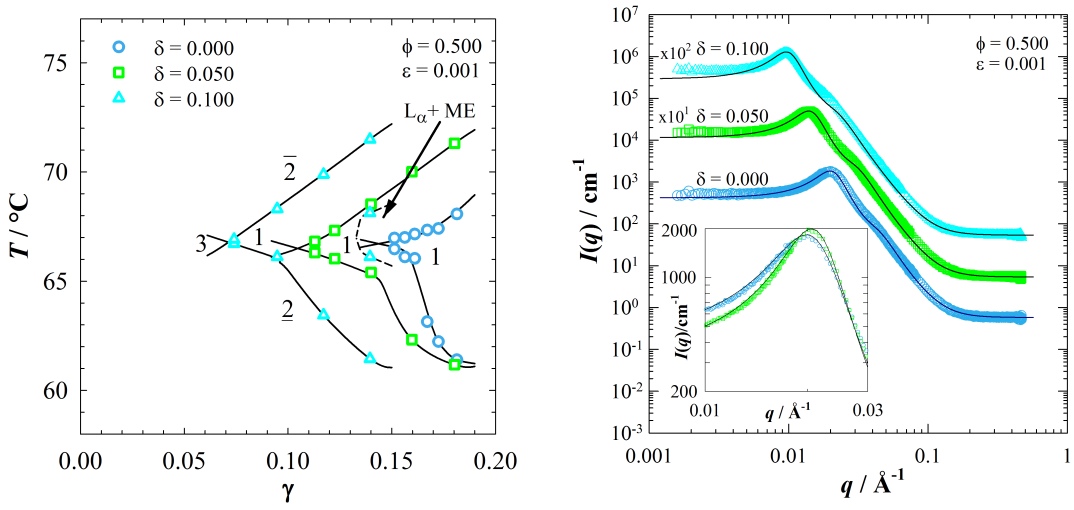

Figure 3: $T(\gamma)$ diagrams of the system H_2O/NaCl – *n*-octacosane – $C_{16}E_6$/Me-P(EO)$_{113}$-*b*-P(C_{12}GE)$_7$, recorded at $\delta = 0$ (○), 0.05 (□) and 0.10 (Δ) with $\phi = 0.500$ and $\varepsilon = 0.001$. The shift of the $\tilde{X}$ points toward lower values of γ upon increasing δ clearly proves the strong efficiency boosting. **Right:** Bulk contrast SANS curves of samples recorded along two pathways: For samples close to the respective $\tilde{X}$ points, the scattering peak shifts to smaller q-values and higher intensities with increasing polymer content. Note that the curves are displaced by a factor of 10. Inset: Samples at $\phi_c = 0.155$ exhibit an increasing sharpness of the scattering peak when increasing δ to $\delta = 0.050$. All curves are analyzed using the *TS* model[53] taking into account double scattering[54,55].

The observed efficiency boosting of Me-P(EO)$_{113}$-*b*-P(C_{12}GE)$_7$ in the *n*-octacosane microemulsion at high temperatures indicates that the copolymer influences the microstructure of the *n*-decane and the *n*-octacosane microemulsion in a similar way. And indeed, as can be seen in Figure 3 (right), the scattering peak of the samples prepared near the $\tilde{X}$ point ($\phi_{C+D} \approx \tilde{\phi}_{C+D} + 0.02$) also strongly shifts to lower q and higher I when δ is increased from $\delta = 0$ to 0.100. Describing the experimental scattering data by eq. (9) (black solid lines) yields an increase of the periodicity d_{TS} by more than a factor two from 307 Å to 634 Å when δ is increased from $\delta = 0$ to 0.100. Interestingly, the amphiphilicity factor, which stays almost constant at $f_a \approx -0.88$, is more negative than the amphiphilicity factor of the *n*-decane microemulsion. Consequently, the value of the

bending rigidity $\varkappa_{SANS} = 0.55\ k_BT$ is larger. Both values indicate a better structural ordering of the $C_{16}E_6$-stabilized *n*-octacosane microemulsion, most probably caused by the longer alkyl chain of the surfactant $C_{16}E_6$ compared to $C_{10}E_4$.

Unfortunately, the influence of Me-P(EO)$_{113}$-*b*-P(C$_{12}$GE)$_7$ on the microemulsion microstructure at $\phi_C = \widetilde{\phi}_{C,0} + 0.02 = 0.155$ was only studied by one sample ($\delta = 0.050$). The inset in Figure 3 (right) shows the respective scattering curve together with the scattering curve of the polymer-free system with a focus on the region around the scattering peak. As observed for the $C_{10}E_4$-stabilized *n*-decane microemulsion, the peak becomes significantly sharper when δ is increased. Accordingly, the analysis of the scattering data provides an increasingly negative f_a value, decreasing from $f_a = -0.88$ to $f_a = -0.92$ and an increase of the amphiphilic film's bending rigidity, which increases from 0.54 k_BT to 0.65 k_BT. For a more detailed analysis of the copolymers influence on the bending rigidity see Figure 8. Note that the composition of the samples, measuring temperatures, as well as values of d_{TS}, ξ_{TS}, f_a and $\varkappa_{SANS}$ are summarized in Table 2.

Table 2: Composition and Measuring Temperature of SANS Samples of Different Microemulsions Boosted by the New Me-P(EO)$_{113}$-*b*-P(C$_{12}$GE)$_7$ Copolymer Together with the Obtained Fit Parameters.[a]

T_{SANS}/ °C	δ	ϕ_C	ϕ_D	ξ_{TS}/Å	d_{TS}/Å	f_a	$\varkappa_{SANS}/k_BT$
D_2O/NaCl – *n*-decane ($C_{10}H_{22}$) – $C_{10}E_4$/Me-P(EO)$_{113}$-*b*-P(C$_{12}$GE)$_7$							
29.0	0	0.144	0	142	272	-0.83	0.44
29.0	0.025	0.125	0.003	178	317	-0.85	0.48
29.0	0.050	0.098	0.005	235	406	-0.86	0.49
29.0	0.075	0.083	0.007	285	484	-0.86	0.50
29.0	0.025	0.143	0.004	174	270	-0.89	0.55

29.0	0.050	0.142	0.007	189	264	-0.91	0.61
29.0	0.075	0.142	0.011	183	255	-0.91	0.61
D_2O/NaCl – *n*-octacosane ($C_{28}H_{58}$) – $C_{16}E_6$/Me-P(EO)$_{113}$-*b*-P(C_{12}GE)$_7$							
65.3	0	0.155	0	195	307	-0.88	0.54
65.3	0.050	0.112	0.006	277	438	-0.88	0.54
65.3	0.100	0.078	0.008	405	634	-0.89	0.55
65.3	0.050	0.154	0.008	228	300	-0.92	0.65
D_2O/NaCl – Sasolwax 5805 – Genapol O 050/080/Me-P(EO)$_{113}$-*b*-P($CO_2C_{12/14}$GE)$_7$							
67.6	0.100	0.114	0.012	241	623	-0.71	0.33

[a]Symmetric microemulsions at constant $\phi = 0.500$ and $\varepsilon = 0.001$ were studied at the temperature T_{SANS} (close to the PIT). Their composition is specified by the copolymer mass fraction δ within the overall amphiphilic mixture, the surfactant and copolymer volume fractions ϕ_C and ϕ_D, respectively. The accuracy of the periodicity d_{TS}, the correlation length ξ_{TS}, the amphiphilicity factor f_a[53–55] and the bending rigidity κ_{SANS}[59] is of the order of ± 3 Å, ± 4 Å, ± 0.015 and ± 0.015 k_BT, respectively.

Role of the Molecular Structure of PEO-*b*-PAlkGE Polymers for the Boosting Effect. So far, the efficiency boosting effect has been studied by means of the copolymer Me-P(EO)$_{113}$-*b*-P(C_{12}GE)$_7$. However, as mentioned before, the outstanding property of PEO-*b*-PAlkGE copolymers is their easy-to-modify molecular structure. Thus, in this section the influence of the AlkGE block size and the alkyl side chain on the polymers' efficiency boosting effect is studied by means of the system H_2O/NaCl – *n*-octacosane –$C_{16}E_6$/Me-P(EO)$_{113}$-*b*-P(C_iGE)$_n$, varying the number *n* of AlkGE repeating units from 3 to 9 and the number *i* of carbon atoms in the alkyl side chain between 12 and 16. On the left side of Figure 4, the phase diagrams recorded at constant $\phi = 0.500$, $\varepsilon = 0.001$ and a polymer mass fraction $\delta = 0.050$ in the overall amphiphile mixture are shown in comparison to the phase diagram of the polymer-free system (○). As can be seen, all of the used Me-P(EO)$_{113}$-*b*-P(C_iGE)$_n$ polymers cause a strong shift of the one phase region and the $\tilde{X}$-point to lower mass

fraction γ of amphiphile. Since all phase boundaries almost lie on top of each other, the influence of the AlkGE block size and the alkyl side chain on the efficiency boosting is shown in the inset by plotting $\tilde{T}$ versus $\tilde{\gamma}$ (the values are compiled in Table S2 of the SI).

The effect of the number n of AlkGE repeating units on the $\tilde{X}$-point is discussed by means of Me-P(EO)$_{113}$-*b*-P(C$_{12}$GE)$_n$ polymers with a dodecyl side chain. By increasing n from 3 to 8, a very systematic shift of $\tilde{\gamma}$ to lower amphiphile mass fractions can be observed. This trend is in agreement with the theoretical prediction of efficiency boosting[21,22,24,26]

$$\ln \tilde{\phi}_{C,i} = \ln \tilde{\phi}^{0}_{C,i} - \Xi\sigma\left(R^2_{ee,w} + R^2_{ee,o}\right), \tag{14}$$

which describes the dependence of the volume fraction $\tilde{\phi}_{C,i}$ of surfactant molecules in the amphiphilic film at the $\tilde{X}$ point as a function of the number density $\sigma = N_D/(S/V)$ of block copolymers within the surfactant membrane and the polymer end-to-end distances $R_{ee,w}$ and $R_{ee,o}$ of the hydrophilic and hydrophobic block, respectively. $\tilde{\phi}^{0}_{C,i}$ is the surfactant volume fraction at the $\tilde{X}$ point of the polymer-free system, Ξ is a pre-factor, $N_D = \phi_D/V_D = \phi_D/(M_D N_A/\varrho_D)$, M_D and ϱ_D are the number density, molar mass and density of the copolymer (D). $S/V = a_C\phi_{C,i}/v_C = a_C\phi_{C,i}/(M_C N_A/\varrho_C)$ is the total specific interface of the amphiphilic film, where M_C and ϱ_C are the molar mass and density of the surfactant (C) molecules and a_C is the area of one surfactant molecule calculated according to reference [48]. Thus, according to eq. (14), an increase of the AlkGE block size should indeed lead to a decrease of the surfactant amount at the $\tilde{X}$ point, which is equivalent to a stronger efficiency boosting.

Considering now the influence of the PEO-*b*-PAlkGE copolymers on the phase inversion temperature $\tilde{T}$, an increase is observed for Me-P(EO)$_{113}$-*b*-P(C$_{12}$GE)$_3$. Comparing the effect of

different copolymers yields an almost systematic decrease of $\tilde{T}$ with an increasing number n of repeating units. These results qualitatively follow the prediction of *Lipowsky*[70], according to which the influence of amphiphilic block copolymers anchored to an interfacial film on its mean curvature H can be described by

$$\Delta H = A \frac{\sigma k_B T (R_{ee,w} - R_{ee,o})}{\varkappa}, \tag{15}$$

where A is a pre-factor. Accordingly, for Me-P(EO)$_{113}$-*b*-P(C$_{12}$GE)$_3$, a shift of $\tilde{T}$ to higher temperatures is expected, as the polymer end-to-end distance $R_{ee,w}$ of the Me-P(EO)$_{113}$ block is larger than the $R_{ee,o}$ of the P(C$_{12}$GE)$_3$ block (see SI, Table S4). Furthermore, the observed decrease of $\tilde{T}$ with an increasing number n of repeating units can be explained by eq. (15). However, based on first SANS measurements of the homopolymer P(C$_{12}$GE)$_{18}$ in *n*-octacosane (see SI, Table S4), this trend is expected to be less pronounced than it was observed. This may indicate that the conformation of the hydrophobic PAlkGE block (as a part of the amphiphilic block copolymer) in the microemulsions is different from the homopolymer's conformation in the pure solvent *n*-octacosane.

Looking at the influence of the number i of carbon atoms in the side chain of the AlkGE unit, no systematic trend on the location of the $\tilde{X}$ point is found. Within the experimental error, the copolymers with a dodecyl (i = 12) and hexadecyl (i = 16) side chain show similar values of $\tilde{\gamma}$ and $\tilde{T}$.

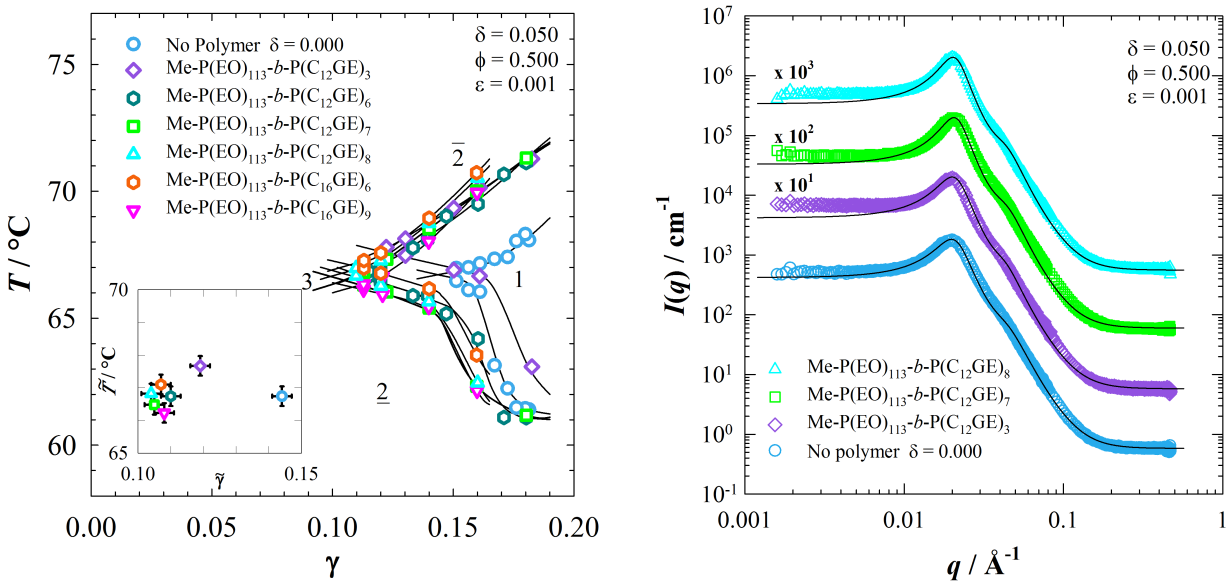

Figure 4. Left: $T(\gamma)$ diagrams of the systems H_2O/NaCl – *n*-octacosane – $C_{16}E_6$/Me-P(EO)$_{113}$-*b*-P(C_iGE)$_n$, recorded at $\phi = 0.500$, $\varepsilon = 0.001$ and $\delta = 0.050$ for the polymers $i = 12$ and $n = 3, 6, 7, 8$ as well as $i = 16$ and $n = 6, 9$ together with the polymer-free system ($\delta = 0$, ○). Inset: $\tilde{X}$ points ($\tilde{T}(\tilde{\gamma})$) of the studied systems to visualize the effect of n and i on the efficiency boosting and the PIT. **Right:** Bulk contrast SANS curves of the polymer-free sample and samples containing different copolymers ($\delta = 0.050$) recorded at $\phi_c = 0.155$. All curves are analyzed using the *TS* model[53] taking into account double scattering[54,55].

The influence of the number n of AlkGE repeating units on the microstructure of D_2O/NaCl – *n*-octacosane – $C_{16}E_6$/Me-P(EO)$_{113}$-*b*-P(C_iGE)$_n$ microemulsions was studied by bulk contrast SANS experiments performed at $\phi_c = \tilde{\phi}_{C,0} + 0.02 = 0.155$. Figure 4 (right) shows the respective scattering curves ($\delta = 0.050$) together with the scattering curve of the polymer-free system ($\delta = 0$). As observed for the microemulsions studied so far, at constant ϕ_c, the sharpness of the peak, which stays almost at the same q_{max}, increases upon addition of the PEO-*b*-PAlkGE copolymers. In agreement with the different degree of efficiency boosting found in the phase behavior studies, the value of the amphiphilicity factor becomes only slightly more negative when adding Me-P(EO)$_{113}$-*b*-P(C_iGE)$_3$, i.e. with the factor decreasing only slightly from $f_a = -0.88$ to $f_a = -0.89$, while for the

copolymers with $n = 7$ and 8, a value of $f_a = -0.92$ is found. Accordingly, the value of the amphiphilic film's bending rigidity increases from 0.54 k_BT for the polymer-free system to 0.57, 0.65 and 0.64 k_BT for the Me-P(EO)$_{113}$-*b*-P(C$_i$GE)$_n$-doped systems with n = 3, 7 and 8, respectively. Note that the composition of the samples, measuring temperatures, as well as values of d_{TS}, ξ_{TS}, f_a and $\varkappa_{SANS}$ are summarized in Table 3.

Table 3: Composition and Measuring Temperature of SANS Samples of the D_2O/NaCl – *n*-octacosane – $C_{16}E_6$ Microemulsions Boosted by Different Me-P(EO)$_{113}$-*b*-P(C$_{12}$GE)$_n$ Copolymers Together with the Obtained Fit Parameters.[a]

n	T_{SANS}/°C	δ	ϕ_C	ϕ_D	ξ_{TS}/Å	d_{TS}/Å	f_a	$\varkappa_{SANS}/k_BT$
	65.3	0	0.155	0	195	307	-0.88	0.54
3	67.6	0.050	0.154	0.008	203	305	-0.89	0.57
7	65.3	0.050	0.154	0.008	228	300	-0.92	0.65
8	65.3	0.050	0.154	0.008	230	304	-0.92	0.64

[a]Symmetric microemulsions at constant $\phi = 0.500$ and $\varepsilon = 0.001$ were studied at the temperature T_{SANS} (close to the PIT). Their composition is specified by the copolymer mass fraction δ within the overall amphiphilic mixture, the surfactant and copolymer volume fractions ϕ_C and ϕ_D, respectively. The accuracy of the periodicity d_{TS}, the correlation length ξ_{TS}, the amphiphilicity factor f_a[53–55] and the bending rigidity κ_{SANS}[59] is of the order of ± 3 Å, ± 4 Å, ± 0.015 and ± 0.015 k_BT, respectively.

Efficiency Boosting of "Carbonated" PEO-*b*-PCO$_2$AlkGE Polymers in H_2O/NaCl – *n*-Octacosane – $C_{16}E_6$. In order to bring the PEO-*b*-PAlkGE diblock copolymers to application, technical-grade Me-P(EO)$_{113}$-*b*-P(CO$_2$C$_{12/14}$GE)$_n$ polycarbonate derivatives were synthesized and their influence on the phase behavior of the H_2O/NaCl – *n*-octacosane – $C_{16}E_6$ system was studied at $\phi = 0.500$, $\varepsilon = 0.001$ and $\delta = 0.050$. To distinguish between the effects of the additional

carbonate group and the technical-grade $C_{12/14}$ side chain in the AlkGE repeating units, "carbonated" Me-P(EO)$_{113}$-*b*-P(CO_2C_{12}GE)$_n$ copolymers with a defined C_{12} side chain were synthesized as well.

In Figure 5 (left), the effects of Me-P(EO)$_{113}$-*b*-P(C_{12}GE)$_3$, Me-P(EO)$_{113}$-*b*-P(CO_2C_{12}GE)$_3$ and Me-P(EO)$_{113}$-*b*-P($CO_2C_{12/14}$GE)$_3$ on the phase behavior of the H_2O/NaCl – *n*-octacosane – $C_{16}E_6$ system are compared in form of the well-known $T(\gamma)$-section. As can be seen, all three copolymers cause a shift of the one phase region and the $\tilde{X}$-point to lower mass fractions γ of amphiphile. Interestingly, the copolymer Me-P(EO)$_{113}$-*b*-P(CO_2C_{12}GE)$_3$ enables the strongest efficiency boosting, which might be related to the somewhat larger PAlkGE block. Consequently, the technical-grade nature of the $C_{12/14}$ side chain must be the reason for the weaker efficiency boosting obtained for the technical-grade P(EO)$_{113}$-*b*-P($CO_2C_{12/14}$GE)$_3$ copolymer.

On the right side of Figure 5, the effect of the different PAlkGE blocks on the phase behavior of the H_2O/NaCl – *n*-octacosane – $C_{16}E_6$ system is shown by means of Me-P(EO)$_{113}$-*b*-P(C_{12}GE)$_7$, Me-P(EO)$_{113}$-*b*-P(CO_2C_{12}GE)$_9$ and Me-P(EO)$_{113}$-*b*-P($CO_2C_{12/14}$GE)$_7$. Since these copolymers possess a larger PAlkGE block, a stronger decrease of $\tilde{\gamma}$, i.e. a stronger efficiency boosting than for the $n = 3$ copolymers is enabled. Comparing the boosting effects among these larger copolymers, the smallest $\tilde{\gamma}$ value is found for Me-P(EO)$_{113}$-*b*-P(CO_2C_{12}GE)$_9$, since it possesses the largest PAlkGE block (eq. (14)). A slightly larger $\tilde{\gamma}$ value, i.e. weaker efficiency boosting, is found for Me-(PEO)$_{113}$-*b*-P(C_{12}GE)$_7$. Regarding a technical application, it is promising that the efficiency boosting effect of the technical-grade Me-P(EO)$_{113}$-*b*-P($CO_2C_{12/14}$GE)$_7$ copolymer is only slightly weaker than observed with the "pure" Me-P(EO)$_{113}$-*b*-P(C_{12}GE)$_7$. For a more detailed comparison of the efficiency boosting effects of the different polymers, the reader is referred to Table S2 in the SI, where all $\tilde{\gamma}$ and $\tilde{T}$ values are compiled.

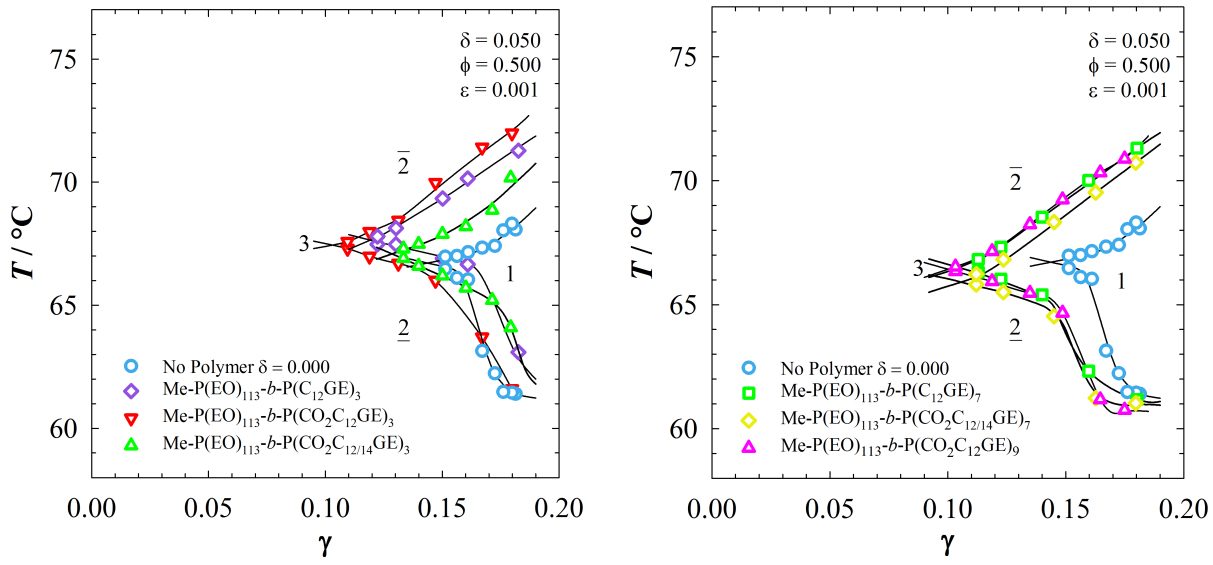

Figure 5: $T(\gamma)$ diagrams of the systems H_2O/NaCl – *n*-octacosane – $C_{16}E_6$/PEO-*b*-PAlkGE recorded at $\phi = 0.500$ and $\varepsilon = 0.001$ for $\delta = 0$ (polymer-free system) and $\delta = 0.050$ with a varying molecular structure of the hydrophobic PAlkGE block, ranging from $P(C_{12}GE)_n$ to the carbonated $P(CO_2C_{12}GE)_n$ to the technical-grade $P(CO_2C_{12/14}GE)_n$. Note that all copolymers with $n = 3$ (left) and $n = 7$ and 9 (right), including the technical-grade ones, cause a considerable efficiency boosting effect.

Efficiency Boosting of Me-P(EO)$_{113}$-*b*-P(CO$_2$C$_{12/14}$GE)$_7$ in H$_2$O/NaCl – Sasolwax 5805 – Genapol O 050/O 080. As already mentioned in the *Introduction*, the boosting effect of amphiphilic diblock copolymers so far has only scarcely found its way into applications[39], mainly due to a difficult and expensive large-scale polymer synthesis[17] as well as the weakening of the boosting effect with increasing dispersity of the polymer blocks, especially in the case of remaining homopolymers. The results obtained in this study, especially those shown in Figure 5 (right), strongly indicate that the technical-grade Me-P(EO)$_m$-*b*-P(CO$_2$C$_{12/14}$GE)$_n$ copolymers, which can be synthesized at low cost and on large scale with a yield of the order of 60 % (Table S1), are at least capable of strongly increasing the efficiency of the monodisperse nonionic surfactant $C_{16}E_6$ to solubilize water and *n*-octacosane.

In a further step towards an application of the efficiency boosting effect, we studied whether the technical-grade Me-P(EO)$_m$-*b*-P(CO$_2$C$_{12/14}$GE)$_n$ copolymers are able to increase the efficiency of technical-grade (polydisperse) *n*-alkyl polyglycol ether surfactants to solubilize the technical-grade Sasolwax 5805, which is a technical-grade mixture of linear and branched alkanes ranging from C_{19} to C_{46} with an average carbon number of 30.5[44]. Ethoxylated oleyl alcohols of the Genapol O series, more precisely Genapol O 050 and Genapol O 080 (mean ethoxylation degrees of 5 and 8, respectively), were chosen as technical-grade nonionic surfactants.

Based on a very recent study of Sasolwax 5805-containing microemulsions stabilized by technical-grade surfactants of the Genapol type[44], we formulated a symmetric ($\phi = 0.500$) microemulsion of the type H$_2$O/NaCl ($\varepsilon = 0.001$) – Sasolwax 5805 – Genapol O 050/O 080, staring with a 1:1 (*m*/*m*) mixture of the two Genapol surfactants. The phase behavior of this polymer-free technical grade microemulsion system is shown in Figure 6 in form of a $T(\gamma)$ section. As can be seen, the phase boundaries are strongly distorted because the hydrophobic homologues of the technical-grade surfactants are extracted from the amphiphilic film into the oil-rich domains and the oil excess phase. As a consequence, the amphiphilic film becomes increasingly hydrophilic with decreasing γ, shifting not only the phase boundaries but also the hydrophilic lipophilic balance (*HLB*) to higher temperatures.[71] Thereby, the $\tilde{X}$ point is located at $\tilde{\gamma} = 0.155$ and $\tilde{T} \approx 73.7$ °C. Note that an extended two-phase coexistence of a lamellar (L_α) and a microemulsion phase can be found at low temperatures.

By replacing 10wt% of the Genapol O 050/O 080 (1:1) mixture with the technical-grade Me-P(EO)$_{113}$-*b*-P(CO$_2$C$_{12/14}$GE)$_7$ copolymer ($\delta = 0.100$, Δ), the $\tilde{X}$-point is shifted to $\tilde{\gamma} = 0.127$ and $\tilde{T} = 79.6$ °C along the upwards tilted *HLB*-line. Thus, the technical-grade Me-P(EO)$_m$-*b*-

P($CO_2C_{12/14}GE)_n$ copolymers indeed enable efficiency boosting. A further increase in efficiency is obtained by increasing the fraction of the hydrophobic Genapol O 050 in the surfactant mixture to 75wt%, leaving the copolymer content constant at $\delta = 0.100$. Accordingly, the phase boundaries are shifted to lower temperatures and surfactant mass fractions, yielding an $\tilde{X}$-point located at $\tilde{\gamma} = 0.091$ and $\tilde{T} = 74.6$ °C. Furthermore, the phase boundaries are even more distorted because the fraction of the hydrophobic homologues of the technical-grade surfactants extracted from the amphiphilic film with respect to the overall surfactant mass fraction strongly increases with decreasing γ. The results clearly prove that this new type of technical-grade amphiphilic diblock copolymers allows for the formulation of efficient microemulsions, even when a mixture of long-chain oils has to be solubilized. From our results, an even stronger efficiency boosting can be predicted upon further increasing the fraction δ of the technical-grade Me-P($EO)_m$-*b*-P($CO_2C_{12/14}GE)_n$ copolymers in the amphiphile mixture. Note that the $\tilde{T}$ and $\tilde{\gamma}$ values are listed in Table S2 in the SI.

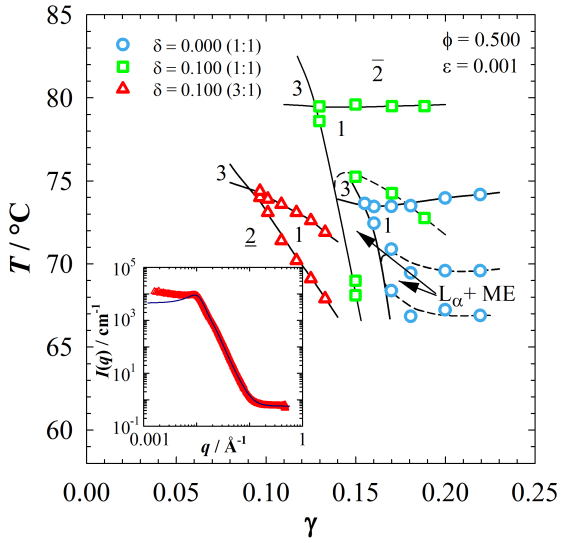

Figure 6. $T(\gamma)$ diagrams of the technical-grade microemulsion system H_2O/NaCl – Sasolwax 5805 – Genapol O 050/O 080/Me-P($EO)_{113}$-*b*-P($CO_2C_{12/14}GE)_7$, recorded at $\phi = 0.500$, $\varepsilon = 0.001$, $\delta = 0.100$ and different surfactant ratios; shown together with the polymer-free system ($\delta = 0$, ○). Two different mixtures

of the Genapol surfactants were used, i.e. 1:1 (□) or 3:1 (Δ) (O 050 : O 080, *m*/*m*). Excitingly, the technical-grade Me-P(EO)$_{113}$-*b*-P(CO$_2$C$_{12/14}$GE)$_7$ copolymer also causes an efficiency boosting in this technical-grade microemulsion system. L_α + ME denotes the coexistence of a lamellar phase (L_α) with a microemulsion phase (ME). Inset: Bulk contrast SANS curve recorded near the $\tilde{X}$ point of the system D$_2$O/NaCl – Sasolwax 5805 – Genapol O 050/O 080/Me-P(EO)$_{113}$-*b*-P(CO$_2$C$_{12/14}$GE)$_7$ with $\delta = 0.100$ and a 3:1 (*m*/*m*) mixture of Genapol O 050 : O 080. The curve was analyzed using the *TS* model[53] taking into account double scattering[54,55].

In order to study the microstructure of this efficiency-boosted technical-grade microemulsion, one bulk contrast SANS curve was recorded for the system D$_2$O/NaCl – *n*-octacosane – Genapol O 050/O 080(3:1)/Me-P(EO)$_{113}$-*b*-P(C$_{12}$GE)$_7$ with $\phi = 0.500$, $\varepsilon = 0.001$ and $\delta = 0.100$ near its $\tilde{X}$ point, i.e. at a surfactant volume fraction of $\phi_c = 0.114$ and a temperature of $T = 67.6$ °C. Note that for D$_2$O, the phase boundaries are about 2 K lower than with H$_2$O.[48] The obtained SANS curve is shown in the inset of Figure 6. Qualitatively, the curve resembles the typical shape found for bicontinuous microemulsions. However, two differences with respect to the scattering curves shown so far (Figure 2 to Figure 4) can be observed. On the one hand, the scattering peak is less pronounced, indicating a less ordered structure. On the other hand, an increase of the scattering intensity at low *q* points to the existence of a structure with a larger length scale. As we can exclude a demixing of the sample during the experiment (by checking before and after the experiment), we presume that the SANS curve was not recorded at the *HLB* but close to the lower phase boundary, where cylindrical structures are expected.

The fit of the experimental scattering data by eq. (9) is shown as a black solid line. As can be seen, it describes almost the entire scattering curve except for the low *q*-regime almost quantitatively. A relatively large value of the periodicity of the structure $d_{TS} = 623$ Å is found. In agreement with the qualitative discussion of the data, a less negative value of the amphiphilicity

factor $f_a = -0.71$ and a smaller bending rigidity $\varkappa_{SANS} = 0.33$ are found, indicating a less ordered structure. The sample composition, measuring temperature, d_{TS}, ξ_{TS}, f_a and $\varkappa_{SANS}$ are summarized in Table 2.

Scaling of the PEO-b-P(AlkGE) Efficiency Boosting: A Synopsis. The results obtained so far clearly show that the new amphiphilic poly(ethylene oxide) - poly(alkyl glycidyl ether) copolymers boost the efficiency of microemulsion systems, containing model type oils like *n*-decane, long-chain oils as *n*-octacosane, or even technical-grade waxes. Similar to the boosting of *n*-decane microemulsions by amphiphilic PEP-*b*-PEO copolymers, which was found 20 years ago [16,17,72], the strong efficiency increase facilitated by the new type of PEO-*b*-PAlkGE copolymers is expected to be related to the anchoring of the copolymers in the amphiphilic film. *Gompper et al.* were able to explain the enormous boosting effect in terms of the bending elastic energy[23] of fluctuating polymer-decorated surfactant membranes[21,22]. To obtain an impressive scaling of the efficiency boosting effect, they combined the effect of the membrane-anchored copolymers onto the curvature and the bending moduli $\varkappa$ and $\bar{\kappa}$ predicted by *Lipowsky et al.*[24,25,52,70] with the model of thermally fluctuating amphiphilic films, for which the bicontinuous microemulsion becomes unstable when the renormalized saddle splay modulus $\bar{\varkappa}(\xi)$ approaches zero at the $\tilde{X}$ point[62-64]. This scaling relation (eq. (14)), whose detailed derivation can be found elsewhere[21,22], allows to predict the increase of the efficiency (characterized by the volume fraction $\tilde{\phi}_{C,i}$ of surfactant molecules in the amphiphilic film at the $\tilde{X}$ point) as a function of the number density σ of block copolymers in the membrane and the end-to-end distances $R_{ee,w}$ and $R_{ee,o}$ of the hydrophilic and hydrophobic block, respectively.

By using this scaling description, the efficiency boosting effect of the new type of PEO-*b*-PAlkGE diblock copolymers in the different microemulsion systems can not only be analyzed on a quantitative level but also allows for a comparison between the respective degrees of efficiency boosting of PEO-*b*-PAlkGE and PEP-*b*-PEO copolymers. However, in order to perform the analysis according to eq. (14), not only $\widetilde{\phi}_{C,i}$ and $\widetilde{\phi}^{0}_{C,i}$ must be calculated using eq. (6) considering the monomeric solubilities of the surfactants in the respective oil, but $\sigma = N_D/(S/V)$, $R_{ee,w}$ and $R_{ee,o}$ are also required. Although the R_g value and therefore the $R_{ee,w}$ value (calculated via $R_{ee} = 6^{1/2} R_g$) of a larger PEO block (41500 g mol^{-1}) in D_2O can be found in literature[73], we performed additional SANS experiments both at T = 25 °C and T = 60 °C to study the temperature dependence of $R_{ee,w}$ of our PEO block, which possesses a molecular weight of M_w = 5290 g mol^{-1}. Furthermore, a few SANS experiments were performed on PAlkGE homopolymers in *n*-decane and *n*-octacosane at $T \approx 25$ °C and T = 67 °C to determine $R_{ee,o}$. The scattering data (Figure S24) of PEO were analyzed by using a two-correlation-length model taking into account the scattering contribution of occurring clusters at low q[73–75], while the data for the PAlkGE homopolymers were described by the *Guinier* model[76]. Interestingly, within the measuring error no dependence of the end-to-end distances on temperature and solvent was found (see values of $R_{ee,o}$ and $R_{ee,w}$ in Table S4). The $R_{ee,o}$ values of the PAlkGE blocks containing 3 to 9 AlkGE repeating units were obtained considering the dependence of end-to-end distances $R_{ee,o}$ on the molecular weight, which was similarly found for PEO polymers by *Kawaguchi et al.*[77], i.e. $R_{ee,o} = 2.2707 M_w^{0.314}$ (Figure S25).

The determination of $\widetilde{\phi}_{C,i}$,$\widetilde{\phi}^{0}_{C,i}$, σ, $R_{ee,w}$ and $R_{ee,o}$ allows to analyze the efficiency boosting effect by a scaling representation via plotting $\ln(\widetilde{\phi}_{C,i}/\widetilde{\phi}^{0}_{C,i})$ versus the surface coverage of the membrane by the respective block copolymers $\sigma(R_{ee,w}^2 + R_{ee,o}^2)$. In a first step, in Figure 7 the efficiency boosting

of the new type of PEO-*b*-PAlkGE and the literature-known PEP-*b*-PEO[72] copolymers is compared by means of the model microemulsion H_2O/NaCl – *n*-decane – $C_{10}E_4$. The plot contains data from the Me-P(EO)$_{113}$-*b*-P(C_iGE)$_n$ copolymers with $i = 12$ and $n = 3$, 6, 7 and 8. As can be seen, for the model *n*-decane microemulsion, the data of PEO-*b*-PAlkGE (□) boosted systems fall onto a single straight line, which confirms the scaling relation (eq. (14)) and proves that the copolymers indeed modify the saddle-splay modulus of the surfactant membrane. Interestingly, the data of PEO-*b*-PAlkGE (□) and PEP-*b*-PEO (○)[72] copolymers fall almost on top of each other, yielding almost identical slopes of Ξ(PEO-*b*-PAlkGE) = 1.54 ± 0.08 and Ξ(PEP-*b*-PEO) = 1.51 ± 0.06[72], respectively. The slopes are roughly twice as large as the theoretical estimate for ideal chains (Ξ(ideal chains) = π/5) due to the fact that self-avoiding chains may have a more pronounced effect on the saddle-splay modulus than ideal chains.[21,78,79]

In the next step, the scaling relation is applied to the efficiency boosting of the new PEO-*b*-PAlkGE in the H_2O/NaCl – *n*-octacosane – $C_{16}E_6$ microemulsion (Figure 7: ◊, Δ). The figure contains data from Me-P(EO)$_{113}$-*b*-P(C_iGE)$_n$ copolymers with $i = 12$, $i = 16$ and $n = 3$, 6, 7, 8, 9 as well as results obtained for Me-P(EO)$_{113}$-*b*-P(CO_2C_iGE)$_n$ with $i = 12$, 12/14 and $n = 3$, 7, 9. As can be seen, the data (with the exception of most of the $n = 3$ (Δ) copolymer data), fall onto a single straight line, confirming that the scaling relation (eq. (14)) also applies for *n*-octacosane microemulsions formed at high temperatures of around 60 °C. However, the slope of Ξ(PEO-*b*-PAlkGE) = 1.09 ± 0.05 is somewhat smaller than the one found for the *n*-decane microemulsions and may indicate that polymers at higher temperatures come closer to the behavior of ideal chains. Furthermore, while the data points of the technical-grade Me-P(EO)$_{113}$-*b*-P($CO_2C_{12/14}$GE)$_7$ follow this scaling relation, most of the $n = 3$ (Δ) copolymer data do not fall on the line. A possible reason might be the rather small size of the PAlkGE block, which decreases the tendency of these

polymers to tether to the surfactant membrane, when *n*-octacosane is used as the hydrophobic solvent at high temperatures. Note that for the *n*-decane microemulsion, efficiency boosting of the Me-P(EO)$_{113}$-*b*-P(C$_{12}$GE)$_3$ obeys the general trend.

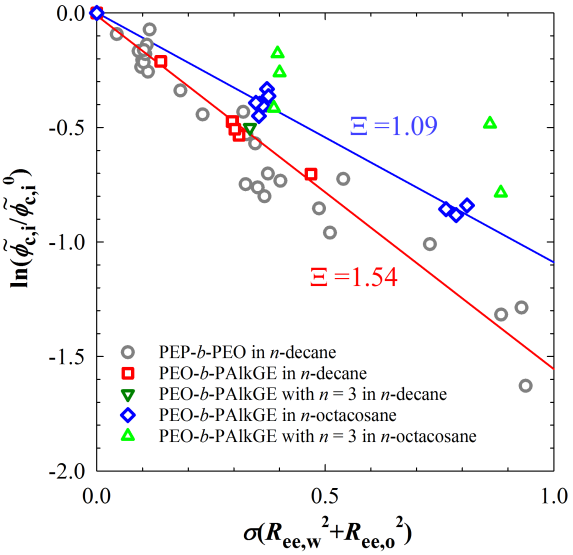

Figure 7. Normalized logarithmic volume fraction of surfactant in the interface at the $\tilde{X}$ point $\ln(\tilde{\phi}_{C,i}/\tilde{\phi}^{0}_{C,i})$, plotted against the polymer coverage of the membrane $\sigma(R_{ee,w}^2 + R_{ee,o}^2)$, for the systems H$_2$O/NaCl – *n*-decane – C$_{10}E_4$/PEO-*b*-PAlkGE (□) and H$_2$O/NaCl – *n*-octacosane – C$_{16}$E$_6$/PEO-*b*-PAlkGE (◊). The plot contains data from the Me-P(EO)$_{113}$-*b*-P(C$_i$GE)$_n$ copolymers with $i = 12$ and $n = 3$, 6, 7, 8 as well as the polymers with $i = 16$ and $n = 6$, 9. Additionally, data for the Me-P(EO)$_{113}$-*b*-P(CO$_2$C$_i$GE)$_n$ copolymers with $i = 12$ and $n = 3$, 9 as well as $i = 12/14$ and $n = 3$, 7 are included. Note that the results obtained for the H$_2$O/NaCl – *n*-octacosane – C$_{16}$E$_6$ systems with the $n = 3$ (△) polymers are shown, but were not considered in the linear regression (see text). Literature data obtained by *Jakobs* for the system H$_2$O – *n*-decane – C$_{10}$E$_4$/PEO$_m$-*b*-PEP$_n$ with different PEO-*b*-PEP copolymers[72] are shown for comparison (○).

Influence of the PEO-b-P(AlkGE)s on the Bending Rigidity κ. The analysis of the SANS data was performed with the model of random interfaces derived by *Safran et al.*[59,80,81] to determine the bending rigidity κ_{SANS}. Due to the reasons given above, we decided to not consider recent indications[60,61] that κ_{SANS} is rather a mixture of the bending rigidity and the saddle splay modulus $\bar{\kappa}$.

Taking into consideration the stiffening of the membrane by anchoring of the copolymers in the amphiphilic film[24,25,52,70] as well as its softening through thermal fluctuations[62–64], $\varkappa_{SANS}$ is given by

$$\varkappa_{SANS} = \varkappa_0 + \frac{k_B T}{12}\left(1 + \frac{\pi}{2}\right)\sigma\left(R_{ee,w}^2 + R_{ee,o}^2\right) - \frac{3\,k_B T}{4\pi}\ln\frac{d_{TS}a}{2v_c}, \tag{16}$$

with $\varkappa_0$ being the pure bending rigidity, $d_{TS}/2$ the length scale of the respective systems, $v_c = M_c N_a/\varrho_c$ the molecular volume of the surfactant molecule and a_c being the area of one surfactant molecule calculated according to reference[48] ($C_{10}E_4$: a_c = 54.1 Å^2 and v_c = 579.0 Å^3; $C_{16}E_6$: a_c = 66.5 Å^2 and v_c = 874.4 Å^3).

In Figure 8, the obtained $\varkappa_{SANS}$ values are plotted as a function of the polymeric coverage $\sigma(R_{ee,w}^2 + R_{ee,o}^2)$ of the amphiphilic film for the two systems D_2O/NaCl – *n*-decane – $C_{10}E_4$/Me-P(EO)$_{113}$-*b*-P(C_{12}GE)$_7$ (left) and D_2O/NaCl – *n*-octacosane – $C_{16}E_6$/Me-P(EO)$_{113}$-*b*-P(C_{12}GE)$_7$ (right). Considering at first the values obtained from the analysis of the SANS measurements performed near the respective $\tilde{X}$ points of the systems at $\phi_{c+D} \approx \tilde{\phi}_{C+D} + 0.02$ (○), $\varkappa_{SANS}$ turned out to be nearly constant. Being close to the stability limit of bicontinuous microemulsions, separating into 3 phases at the $\gamma < \tilde{\gamma}$, the effect of membrane stiffening via copolymer anchoring and membrane softening through thermal fluctuations compensate each other. Note that a similar compensation membrane stiffening and softening was already observed by *Jakobs* for the system D_2O – *n*-octane – C_8E_3/PEP$_5$-*b*-PEO$_5$.[72]

Analyzing the second set of experiments (□), which were conducted at a constant surfactant volume fraction $\phi_c = \tilde{\phi}_{C,0} + 0.02$ = const. close to the surfactant volume fraction $\tilde{\phi}_{C,0}$ at the $\tilde{X}$ point of the polymer-free system, a linear increase of $\varkappa_{SANS}$ with increasing polymer decoration of the membrane ($\sigma(R_{ee,w}^2 + R_{ee,o}^2)$) is found. Due to the fact that ϕ_c and therewith the length scale $d_{TS}/2$

of the structure remains constant, the thermal fluctuations provide a constant contribution to $\varkappa_{SANS}$ (eq. (16)), which amounts to 0.61 k_BT and 0.59 k_BT for the *n*-decane and *n*-octacosane system, respectively. Thus, the increase of $\varkappa_{SANS}$ can only be attributed to the increasing polymer decoration. Assuming a linear behavior, slopes of 0.38 and 0.32 were obtained, which - in close agreement with Ξ found for the scaling of the efficiency - are larger than the theoretically expected value for ideal chains of $(1 + \pi/2)/12 = 0.214$. Last but not least, the values of the intercept, i.e. 0.47 ± 0.03 k_BT and 0.54 ± 0.04 k_BT can be used for the determination of the bare bending rigidity $\varkappa_0$, yielding $\varkappa_0(C_{10}E_4/n\text{-decane}) = 1.08 \pm 0.05\ k_BT$ and $\varkappa_0(C_{16}E_6/n\text{-octacosane}) = 1.13 \pm 0.06\ k_BT$ at $T = 302.2$ K and $T = 338.5$ K, respectively. Thus, the pure $C_{10}E_4$ membrane in the microemulsion containing *n*-decane is slightly less rigid compared to the pure $C_{16}E_6$ membrane in the *n*-octacosane microemulsion.

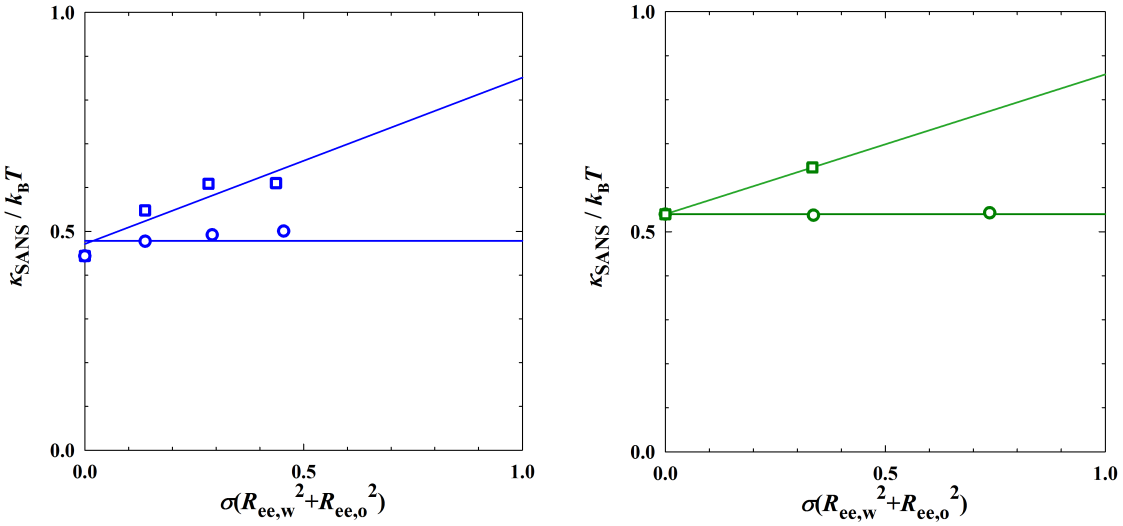

Figure 8. Bending rigidity $\varkappa_{SANS}$ determined by the analysis of the SANS curves according to the model of random interfaces[59], plotted against the polymer coverage of the membrane $\sigma(R_{ee,w}^2 + R_{ee,o}^2)$ for the systems D_2O/NaCl – *n*-decane – $C_{10}E_4$/Me-P(EO)$_{113}$-*b*-P(C_{12}GE)$_7$ (left) and D_2O/NaCl – *n*-octacosane – $C_{16}E_6$/Me-P(EO)$_{113}$-*b*-P(C_{12}GE)$_7$ (right) at constant $\phi = 0.500$ and $\varepsilon = 0.001$. Experiments were performed along two pathways varying δ: (○) close to the respective $\tilde{X}$ points and (□) at constant surfactant volume fraction, i.e. $\phi_c = 0.144$ (left) and $\phi_c = 0.155$ (right).

CONCLUSION

In this study, poly(ethylene oxide)-poly(alkyl glycidyl ether)s (PEO-*b*-PAlkGE) and their "carbonated" poly(ethylene oxide)-poly(carbonate alkyl glycidyl ether) analogs were synthesized as promising efficiency boosters for microemulsions. These new types of amphiphilic block copolymers excel in their facile synthesis, which can be performed at low cost and on a large scale, as well as their easy-to-modify molecular structure. Systematic phase behavior studies revealed that the Me-P(EO)$_{113}$-*b*-P(C$_i$GE)$_n$ copolymers not only strongly increase the efficiency of the medium-chain nonionic surfactant $C_{10}E_4$ to solubilize water and *n*-decane at room temperature, but also boost the efficiency of the longer-chain surfactant $C_{16}E_6$ to stabilize water/*n*-octacosane microemulsions at elevated temperatures. The influence of the molecular structure on the boosting effect was studied by increasing the number *n* of C$_i$GE repeating units from 3 to 9 and by varying the number *i* of carbon atoms in the alkyl side chain between 12 and 16. The observed very systematic increase in efficiency is in agreement with theoretical predictions.[21,22,24,29]

The "carbonated" Me-P(EO)$_{113}$-*b*-P(CO$_2$C$_{12}$GE)$_n$ copolymers and their technical-grade Me-P(EO)$_{113}$-*b*-P(CO$_2$C$_{12/14}$GE)$_n$ derivatives were also found to enable a strong efficiency boosting. By means of the H_2O/NaCl – *n*-octacosane – $C_{16}E_6$ system, we were able to show that the boosting efficiency of the technical-grade Me-P(EO)$_{113}$-*b*-P(CO$_2$C$_{12/14}$GE)$_7$ is only slightly weaker than that of the "pure" Me-P(EO)$_{113}$-*b*-P(C$_{12}$GE)$_7$. In a further step towards application, we added the technical-grade Me-P(EO)$_m$-*b*-P(CO$_2$C$_{12/14}$GE)$_7$ copolymer to a technical-grade microemulsion consisting of brine, Sasolwax 5805 (linear and branched alkanes with an average carbon number of 30.5[44]) and a mixture of technical-grade nonionic surfactants (Genapol O 050/ O 080). We emphasize that our data show that the mass fraction of amphiphiles needed to stabilize this technical-grade

microemulsion can be strongly reduced from 15.5 wt% to 9.1 wt% when only 10wt% of an optimized surfactant mixture are replaced with the Me-P(EO)$_{113}$-*b*-P(CO$_2$C$_{12/14}$GE)$_7$ copolymer. This result could be of interest for industrial applications where reduced surfactant needs would have significant economic and ecological implications.

The scaling description of the efficiency boosting[21,22,24,29] was then used to analyze the boosting of the new type of PEO-*b*-PAlkGE diblock copolymers on a quantitative level and to compare the respective degrees of efficiency boosting of PEO-*b*-PAlkGE and PEP-*b*-PEO copolymers. We found that for *n*-decane microemulsions, the boosting of PEO-*b*-PAlkGE and PEP-*b*-PEO polymers can be scaled on top of each other, when the efficiency is plotted semi-logarithmically versus the polymeric coverage of the amphiphilic film. Interestingly, a somewhat different scaling behavior was observed for *n*-octacosane microemulsions stable at elevated temperatures, suggesting that the polymers show less self-avoidance and rather behave as almost ideal chains.

The influence of the new PEO-*b*-PAlkGE copolymers on the microstructure of the D$_2$O/NaCl – *n*-decane – C$_{10}$E$_4$ systems was studied by systematic SANS experiments performed close to the $\tilde{X}$ point of the boosted microemulsions and at a constant surfactant volume fraction close to the $\tilde{X}$ point of the polymer-free system. Particularly the SANS curves obtained from the latter experiments indicate that the copolymers induce a considerably better ordering of the bicontinuous microstructure. To study the influence of the PEO-*b*-PAlkGE on the membrane's bending rigidity $\varkappa_{SANS,}$ the SANS data were analyzed using the model of random interfaces derived by *Safran et al.*.[59,80,81] We found that the bending rigidity $\varkappa_{SANS}$ remains almost constant for boosted microemulsion prepared near their $\tilde{X}$ point. Being close to the stability limit of bicontinuous microemulsions, the effects of membrane stiffening via copolymer anchoring and membrane softening through thermal

fluctuations compensate each other. For the boosted microemulsions studied at a constant surfactant volume fraction close to the $\tilde{X}$ point of the polymer-free system, however, an increase of $\varkappa_{SANS}$ upon the polymeric coverage of the amphiphilic film is found.

By determining the bare bending rigidities $\varkappa_0$, it was found that the pure $C_{10}E_4$ membrane in the *n*-decane microemulsion ($\varkappa_0(C_{10}E_4/n\text{-decane}) = 1.08\ k_BT$ at $T = 302.2$ K) is slightly less rigid compared to the pure $C_{16}E_6$ membrane in the *n*-octacosane microemulsion ($\varkappa_0(C_{16}E_6/n\text{-octacosane}) = 1.13\ k_BT$ at $T = 338.5$ K).

ASSOCIATED CONTENT

Supporting Information.

Synthesis of the amphiphilic diblock polycarbonates, overview of synthesized homopolymers and diblock copolymers, SEC measurements of the synthesized homopolymers, ^{1}H NMR spectra as well as DSC measurements of the synthesized diblock copolymers, tabular overview of the phase behavior and SANS results, SANS curves of homopolymers and their analysis.

AUTHOR INFORMATION

Corresponding Author

*

Author Contributions

The manuscript was written through contributions of all authors. All authors have given approval to the final version of the manuscript.

ACKNOWLEDGMENT

The authors thank the companies Clariant Produkte (Deutschland) GmbH and SASOL Germany GmbH for providing the technical-grade Genapol surfactants as well as for providing the technical-grade wax Sasolwax 5805. Furthermore, we would like to acknowledge the Institut Laue-Langevin (ILL) in Grenoble (France) for the allocation of beam-time under proposal 9-12-573 [doi: 10.5291/ILL-DATA.9-12-573] and David Bowyer for help with setting up the SANS environment. Additionally, we thank the Jülich Centre for Neutron Science (JCNS) at the Heinz Maier-Leibnitz Zentrum (MLZ) in Munich (Germany) and the National Institute of Standards and Technology (NIST) in Gaithersburg (USA) for providing the facilities for preliminary SANS experiments on PEO and PAlkGE homopolymers in D_2O and deuterated *n*-alkanes as well as the valuable support of the local contacts H. Frielinghaus (JCNS) and Y. Liu (NIST). Also, we acknowledge the help of the SANS teams consisting of K. Abitaev, J. Bruckner, S. Dieterich, J. Fischer, F. Gießelmann, S. Tseng and D. Zauser (Institute of Physical Chemistry, University of Stuttgart) during the SANS measurements. The authors also thank Monika Schmelzer for SEC measurements.

References

(1) Schulman, J. H.; Stoeckenius, W.; Prince, L. M. Mechanism of Formation and Structure of Micro Emulsions by Electron Microscopy. *J. Phys. Chem.* **1959**, *63*, 1677–1680.

(2) Strey, R. Microemulsion microstructure and interfacial curvature. *Colloid Polym. Sci.* **1994**, *272*, 1005–1019.

(3) Langevin, D.; Chen, S.-H. (e.). *Low Interfacial Tensions in Microemulsion Systems*. In: Structure and Dynamics of Strongly Interacting Colloids and Supramolecular Aggregates in Solution; Springer Netherlands: Dordrecht, 1992.

(4) Aveyard, R.; Binks, B. P.; Clark, S.; Mead, J. Interfacial tension minima in oil–water–surfactant systems. Behaviour of alkane–aqueous NaCl systems containing aerosol OT. *J. Chem. Soc., Faraday Trans. 1* **1986**, *82*, 125–142.

(5) Sottmann, T.; Strey, R. Shape Similarities of Ultra-Low Interfacial Tension Curves in Ternary Microemulsion Systems of the Water-Alkane-C_iE_j Type. *Ber. Bunsenges. Phys. Chem.* **1996**, *100*, 237–241.

(6) Sottmann, T.; Strey, R. Ultralow interfacial tensions in water–*n*-alkane–surfactant systems. *J. Chem. Phys.* **1997**, *106*, 8606–8615.

(7) Sottmann, T.; Strey, R. *Microemulsions, In: Fundamentals of Interface and Colloid Science: Soft Colloids*, 1. Aufl.; Fundamentals of Interface and Colloid Science v.v. 5; Elsevier professional: s.l., 2005.

(8) Scheibel, J. J. The evolution of anionic surfactant technology to meet the requirements of the laundry detergent industry. *J. Surfactants Deterg.* **2004**, *7*, 319–328.

(9) Bajpai, D.; Tyagi, V. K. Laundry Detergents: An Overview. *J. Oleo Sci.* **2007**, *56*, 327–340.

(10) Shah, D. O. *Improved oil recovery by surfactant and polymer flooding*; Elsevier, 2012.

(11) Nazar, M. F.; Shah, S. S.; Khosa, M. A. Microemulsions in Enhanced Oil Recovery: A Review. *Pet. Sci. Technol.* **2011**, *29*, 1353–1365.

(12) Anderberg, E. K.; Nyström, C.; Artursson, P. Epithelial transport of drugs in cell culture. VII: Effects of pharmaceutical surfactant excipients and bile acids on transepithelial permeability in monolayers of human intestinal epithelial (Caco-2) cells. *J. Pharm. Sci.* **1992**, *81*, 879–887.

(13) Merchán Arenas, D. R.; Martínez Bonilla, C. A.; Kouznetsov, V. V. Aqueous SDS micelle-promoted acid-catalyzed domino ABB' imino Diels-Alder reaction: a mild and efficient synthesis of privileged 2-methyl-tetrahydroquinoline scaffolds. *Org. Biomol. Chem.* **2013**, *11*, 3655–3663.

(14) La Sorella, G.; Strukul, G.; Scarso, A. Recent advances in catalysis in micellar media. *Green Chem.* **2015**, *17*, 644–683.

(15) Sottmann, T. Solubilization efficiency boosting by amphiphilic block co-polymers in microemulsions. *Curr. Opin. Colloid Interface Sci.* **2002**, *7*, 57–65.

(16) Jakobs, B.; Sottmann, T.; Strey, R.; Allgaier, J.; d. Richter. Amphiphilic Block Copolymers as Efficiency Boosters for Microemulsions. *Langmuir* **1999**, *15*, 6707–6711.

(17) Jakobs, B.; Sottmann, T.; Strey, R. Efficiency boosting with amphiphilic block copolymers: a new approach to microemulsion formulation. *Tenside, Surfactants, Deterg.* **2000**, *37*, 357–364.

(18) Allgaier, J.; Poppe, A.; Willner, L.; Richter, D. Synthesis and Characterization of Poly[1,4-isoprene- b -(ethylene oxide)] and Poly[ethylene- co -propylene- b -(ethylene oxide)] Block Copolymers. *Macromolecules* **1997**, *30*, 1582–1586.

(19) Poppe, A.; Willner, L.; Allgaier, J.; Stellbrink, J.; Richter, D. Structural Investigation of Micelles Formed by an Amphiphilic PEP−PEO Block Copolymer in Water. *Macromolecules* **1997**, *30*, 7462–7471.

(20) Frank, C.; Sottmann, T.; Stubenrauch, C.; Allgaier, J.; Strey, R. Influence of amphiphilic block copolymers on lyotropic liquid crystals in water-oil-surfactant systems. *Langmuir* **2005**, *21*, 9058–9067.

(21) Endo, H.; Allgaier, J.; Gompper, G.; Jakobs, B.; Monkenbusch, M.; d. Richter; Sottmann, T.; Strey, R. Membrane decoration by amphiphilic block copolymers in bicontinuous microemulsions. *Phys. Rev. Lett.* **2000**, *85*, 102–105.

(22) Gompper, G.; Endo, H.; Mihailescu, M.; Allgaier, J.; Monkenbusch, M.; d. Richter; Jakobs, B.; Sottmann, T.; Strey, R. Measuring bending rigidity and spatial renormalization in bicontinuous microemulsions. *Europhys. Lett.* **2001**, *56*, 683–689.

(23) Helfrich, W. Elastic properties of lipid bilayers: theory and possible experiments: Theory and Possible Experiments. *Z. Naturforsch., C: J. Biosci.* **1973**, *28*, 693–703.

(24) Lipowsky, R. Bending of Membranes by Anchored Polymers. *Europhys. Lett.* **1995**, *30*, 197–202.

(25) Lipowsky, R.; Döbereiner, H.-G.; Hiergeist, C.; Indrani, V. Membrane curvature induced by polymers and colloids. *Phys. A* **1998**, *249*, 536–543.

(26) Endo, H.; Mihailescu, M.; Monkenbusch, M.; Allgaier, J.; Gompper, G.; d. Richter; Jakobs, B.; Sottmann, T.; Strey, R.; Grillo, I. Effect of amphiphilic block copolymers on the structure and phase behavior of oil–water-surfactant mixtures. *J. Chem. Phys.* **2001**, *115*, 580–600.

(27) Nilsson, M.; Söderman, O.; Johansson, I. The effect of polymers on the phase behavior of balanced microemulsions: diblock-copolymer and comb-polymers. *Colloid Polym. Sci.* **2006**, *284*, 1229–1241.

(28) Byelov, D.; Frielinghaus, H.; Holderer, O.; Allgaier, J.; d. Richter. Microemulsion efficiency boosting and the complementary effect. 1. Structural properties. *Langmuir* **2004**, *20*, 10433–10443.

(29) Gompper, G.; d. Richter; Strey, R. Amphiphilic block copolymers in oil-water-surfactant mixtures: efficiency boosting, structure, phase behaviour and mechanism: Efficiency boosting, structure, phase behaviour and mechanism. *J. Phys.: Condens. Matter* **2001**, *13*, 9055–9074.

(30) Klemmer, H. F. M.; Allgaier, J.; Frielinghaus, H.; Holderer, O.; Ohl, M. Influence of the amphiphilicity profile of copolymers on the formation of liquid crystalline mesophases in microemulsions. *Colloid Polym. Sci.* **2017**, *295*, 911–923.

(31) Kunze, L.; Tseng, S.-Y.; Schweins, R.; Sottmann, T.; Frey, H. Nonionic Aliphatic Polycarbonate Diblock Copolymers Based on CO2, 1,2-Butylene Oxide, and mPEG: Synthesis, Micellization, and Solubilization. *Langmuir* **2019**, *35*, 5221–5231.

(32) Foster, T.; Sottmann, T.; Schweins, R.; Strey, R. Small-angle-neutron-scattering from giant water-in-oil microemulsion droplets. II. Polymer-decorated droplets in a quaternary system. *The Journal of Chemical Physics* **2008**, *128*, 64902.

(33) Frank, C.; Frielinghaus, H.; Allgaier, J.; Richter, D. Hydrophilic alcohol ethoxylates as efficiency boosters for microemulsions. *Langmuir* **2008**, *24*, 6036–6043.

(34) Brodeck, M.; Maccarrone, S.; Saha, D.; Willner, L.; Allgaier, J.; Mangiapia, G.; Frielinghaus, H.; Holderer, O.; Faraone, A.; Richter, D. Asymmetric polymers in bicontinuous microemulsions and their accretion to the bending of the membrane. *Colloid Polym. Sci.* **2015**, *293*, 1253–1265.

(35) Hoehn, S.; Schulreich, C.; Hellweg, T. Efficiency Boosting in Technical Grade Sugar Surfactant Based Microemulsions Using Pluronics. *Tenside, Surfactants, Deterg.* **2014**, *51*, 32–39.

(36) Takahashi, Y.; Shirahata, H.; Nishimura, T.; Murai, M.; Wakita, K.; Kondo, Y. Boosting Effect of Amphiphilic Random Copolymers for Bicontinuous Phases. *J. Oleo Sci.* **2018**, *67*, 531–537.

(37) Marchal, F.; Guenoun, P.; Daillant, J.; Holley, D. W.; Mays, J. W. Unprecedented microemulsion boosting effect induced by a charged diblock copolymer: bending modulus and curvature frustration of the surfactant film. *Soft Matter* **2009**, *5*, 4006.

(38) Tchekountieu Mboumi, L. J. *Technisch relevante amphiphile Blockcopolymere in Mikroemulsionen: Dissertation*, 2010.

(39) Beisser, R.; Allgaier, J.; Hillerich, J. Patent: Microemulsion-based cleaning agent comprising an anionic/nonionic surfactant mixture.

(40) Verkoyen, P.; Johann, T.; Blankenburg, J.; Czysch, C.; Frey, H. Polymerization of long chain alkyl glycidyl ethers: a platform for micellar gels with tailor-made melting points. *Polym. Chem.* **2018**, *9*, 5327–5338.

(41) Petrov, P.; Rangelov, S.; Novakov, C.; Brown, W.; Berlinova, I.; Tsvetanov, C.B. Core-corona nanoparticles formed by high molecular weight poly(ethylene oxide)-b-poly(alkylglycidyl ether) diblock copolymers. *Polymer* **2002**, *43*, 6641–6651.

(42) Liu, F.; Frere, Y.; Francois, J. Association properties of poly(ethylene oxide) modified by pendant aliphatic groups. *Polymer* **2001**, *42*, 2969–2983.

(43) Satoh, Y.; Miyachi, K.; Matsuno, H.; Isono, T.; Tajima, K.; Kakuchi, T.; Satoh, T. Synthesis of Well-Defined Amphiphilic Star-Block and Miktoarm Star Copolyethers via t -Bu-P

4 -Catalyzed Ring-Opening Polymerization of Glycidyl Ethers. *Macromolecules* **2016**, *49*, 499–509.

(44) Schneider, K.; Ott, T. M.; Schweins, R.; Frielinghaus, H.; Lade, O.; Sottmann, T. Phase Behavior and Microstructure of Symmetric Nonionic Microemulsions with Long-Chain n -Alkanes and Waxes. *Ind. Eng. Chem. Res.* **2019**, *58*, 2583–2595.

(45) Kahlweit, M.; Strey, R.; Busse, G. Microemulsions: a qualitative thermodynamic approach. *J. Phys. Chem.* **1990**, *94*, 3881–3894.

(46) Kahlweit, M.; Strey, R. Phase Behavior of Ternary Systems of the Type H2O-Oil-Nonionic Amphiphile (Microemulsions). *Angew. Chem. Int. Ed. Engl.* **1985**, *24*, 654–668.

(47) Burauer, S.; Sachert, T.; Sottmann, T.; Strey, R. On microemulsion phase behavior and the monomeric solubility of surfactant. *Phys. Chem. Chem. Phys.* **1999**, *1*, 4299–4306.

(48) Sottmann, T.; Strey, R.; Chen, S.-H. A small-angle neutron scattering study of nonionic surfactant molecules at the water–oil interface: Area per molecule, microemulsion domain size, and rigidity. *J. Chem. Phys.* **1997**, *106*, 6483–6491.

(49) Shi, W.; McGrath, A. J.; Li, Y.; Lynd, N. A.; Hawker, C. J.; Fredrickson, G. H.; Kramer, E. J. Cooperative and Sequential Phase Transitions in it -Poly(propylene oxide)- b -poly(ethylene oxide)- b - it -poly(propylene oxide) Triblock Copolymers. *Macromolecules* **2015**, *48*, 3069–3079.

(50) McGrath, A. J.; Shi, W.; Rodriguez, C. G.; Kramer, E. J.; Hawker, C. J.; Lynd, N. A. Synthetic Strategy for Preparing Chiral Double-semicrystalline Polyether Block Copolymers. *Polym. Chem.* **2015**, *6*, 1465–1473.

(51) Shin, D.; Shin, K.; Aamer, K. A.; Tew, G. N.; Russell, T. P.; Lee, J. H.; Jho, J. Y. A Morphological Study of a Semicrystalline Poly(l -lactic acid- b -ethylene oxide- b - l -lactic acid) Triblock Copolymer. *Macromolecules* **2005**, *38*, 104–109.

(52) Hiergeist, C.; Lipowsky, R. Elastic Properties of Polymer-Decorated Membranes. *J. Phys. II France* **1996**, *6*, 1465–1481.

(53) Teubner, M.; Strey, R. Origin of the scattering peak in microemulsions. *J. Chem. Phys.* **1987**, *87*, 3195–3200.

(54) Schelten, J.; Schmatz, W. Multiple-scattering treatment for small-angle scattering problems. *J. Appl. Crystallogr.* **1980**, *13*, 385–390.

(55) Silas, J. A.; Kaler, E. W. Effect of multiple scattering on SANS spectra from bicontinuous microemulsions. *J. Colloid Interface Sci.* **2003**, *257*, 291–298.

(56) Gradzielski, M.; Langevin, D.; Sottmann, T.; Strey, R. Small angle neutron scattering near the wetting transition: Discrimination of microemulsions from weakly structured mixtures. *The Journal of Chemical Physics* **1996**, *104*, 3782–3787.

(57) Schubert, K.‐V.; Strey, R. Small‐angle neutron scattering from microemulsions near the disorder line in water/formamide‐octane‐C_iE_j systems. *J. Chem. Phys.* **1991**, *95*, 8532–8545.

(58) Schubert, K.‐V.; Strey, R.; Kline, S. R.; Kaler, E. W. Small angle neutron scattering near Lifshitz lines: Transition from weakly structured mixtures to microemulsions. *J. Chem. Phys.* **1994**, *101*, 5343–5355.

(59) Pieruschka, P.; Safran, S. A.; Marčelja, S. T. Comment on ‘‘Fluctuating interfaces in microemulsion and sponge phases’’. *Phys. Rev. E* **1995**, *52*, 1245–1247.

(60) Peltomäki, M.; Gompper, G.; Kroll, D. M. Scattering intensity of bicontinuous microemulsions and sponge phases. *J. Chem. Phys.* **2012**, *136*, 134708.

(61) Holderer, O.; Frielinghaus, H.; Monkenbusch, M.; Klostermann, M.; Sottmann, T.; Richter, D. Experimental determination of bending rigidity and saddle splay modulus in bicontinuous microemulsions. *Soft Matter* **2013**, *9*, 2308.

(62) Morse, D. C. Topological instabilities and phase behavior of fluid membranes. *Phys. Rev. E* **1994**, *50*, 2423-2426.

(63) Gompper, G.; Kroll, D. M. Membranes with Fluctuating Topology: Monte Carlo Simulations. *Phys. Rev. Lett.* **1998**, *81*, 2284–2287.

(64) Golubović, L. Passages and droplets in lamellar fluid membrane phases. *Phys. Rev. E* **1994**, *50*, 2419-2422.

(65) Lyklema, J. *Fundamentals of Interface and Colloid Science: Soft Colloids*. In: Fundamentals of Interface and Colloid Science, 1. Aufl.; Fundamentals of Interface and Colloid Science v.v. 5; Elsevier professional: s.l., 2005.

(66) Aubry, J.-M.; Ontiveros, J. F.; Salager, J.-L.; Nardello-Rataj, V. Use of the normalized hydrophilic-lipophilic-deviation (HLDN) equation for determining the equivalent alkane carbon number (EACN) of oils and the preferred alkane carbon number (PACN) of nonionic surfactants by the fish-tail method (FTM). *Adv. Colloid Interface Sci.* **2020**, *276*, 102099.

(67) Sagalowicz, L.; Leser, M. E.; Watzke, H. J.; Michel, M. Monoglyceride self-assembly structures as delivery vehicles. *Trends in Food Science & Technology* **2006**, *17*, 204–214.

(68) Attard, G. S.; Glyde, J. C.; Göltner, C. G. Liquid-crystalline phases as templates for the synthesis of mesoporous silica. *Nature* **1995**, *378*, 366–368.

(69) Solans, C. *Industrial applications of microemulsions*; Surfactant science series 66; Dekker: New York, NY, 1997.

(70) Lipowsky, R. Flexible membranes with anchored polymers. *Colloids Surf. A* **1997**, *128*, 255–264.

(71) Sottmann, T.; Lade, M.; Stolz, M.; Schomäcker, R. Phase behavior of non-ionic microemulsions prepared from technical-grade surfactants. *Tenside, Surfactants, Deterg.* **2002**, *39*, 20–28.

(72) Jakobs, B. *Amphiphile Blockcopolymere als Efficiency Booster für Tenside*, 1st ed.; Cuvillier Verlag: Göttingen, 2001.

(73) Hammouda, B.; Ho, D. L. Insight into chain dimensions in PEO/water solutions. *J. Polym. Sci. Part B: Polym. Phys.* **2007**, *45*, 2196–2200.

(74) Hammouda, B.; Ho, D. L.; Kline, S. Insight into Clustering in Poly(ethylene oxide) Solutions. *Macromolecules* **2004**, *37*, 6932–6937.

(75) Hammouda, B.; Ho, D.; Kline, S. SANS from Poly(ethylene oxide)/Water Systems. *Macromolecules* **2002**, *35*, 8578–8585.

(76) Glatter, O.; Kratky, O. *Small angle X-ray scattering*, 2nd printing 36; Academic Press: London, 1982.

(77) Kawaguchi, S.; Imai, G.; Suzuki, J.; Miyahara, A.; Kitano, T.; Ito, K. Aqueous solution properties of oligo- and poly(ethylene oxide) by static light scattering and intrinsic viscosity. *Polymer* **1997**, *38*, 2885–2891.

(78) Auth, T.; Gompper, G. Self-avoiding linear and star polymers anchored to membranes. *Physical review. E, Statistical, nonlinear, and soft matter physics* **2003**, *68*, 51801.

(79) Auth, T.; Gompper, G. Fluctuation spectrum of membranes with anchored linear and star polymers. *Physical review. E, Statistical, nonlinear, and soft matter physics* **2005**, *72*, 31904.

(80) Pieruschka, P.; Safran, S. A. Random Interface Model of Sponge Phases. *Europhys. Lett.* **1995**, *31*, 207–212.

(81) Pieruschka, P.; Safran, S. A. Random Interfaces and the Physics of Microemulsions. *Europhys. Lett.* **1993**, *22*, 625–630.

SUPPORTING INFORMATION

Efficiency Boosting of Surfactants with Poly(ethylene oxide)—Poly(alkyl glycidyl ether)s – A New Class of Amphiphilic Polymers

*Kristina Schneider[§,a], Patrick Verkoyen[§,b], Maximilian Krappel[a], Christina Gardiner[a], R. Schweins[c], Holger Frey[b], Thomas Sottmann[a]**

a. Institute of Physical Chemistry, University of Stuttgart, Pfaffenwaldring 55, 70569 Stuttgart, Germany

b. Department of Chemistry, Johannes Gutenberg University Mainz, Duesbergweg 10-14, 55128 Mainz, Germany.

c. Institut Laue-Langevin, DS/LSS, 71 avenue des Martyrs, CS 20156, 38042 Grenoble CEDEX 9, France

*Corresponding author: thomas.sottmann@ipc.uni-stuttgart.de, Tel. +49(0)711-685-64494, Fax. +49(0)711-685-64443

[§]These authors have contributed equally: Kristina Schneider and Patrick Verkoyen.

Table of Contents

1. Route of Synthesis of Amphiphilic Diblock Polycarbonates and Overview of the Synthesized Homopolymers and Diblock Copolymers

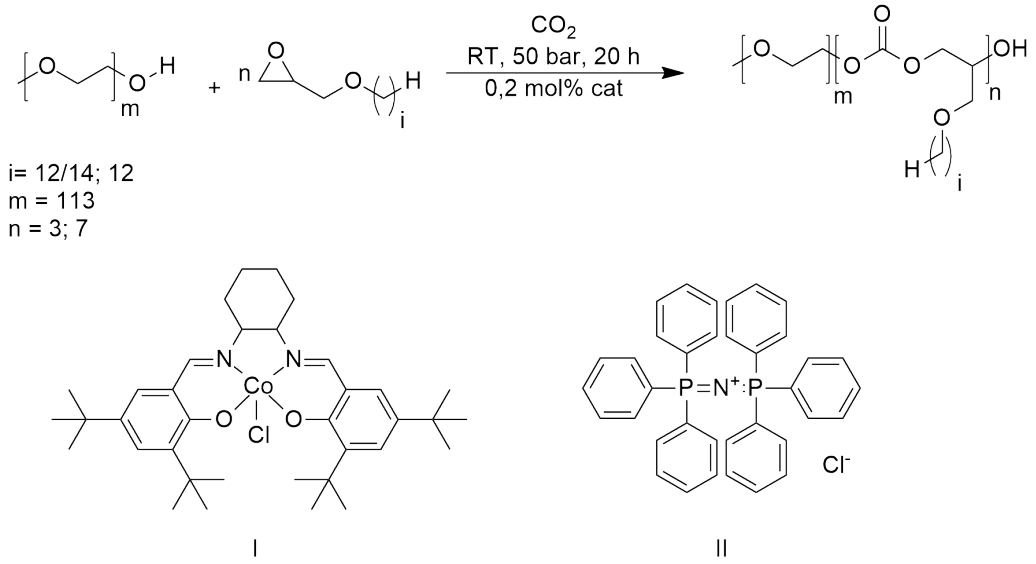

Scheme 1. Synthesis of amphiphilic diblock polycarbonates using Me-PEO as chain transfer agent, long-chain alkyl glycidyl ethers (C_{12}GE and a $C_{12/14}$GE technical-grade mixture) and carbon dioxide as monomers. For polymerization, the catalyst I and the co-catalyst II were used.

Table S1. Synthesized homopolymers and diblock copolymers, calculated molar masses $M_{n,theo}$, experimentally determined molar masses $M_{n,exp}$ and $M_{w,exp}$, as well as molar mass distributions $Đ$ obtained from SEC[b], melting temperatures (T_m) of the two polymer blocks and yields.

Polymer sample	$M_{n,theo}$/ g mol^{-1}	$M_{n,exp}$/ g mol^{-1} [a]	$M_{w,exp}$/ g mol^{-1} [a]	$Đ$ [a]	T_m/ °C [b]	ΔH_m/ J g^{-1} [b]	Yield/ %
BnO-P(C_{12}GE)$_6$	1710	2500	2680	1.06	-	-	80
BnO-P(C_{12}GE)$_{14}$	3649	3600	3960	1.09	-	-	83
BnO-P(C_{12}GE)$_{18}$	4619	4600	4820	1.06	-	-	79
Me-P(EO)$_{113}$-*b*-P(C_{12}GE)$_3$	5699	5400	5810	1.05	-4; 55	2; 136	92
Me-P(EO)$_{113}$-*b*-P(C_{12}GE)$_6$	6426	5800	6520	1.08	1; 53	5; 75	98
Me-P(EO)$_{113}$-*b*-P(C_{12}GE)$_7$	6668	6500	6880	1.06	-	-	80
Me-P(EO)$_{113}$-*b*-P(C_{12}GE)$_8$	6911	6500	6750	1.06	3; 53	14; 131	68
Me-P(EO)$_{113}$-*b*-P(C_{16}GE)$_3$	5866	5400	5660	1.04	56	148	87
Me-P(EO)$_{113}$-*b*-P(C_{16}GE)$_6$	6760	5800	6460	1.06	35; 53	10; 114	82
Me-P(EO)$_{113}$-*b*-P(C_{16}GE)$_9$	7654	6600	6420	1.05	38; 52	20; 103	70
Me-P(EO)$_{113}$-*b*-P(CO_2C_{12}GE)$_3$	5831	5900	6180	1.04	-3; 54	6; 131	40
Me-P(EO)$_{113}$-*b*-P(CO_2C_{12}GE)$_6$	7549	6600	6990	1.05	-2; 54	8; 113	60
Me-P(EO)$_{113}$-*b*-P($CO_2C_{12/14}$GE)$_3$	5872	5500	6160	1.06	3; 55	9; 125	59
Me-P(EO)$_{113}$-*b*-P($CO_2C_{12/14}$GE)$_7$	7072	6800	7150	1.05	-3; 53	6; 107	28

[a] Determined by SEC (eluent: DMF, calibration: PEO standards, and THF, PS standards for the homopolymers); [b] measured by DSC, the first-mentioned melting temperature (T_m) can be assigned to the alkyl glycidyl ether (chain) block and the second T_m can be assigned to the PEO block, respectively. ΔH_m represents the determined melting enthalpy.

2. SEC Measurements of the Synthesized Homopolymers

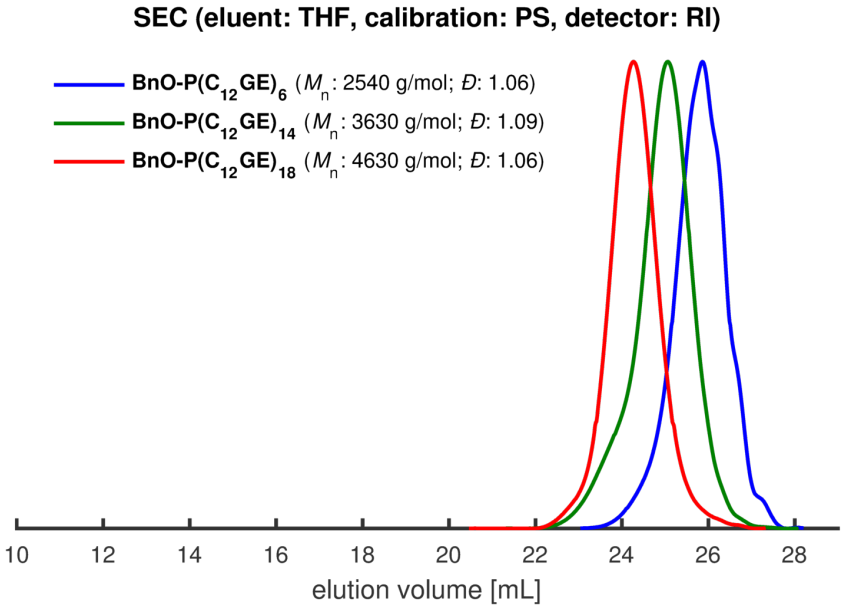

Figure S1. SEC traces of the synthesized homopolymers using C_{12}GE and Benzyloxy ethanol (BnO) as initiator (eluent: THF, calibration: PS standards).

3. DSC Curves of the Synthesized Diblock Copolymers

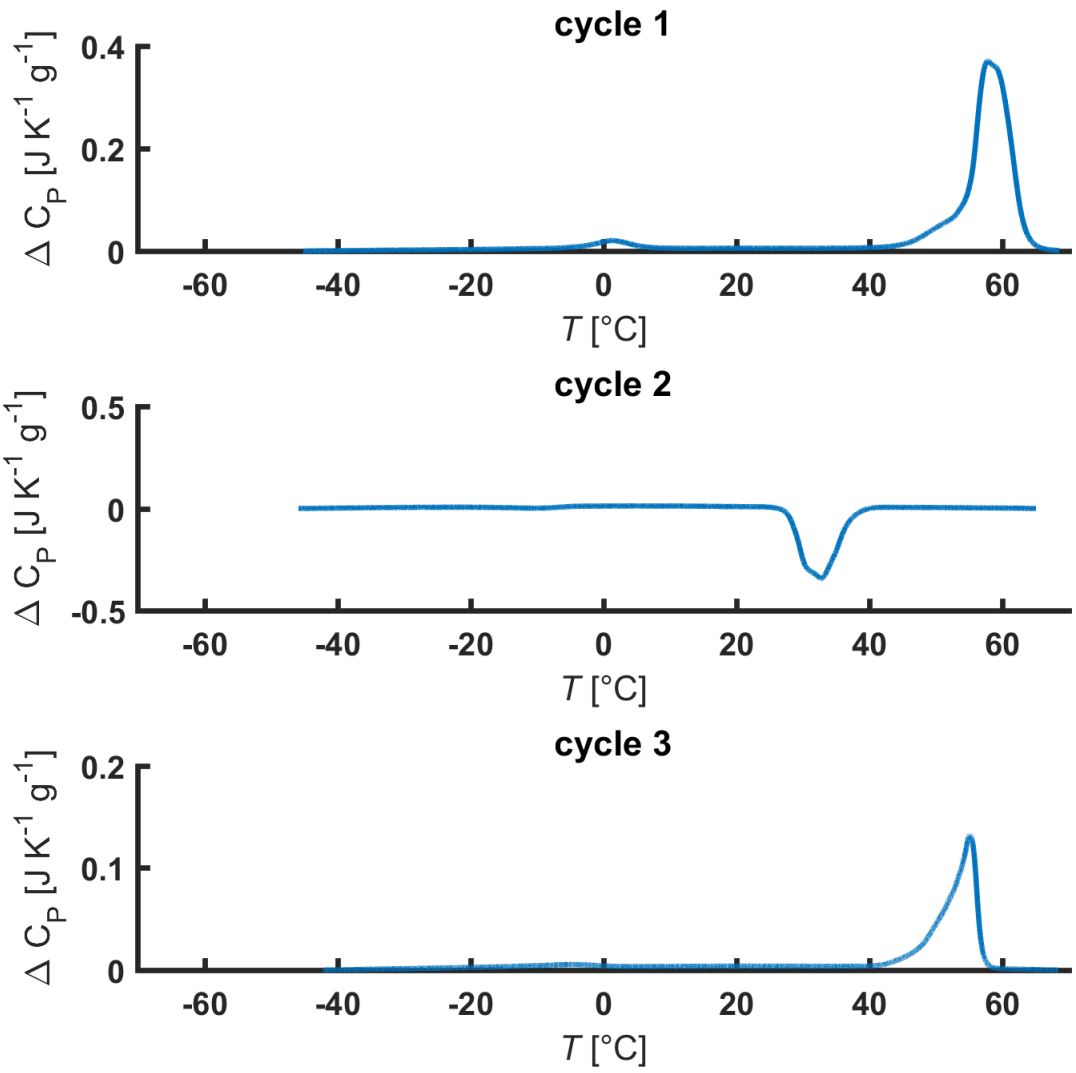

Figure S2. Heating, cooling, and heating cycles of the synthesized diblock copolymer Me-P(EO)$_{113}$-*b*-P(C$_{12}$GE)$_3$; Heating rates: first heating cycle: 20 K min^{-1}, cooling and second heating cycle: 10 K min^{-1}.

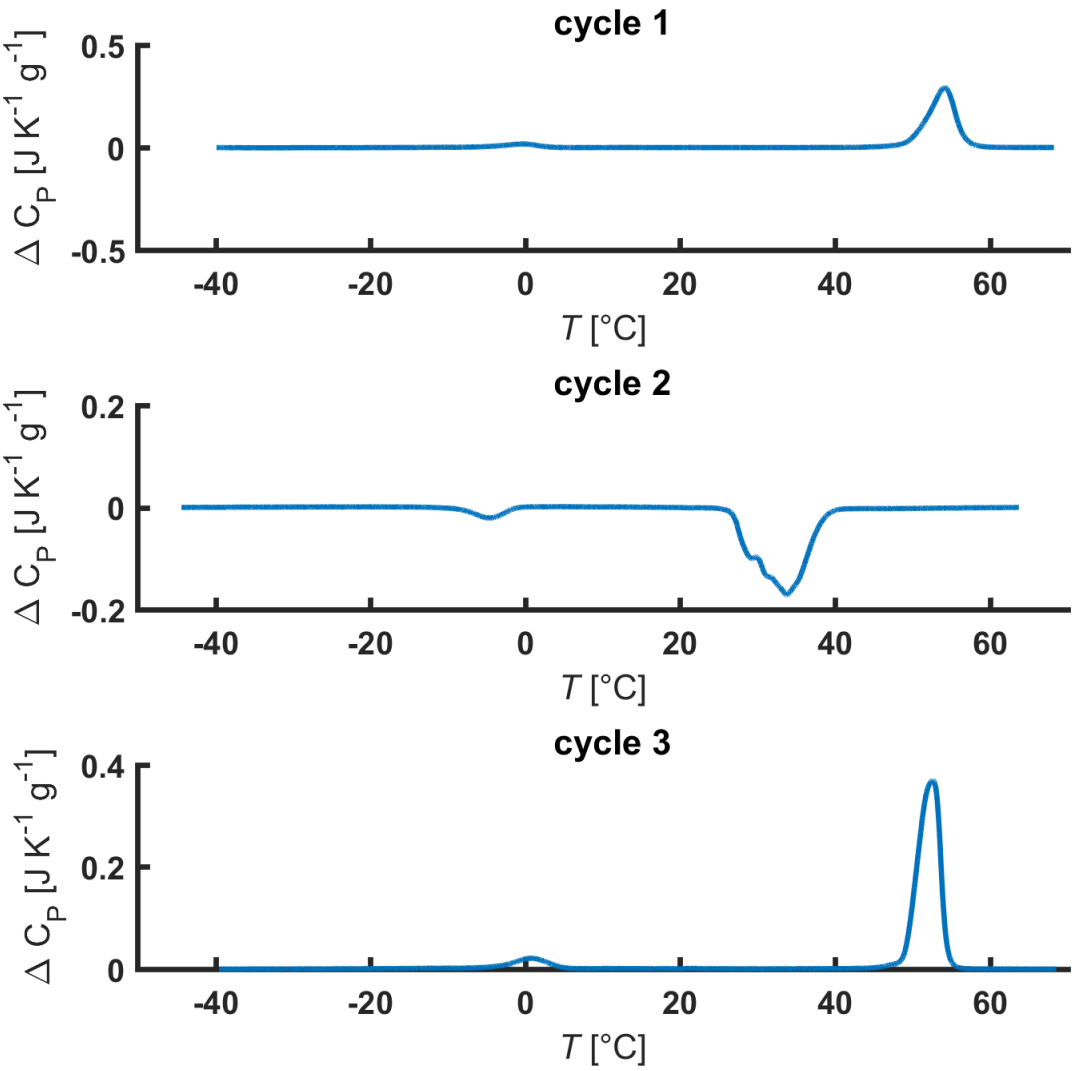

Figure S3. Heating, cooling, and heating cycles of the synthesized diblock copolymer Me-P(EO)$_{113}$-*b*-P(C$_{12}$GE)$_6$; Heating rates: first heating cycle: 20 K min^{-1}, cooling and second heating cycle: 10 K min^{-1}.

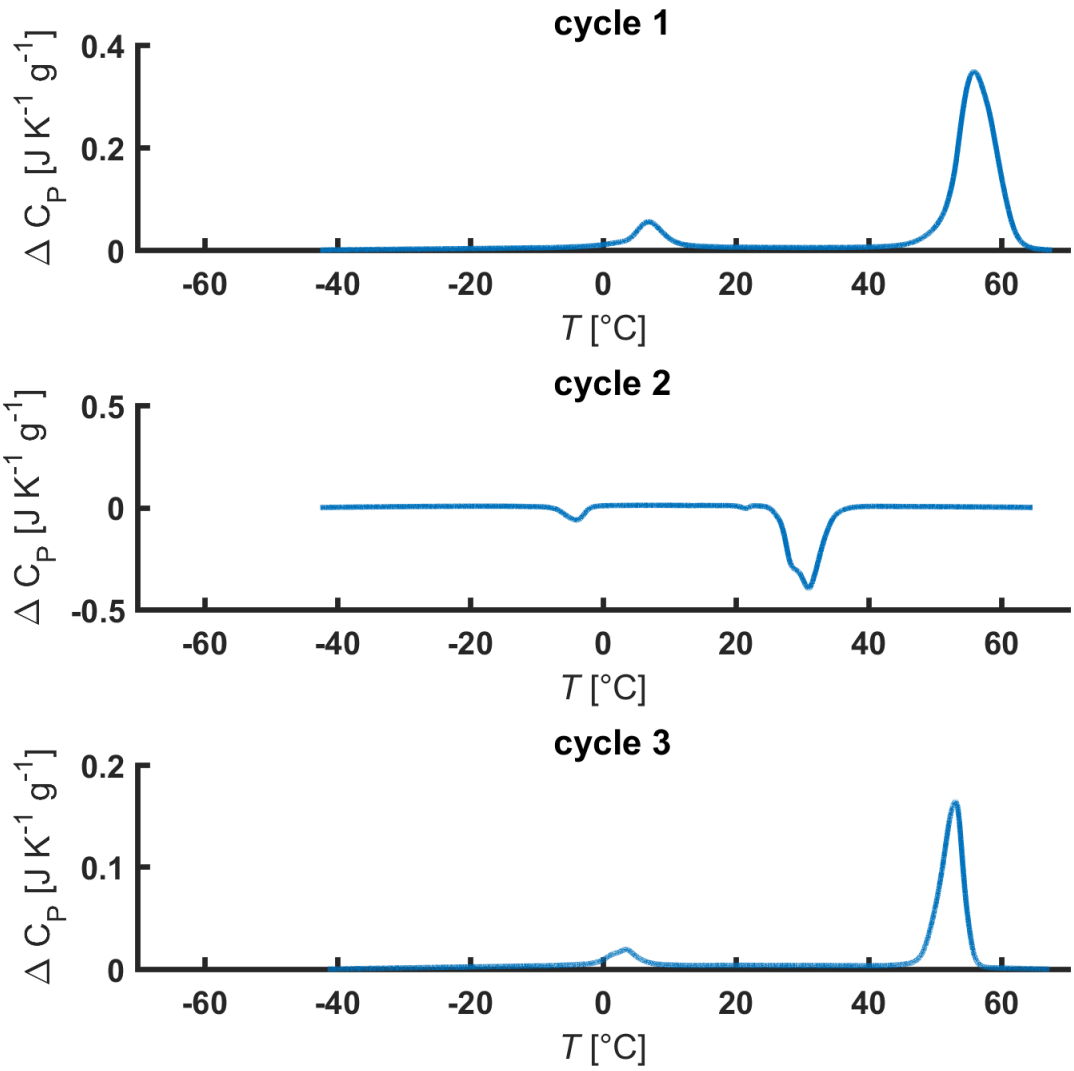

Figure S4. Heating, cooling, and heating cycles of the synthesized diblock copolymer Me-P(EO)$_{113}$-*b*-P(C$_{12}$GE)$_8$; Heating rates: first heating cycle: 20 K min^{-1}, cooling and second heating cycle: 10 K min^{-1}.

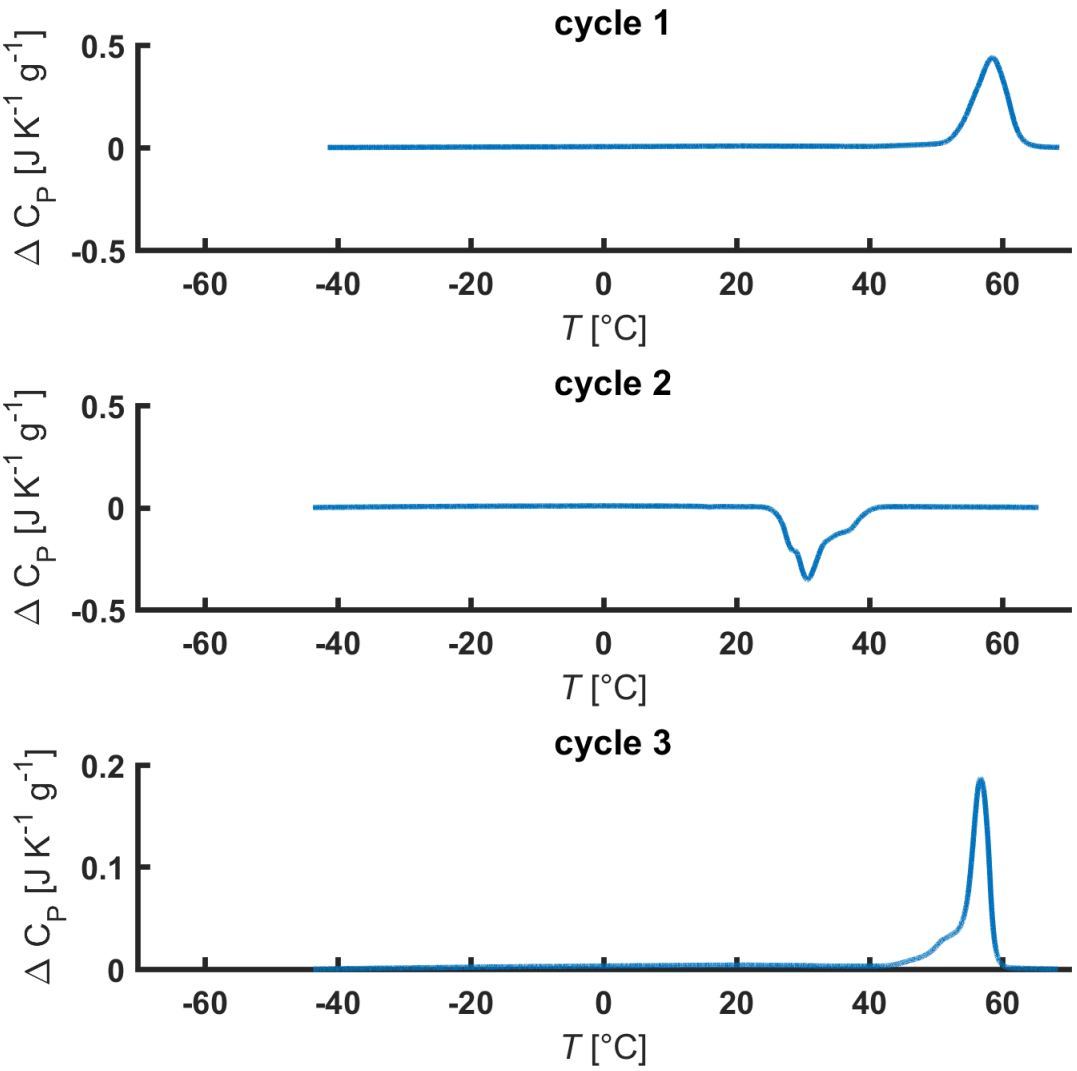

Figure S5. Heating, cooling, and heating cycles of the synthesized diblock copolymer Me-P(EO)$_{113}$-*b*-P(C$_{16}$GE)$_3$; Heating rates: first heating cycle: 20 K min^{-1}, cooling and second heating cycle: 10 K min^{-1}.

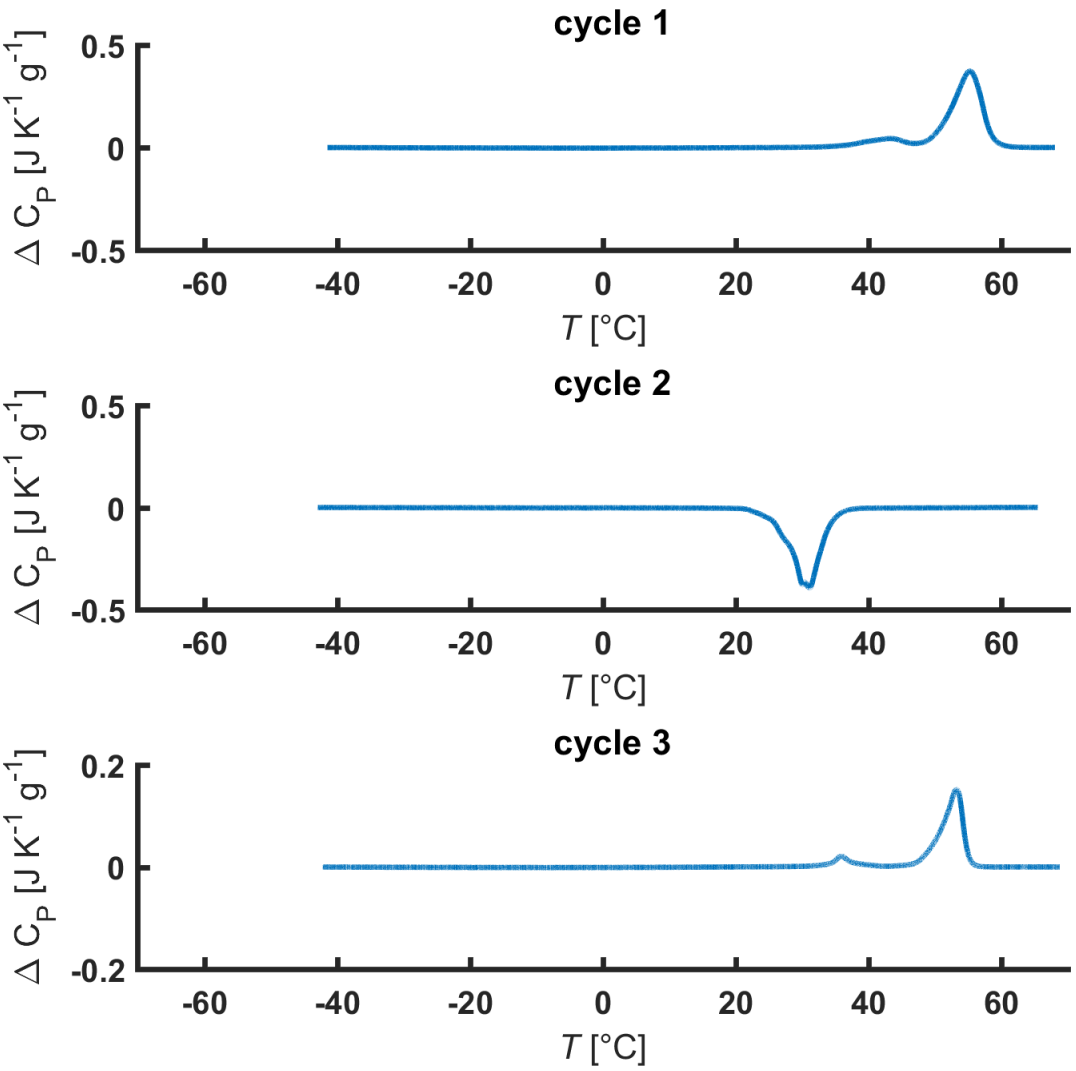

Figure S6. Heating, cooling, and heating cycles of the synthesized diblock copolymer Me-P(EO)$_{113}$-*b*-P(C$_{16}$GE)$_6$; Heating rates: first heating cycle: 20 K min^{-1}, cooling and second heating cycle: 10 K min^{-1}.

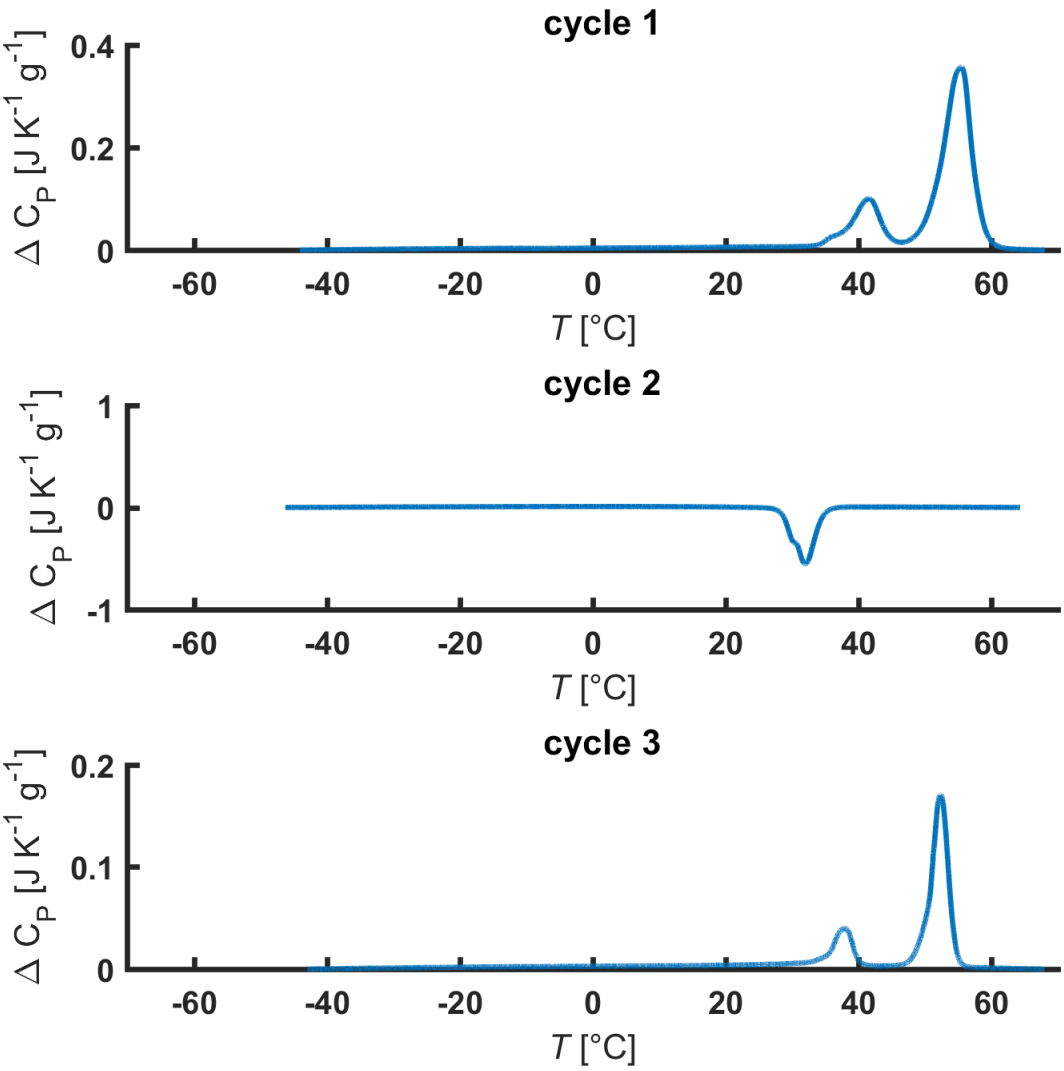

Figure S7. Heating, cooling, and heating cycles of the synthesized diblock copolymer Me-P(EO)$_{113}$-*b*-P(C$_{16}$GE)$_9$; Heating rates: first heating cycle: 20 K min^{-1}, cooling and second heating cycle: 10 K min^{-1}.

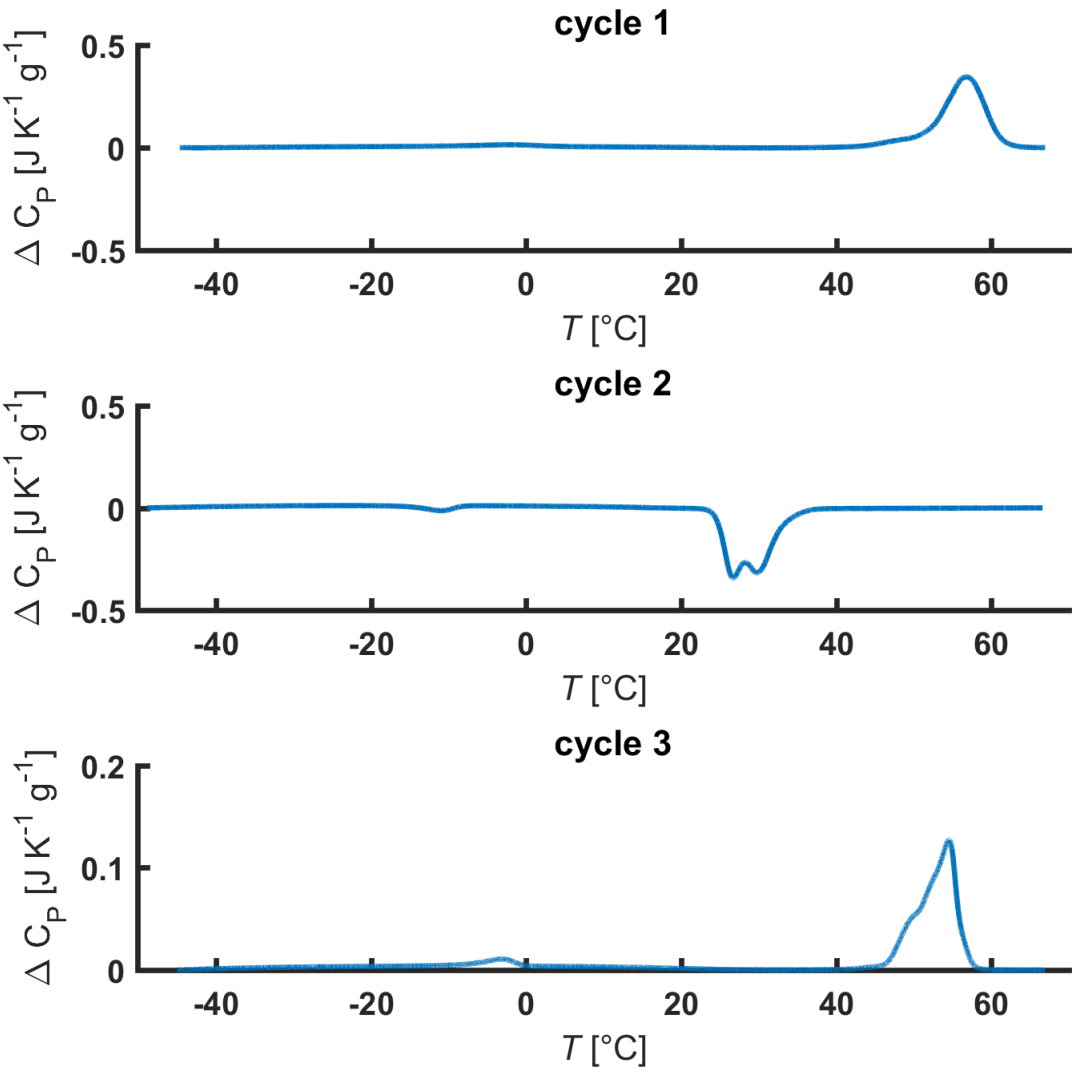

Figure S8. Heating, cooling, and heating cycles of the synthesized diblock copolymer Me-P(EO)$_{113}$-*b*-P(CO$_2$C$_{12}$GE)$_3$; Heating rates: first heating cycle: 20 K min^{-1}, cooling and second heating cycle: 10 K min^{-1}.

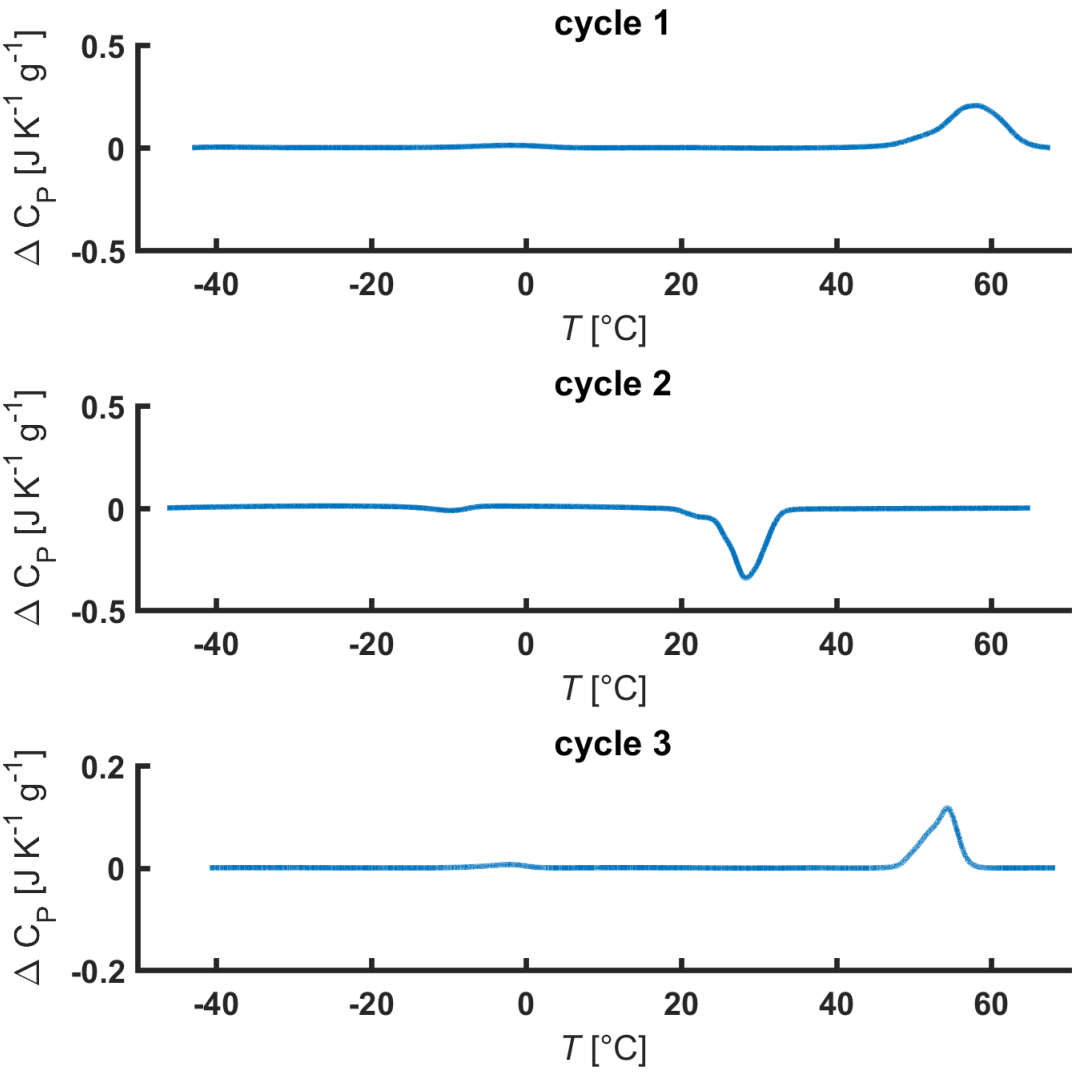

Figure S9. Heating, cooling, and heating cycles of the synthesized diblock copolymer Me-P(EO)$_{113}$-*b*-P(CO$_2$C$_{12}$GE)$_9$; Heating rates: first heating cycle: 20 K min^{-1}, cooling and second heating cycle: 10 K min^{-1}.

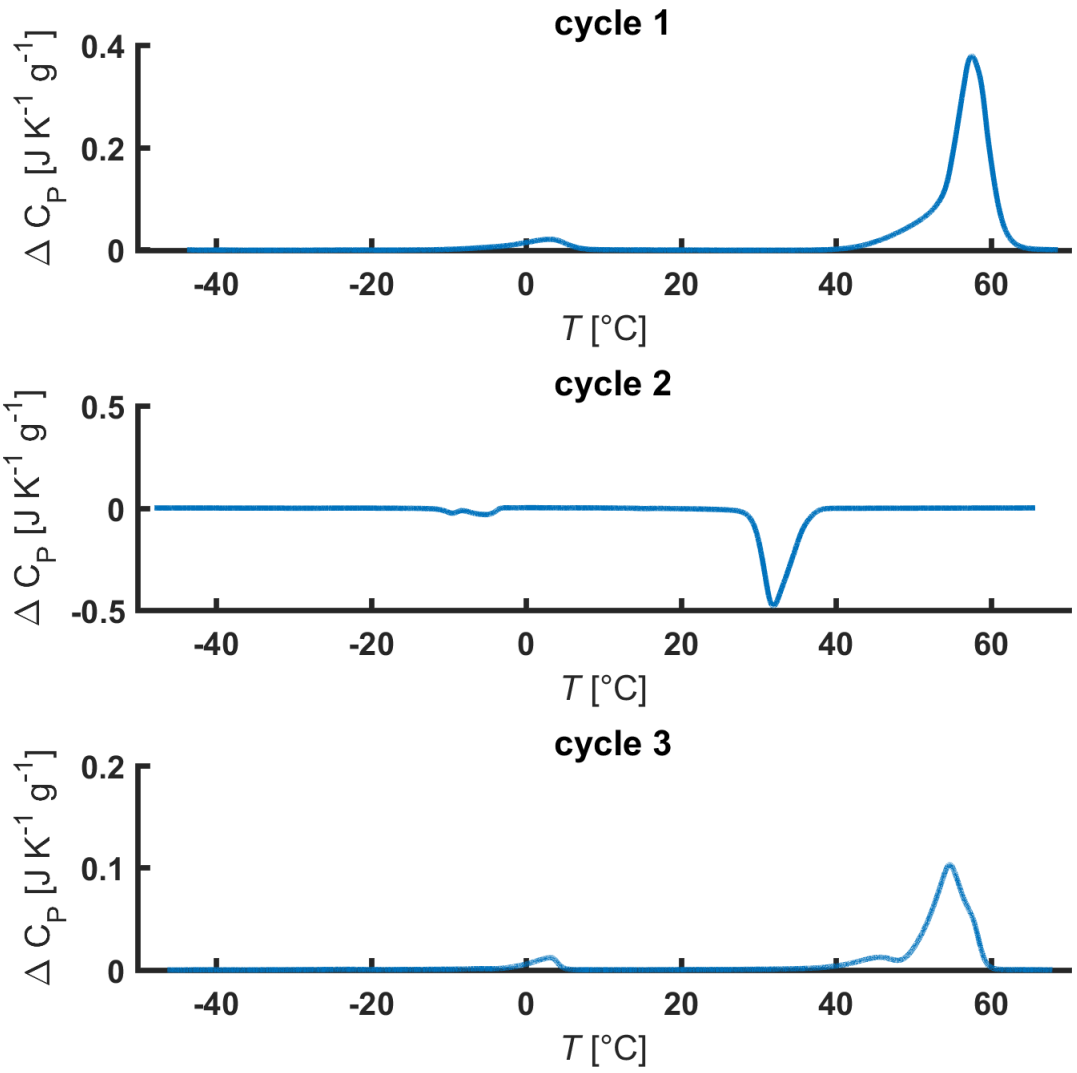

Figure S10. Heating, cooling, and heating cycles of the synthesized diblock copolymer Me-P(EO)$_{113}$-*b*-P(CO$_2$C$_{12/14}$)$_3$; Heating rates: first heating cycle: 20 K min^{-1}, cooling and second heating cycle: 10 K min^{-1}.

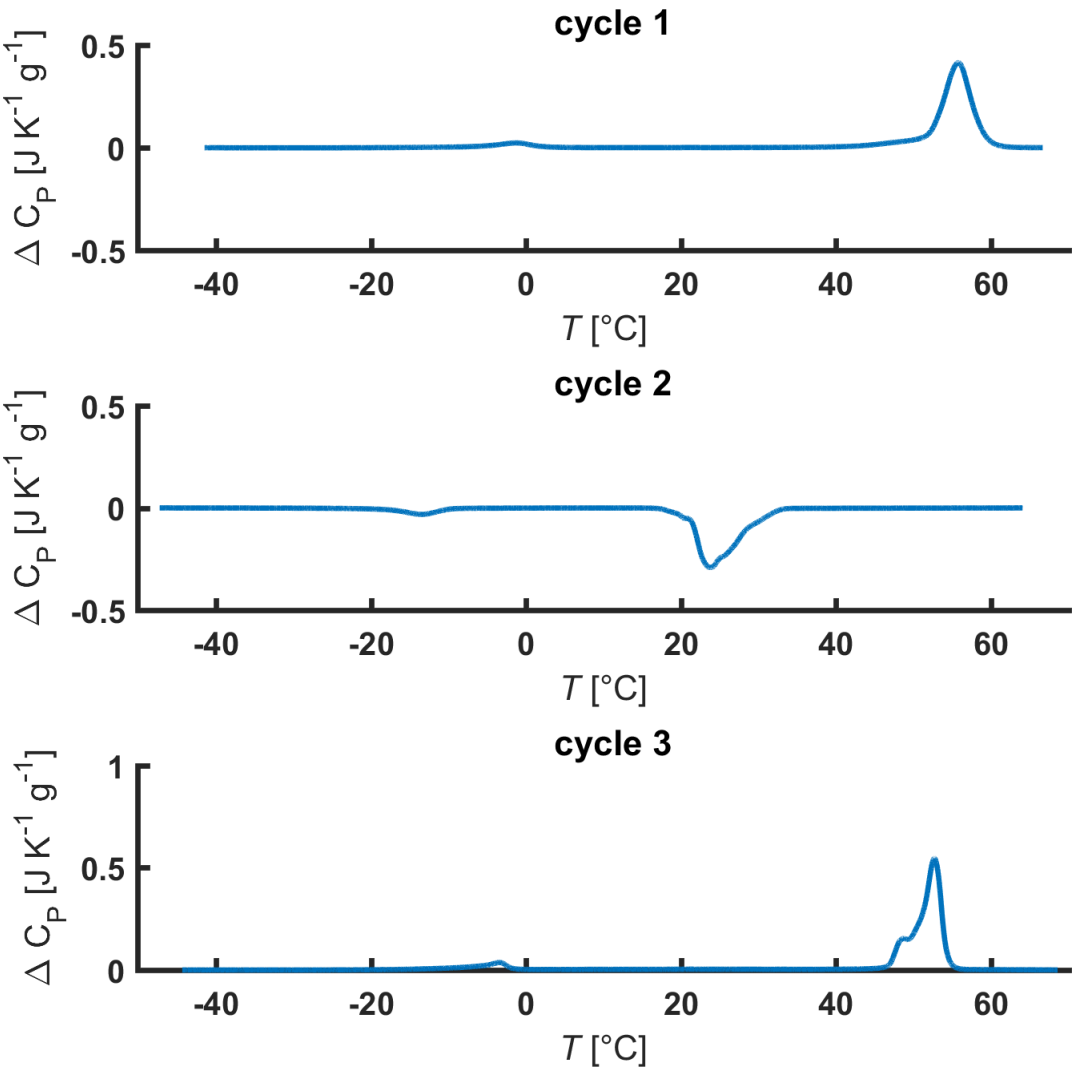

Figure S11. Heating, cooling, and heating cycles of the synthesized diblock copolymer Me-P(EO)$_{113}$-*b*-P(CO$_2$C$_{12/14}$)$_7$; Heating rates: first heating cycle: 20 K min^{-1}, cooling and second heating cycle: 10 K min^{-1}.

4. ^{1}H NMR Spectra of the Diblock Copolymers

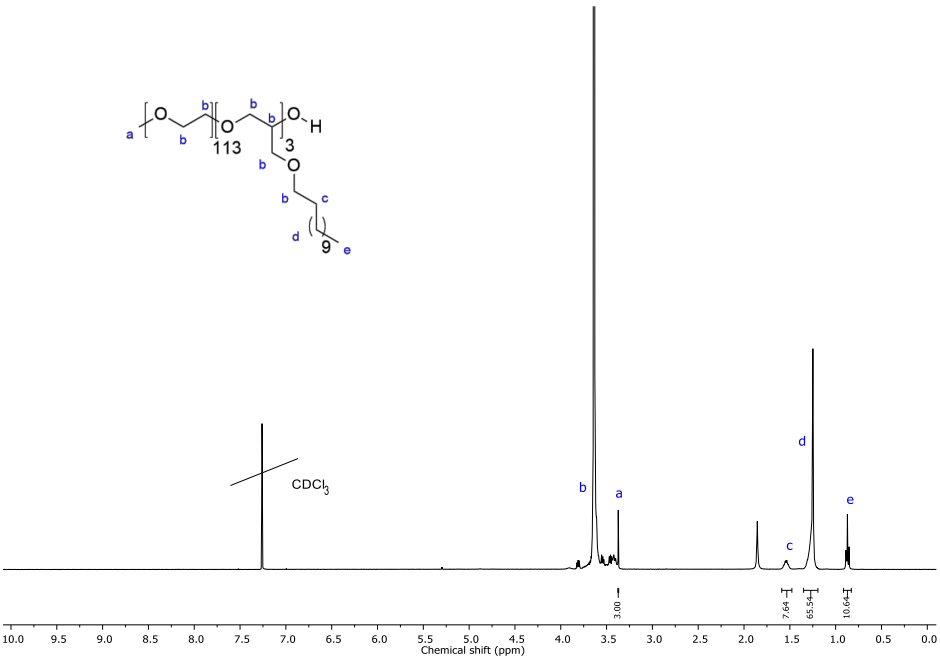

Figure S12. ^{1}H NMR spectrum (300 MHz, chloroform-d) of Me-P(EO)$_{113}$-*b*-P(C$_{12}$GE)$_3$.

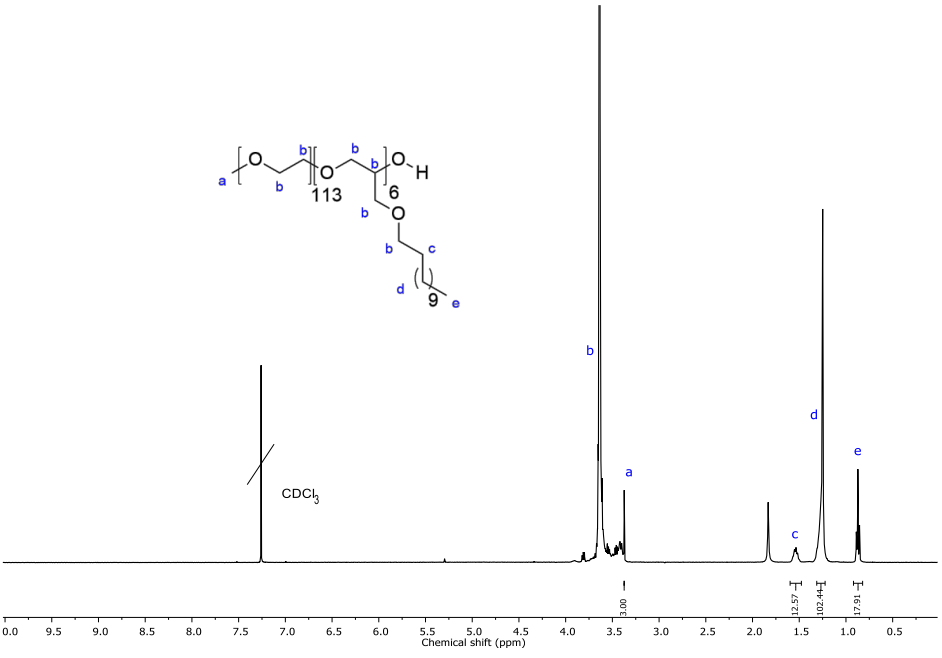

Figure S13. ^{1}H NMR spectrum (300 MHz, chloroform-d) of Me-P(EO)$_{113}$-*b*-P(C$_{12}$GE)$_6$.

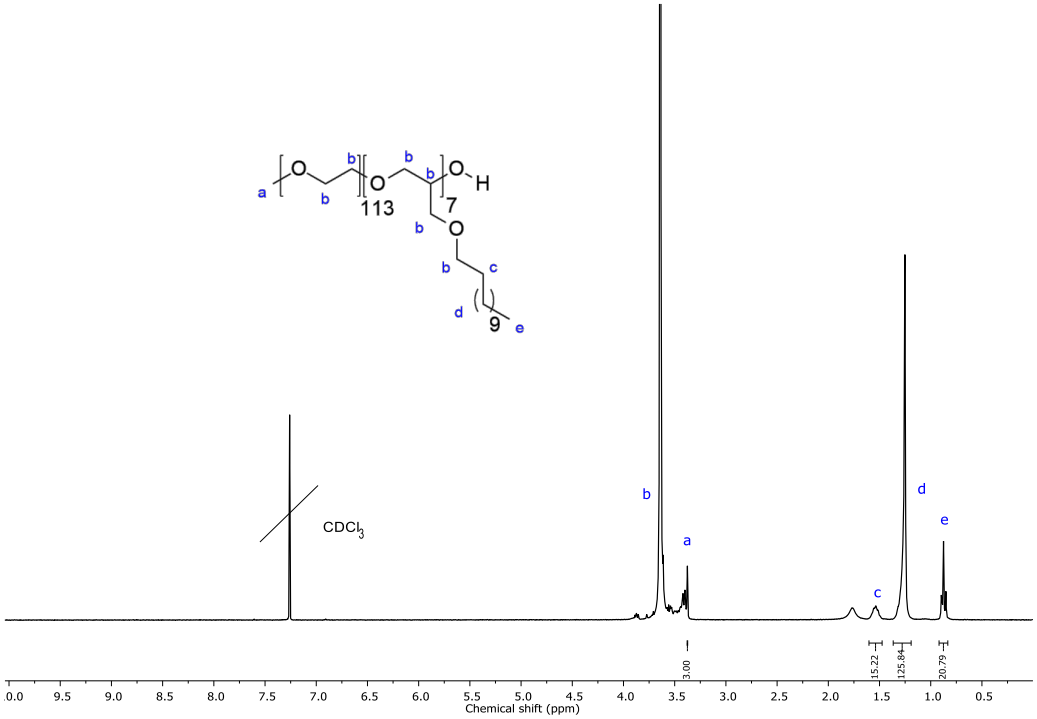

Figure S14. ^{1}H NMR spectrum (300 MHz, chloroform-d) of Me-P(EO)$_{113}$-*b*-P(C$_{12}$GE)$_{7}$.

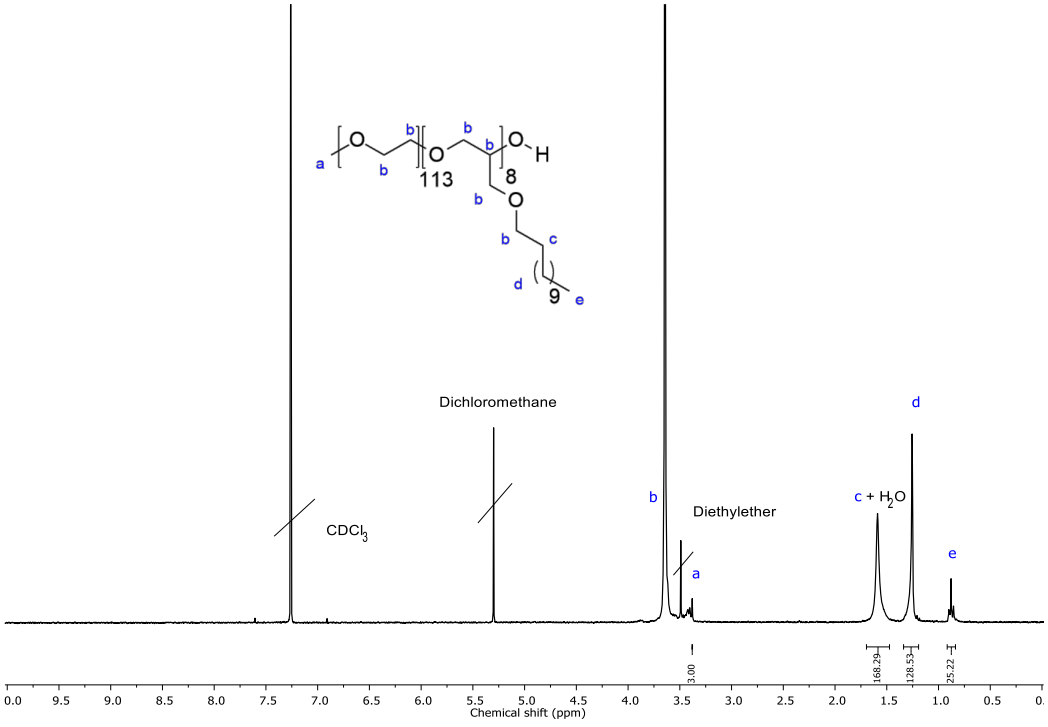

Figure S15. ^{1}H NMR spectrum (300 MHz, chloroform-d) of Me-P(EO)$_{113}$-*b*-P(C$_{12}$GE)$_{8}$.

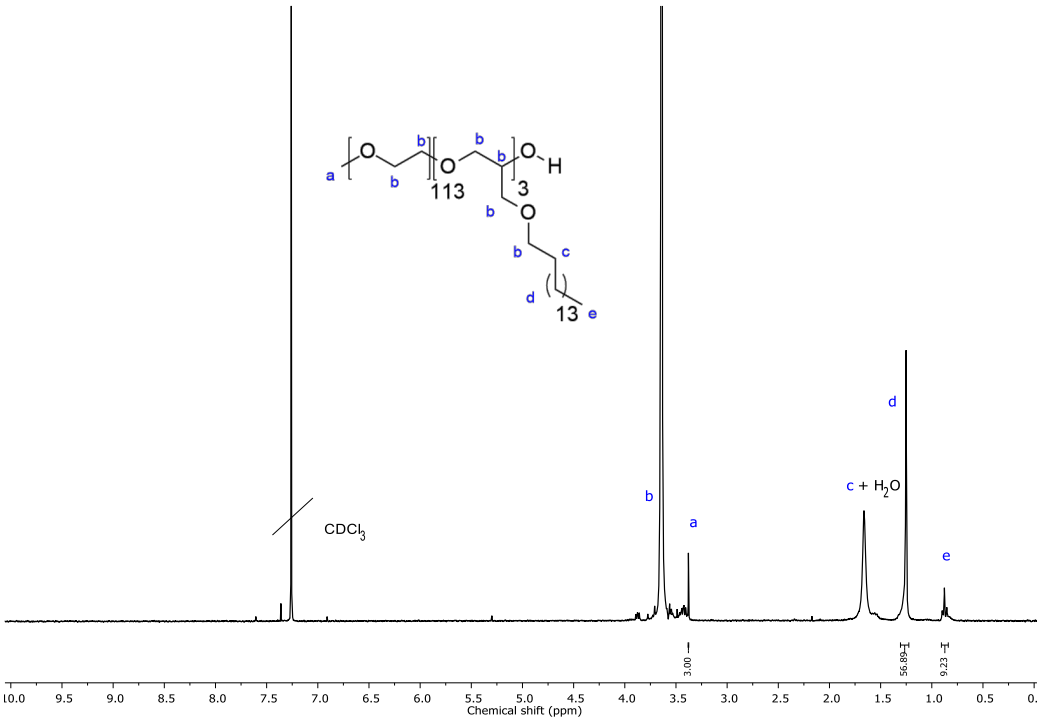

Figure S16. ^{1}H NMR spectrum (300 MHz, chloroform-d) of Me-P(EO)$_{113}$-*b*-P(C$_{16}$GE)$_{3}$.

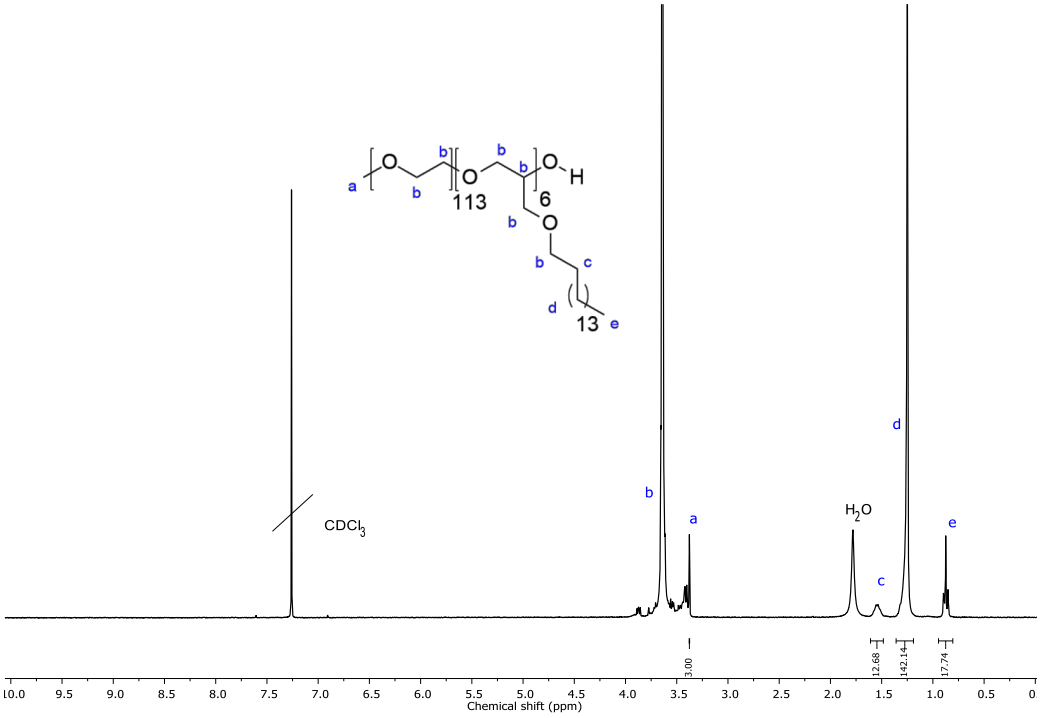

Figure S17. ^{1}H NMR spectrum (300 MHz, chloroform-d) of Me-P(EO)$_{113}$-*b*-P(C$_{16}$GE)$_{6}$.

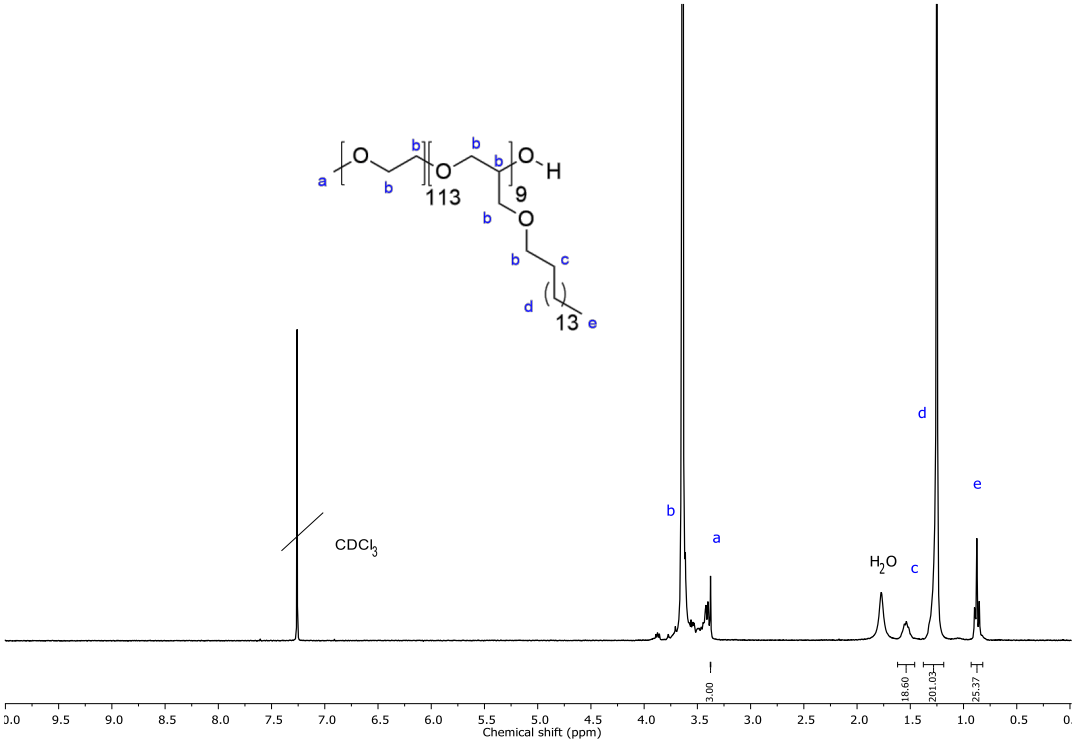

Figure S18. ^{1}H NMR spectrum (300 MHz, chloroform-d) of Me-P(EO)$_{113}$-*b*-P(C$_{16}$GE)$_{9}$.

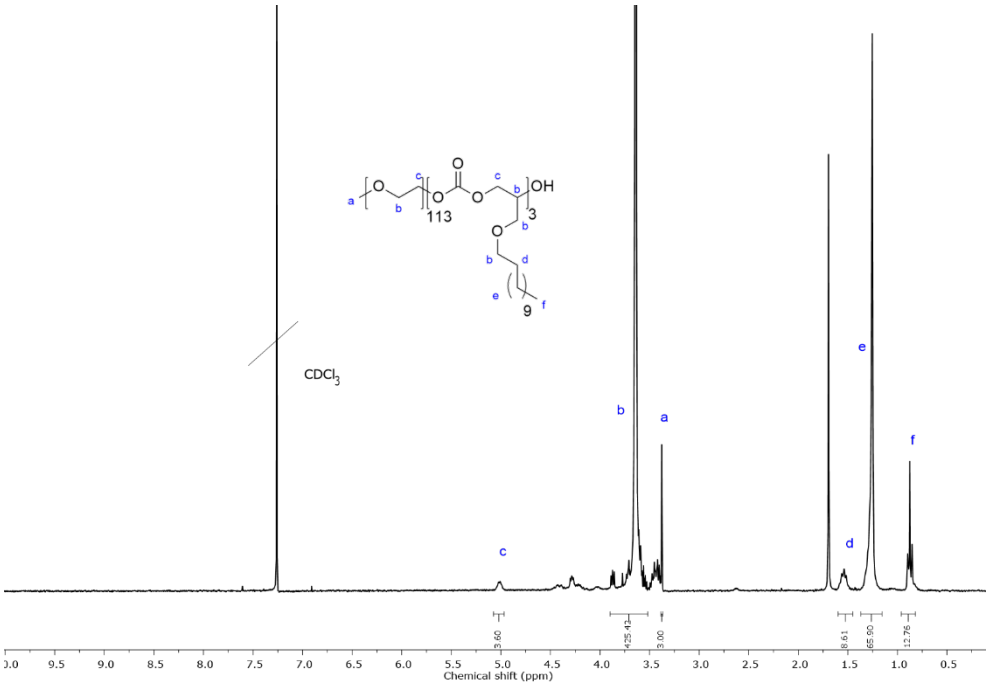

Figure S19. ^{1}H NMR spectrum (300 MHz, chloroform-d) of Me-P(EO)$_{113}$-*b*-P(CO$_{2}$C$_{12}$GE)$_{3}$.

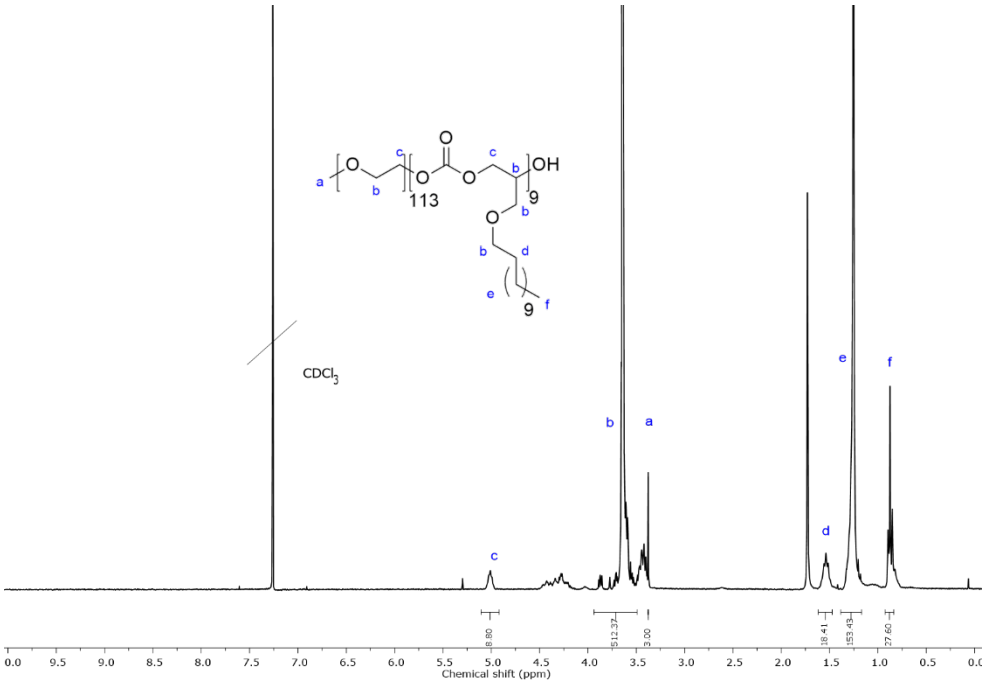

Figure S20. ^{1}H NMR spectrum (300 MHz, chloroform-d) of Me-P(EO)$_{113}$-*b*-P(CO$_2$C$_{12}$GE)$_9$.

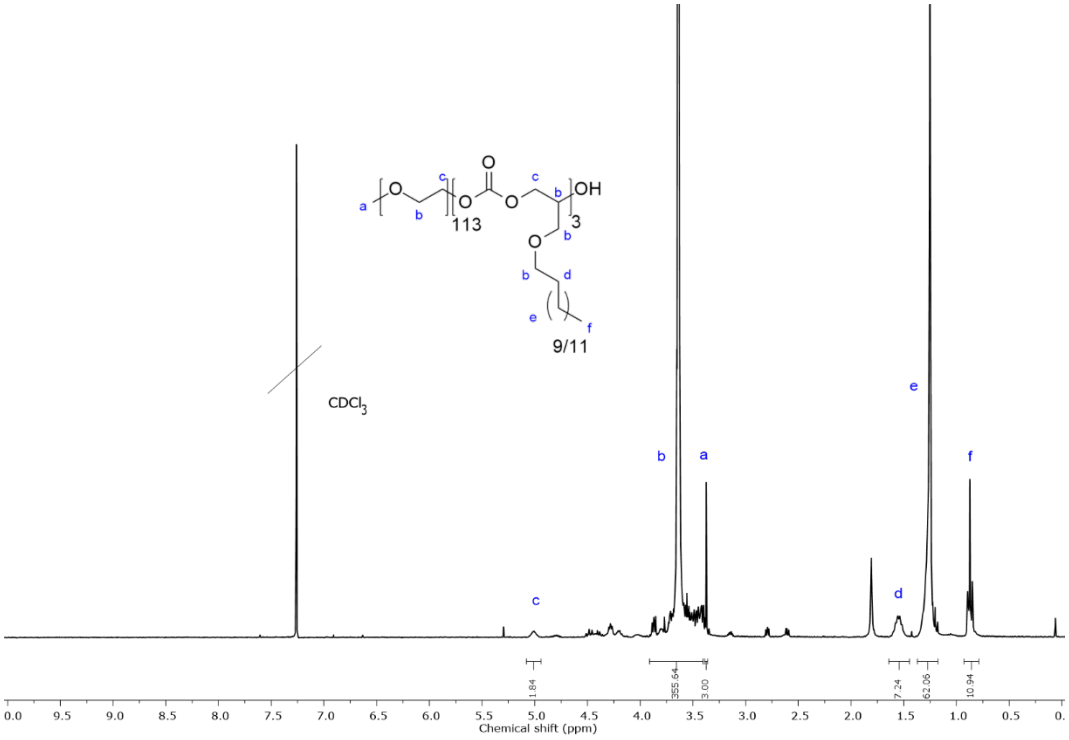

Figure S21. ^{1}H NMR spectrum (300 MHz, chloroform-d) of Me-P(EO)$_{113}$-*b*-P(CO$_2$C$_{12/14}$GE)$_3$.

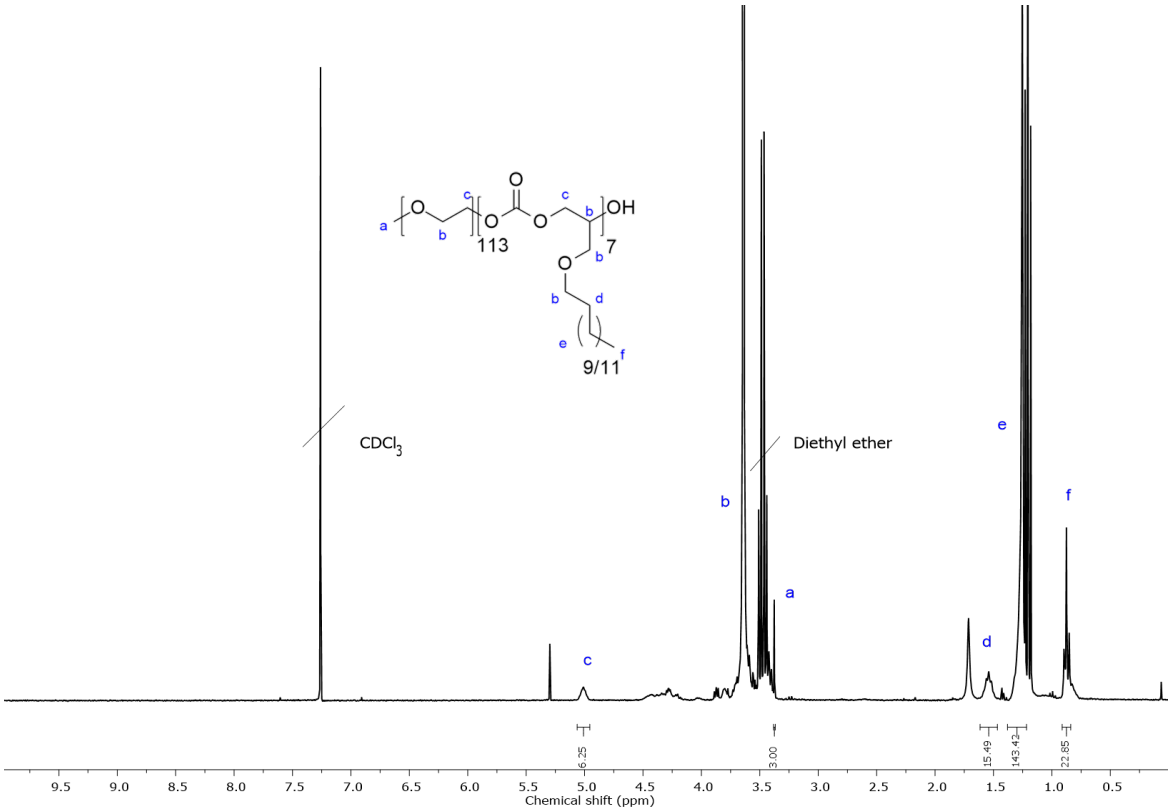

Figure S22. ^{1}H NMR spectrum (300 MHz, chloroform-d) of Me-P(EO)$_{113}$-*b*-P(CO$_2$C$_{12/14}$GE)$_7$.

5. Tabular Overview of the Phase Behavior Studies

Table S2. Sample composition, $\tilde{X}$ point parameters ($\tilde{\gamma}$ and $\tilde{T}$) and surfactant mass fraction $\tilde{\phi}_{C,i}$ within the interface at the $\tilde{X}$ point of the pseudo-ternary systems at constant $\phi = 0.500$ and $\varepsilon = 0.001$[a], together with the molecular masses $M_{w,PEO}$ and $M_{w,PAlkGE}$ of the PEO and the ,PAlkGE blocks as well as the end-to-end distances $R_{ee,w}$ and $R_{ee,o}$ calculated from an equation derived by Kawaguchi et al. (see ref.[1]).

Polymer	δ	$\tilde{\gamma}$	$\tilde{T}$/°C	$\tilde{\phi}_{C,i}$	$M_{w,PEO}$/ g mol^{-1}	$R_{ee,w}$/Å	$M_{w,PAlkGE}$ g mol^{-1}	$R_{ee,o}$/Å
H_2O/NaCl – *n*-decane ($C_{10}H_{22}$) – $C_{10}E_4$/pure PEO-*b*-PAlkGE								
No polymer	0.000	0.135	30.6	0.124	-	-	-	-
Me-P(EO)$_{113}$-*b*-P(C_{12}GE)$_3$	0.050	0.090	31.5	0.071	5195	71.8	616	17.1
Me-P(EO)$_{113}$-*b*-P(C_{12}GE)$_6$	0.050	0.088	31.2	0.068	5195	71.8	1331	21.7
Me-P(EO)$_{113}$-*b*-P(C_{12}GE)$_7$	0.025	0.114	31.1	0.094	5195	71.8	1691	23.4
Me-P(EO)$_{113}$-*b*-P(C_{12}GE)$_7$	0.050	0.0923	30.9	0.073	5195	71.8	1691	23.4
Me-P(EO)$_{113}$-*b*-P(C_{12}GE)$_7$	0.075	0.0774	31.0	0.058	5195	71.8	1691	23.4
Me-P(EO)$_{113}$-*b*-P(C_{12}GE)$_8$	0.050	0.0896	31.0	0.070	5195	71.8	1556	22.8
H_2O/NaCl – *n*-octacosane ($C_{28}H_{58}$) – $C_{16}E_6$/pure or technical-grade PEO-*b*-PAlkGE								
No polymer	0.000	0.144	66.8	0.130	-	-	-	-
Me-P(EO)$_{113}$-*b*-P(C_{12}GE)$_3$	0.050	0.119	67.7	0.101	5195	71.8	616	17.1
Me-P(EO)$_{113}$-*b*-P(CO_2C_{12}GE)$_3$	0.050	0.103	67.5	0.086	5195	71.8	982	19.8
Me-P(EO)$_{113}$-*b*-P($CO_2C_{12/14}$GE)$_3$	0.050	0.128	67.1	0.109	5195	71.8	592	16.9
Me-P(EO)$_{113}$-*b*-P(C_{12}GE)$_6$	0.050	0.105	66.5	0.087	5195	71.8	1331	21.7
Me-P(EO)$_{113}$-*b*-P(C_{12}GE)$_7$	0.050	0.105	66.5	0.088	5195	71.8	1691	23.4

Me-P(EO)$_{113}$-*b*-P(C$_{12}$GE)$_7$	0.100	0.071	66.8	0.054	5195	71.8	1691	23.4
Me-P(EO)$_{113}$-*b*-P(CO$_2$C$_{12/14}$GE)$_7$	0.050	0.105	66.5	0.088	5195	71.8	1960	24.5
Me-P(EO)$_{113}$-*b*-P(CO$_2$C$_{12}$GE)$_9$	0.050	0.100	66.4	0.083	5195	71.8	1794	23.9
Me-P(EO)$_{113}$-*b*-P(C$_{12}$GE)$_8$	0.050	0.104	66.8	0.087	5195	71.8	1556	22.8
Me-P(EO)$_{113}$-*b*-P(C$_{16}$GE)$_6$	0.050	0.111	66.7	0.093	5195	71.8	1271	21.4
Me-P(EO)$_{113}$-*b*-P(C$_{16}$GE)$_9$	0.050	0.108	66.2	0.091	5195	71.8	1229	21.2
H$_2$O/NaCl – Sasolwax 5805 – Genapol O 050/080/ Me-P(EO)$_{113}$-*b*-P(CO$_2$C$_{12/14}$GE)$_7$								
Mass ratio surfactant mixture	δ	$\tilde{\gamma}$	$\tilde{T}$/°C	$M_{w,PEO}$/ gmol^{-1}	$R_{ee,w}$/Å	$M_{W,PALKGE}$/ gmol^{-1}	$R_{ee,o}$/Å	
1:1	0.000	0.155	73.7	-	-	-	-	
1:1	0.100	0.127	79.6	5195	71.8	1960	24.5	
3:1	0.100	0.091	74.6	5195	71.8	1960	24.5	

[a] Note that for the technical-grade systems, the weight ratio of the two technical-grade surfactants are also given.

6. Complete SANS Curves Recorded at $\phi_c = \widetilde{\phi}_{C,0} + 0.02$

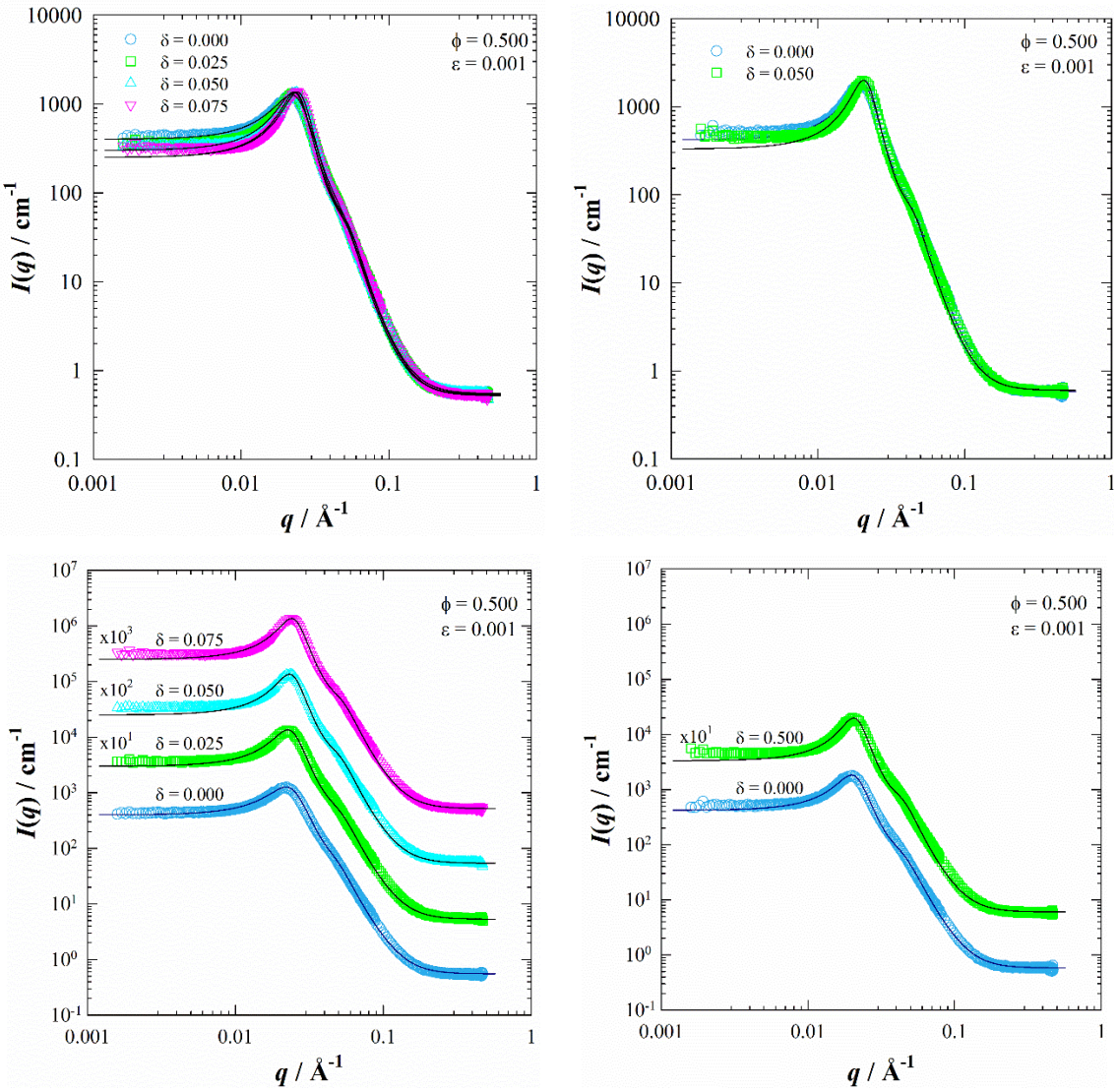

Figure S23. Left: Top :Bulk contrast SANS curves obtained for D_2O/NaCl – *n*-decane – $C_{10}E_6$/Me-P(EO)$_{113}$-*b*-P(C_{12}GE)$_7$ samples recorded close to the $\tilde{X}$ point of the polymer-free system at $\phi_c = \widetilde{\phi}_{C,0} + 0.02 = 0.144$. Bottom: Curves from the top figure displaced by a factor of 10. **Right:** Bulk contrast SANS curves obtained for D_2O/NaCl – *n*-octacosane – $C_{16}E_6$/Me-P(EO)$_{113}$-*b*-P(C_{12}GE)$_7$ samples recorded close to the $\tilde{X}$ point of the polymer-free system at $\phi_c = \widetilde{\phi}_{C,0} + 0.02 = 0.155$. Bottom: Curves from the top figure displaced by a factor of 10. Note that all shown curves were analyzed using the TS model[2] taking into account double scattering[3,4].

7. Tabular Overview of the Parameters Used to Fit the SANS Curves

Table S3: Composition of the bulk-contrast SANS samples, the corresponding fit parameters of the Teubner-Strey (*TS*) model[2] taking into account double scattering[3,4] as well as the bending rigidity determined from the model of random interfaces[5], alongside the transmission values of the respective SANS measurements.[a]

δ	ϕ_C	ϕ_D	q_{max}/Å^{-1}	I_{max}/cm^{-1}	I_0/cm^{-1}	$I_{incoh.}$/cm^{-1}	f	x	transmission
D_2O/NaCl – *n*-decane ($C_{10}H_{22}$) – $C_{10}E_4$/Me-P(EO)$_{113}$-*b*-P(C_{12}GE)$_7$									
0.000	0.144	0.000	0.022	1280	400	0.550	0.020	1.00	0.66
0.025	0.125	0.003	0.019	1980	550	0.540	0.025	1.30	0.67
0.050	0.098	0.005	0.015	4150	1100	0.520	0.030	1.60	0.67
0.075	0.083	0.007	0.013	6560	1700	0.500	0.030	1.60	0.68
0.025	0.143	0.004	0.023	1370	300	0.530	0.020	1.60	0.66
0.050	0.142	0.007	0.023	1370	250	0.540	0.020	1.60	0.66
0.075	0.142	0.011	0.024	1380	250	0.520	0.020	1.60	0.66
D_2O/NaCl – *n*-octacosane ($C_{28}H_{58}$) – $C_{16}E_6$/Me-P(EO)$_{113}$-*b*-P(C_{12}GE)$_7$									
0.000	0.155	0.000	0.020	1855	420	0.580	0.022	1.60	0.65
0.050	0.112	0.006	0.014	5050	1150	0.540	0.030	1.60	0.66
0.100	0.078	0.008	0.010	13000	2900	0.540	0.025	2.00	0.68
0.050	0.154	0.008	0.021	2020	330	0.600	0.020	1.60	0.65
D_2O/NaCl – Sasolwax 5805 – Genapol O 050/080/Me-P(EO)$_{113}$-*b*-P($CO_2C_{12/14}$GE)									
0.100	0.114	0.012	0.009	9100	4500	0.580	0.022	1.00	0.65

n	δ	ϕ_C	ϕ_D	q_{max}/ Å^{-1}	I_{max}/c m^{-1}	I_0/cm^{-1}	$I_{incoh.}$/cm^{-1}	f	x	Trans-mission
D_2O/NaCl – *n*-octacosane ($C_{28}H_{58}$) – $C_{16}E_6$/Me-P(EO)$_{113}$-*b*-P(C_{12}GE)$_n$										
-	0.000	0.155	0.000	0.020	1855	420	0.580	0.022	1.60	0.65
3	0.050	0.154	0.008	0.020	2050	420	0.580	0.020	1.20	0.65
7	0.050	0.154	0.008	0.014	5050	1150	0.540	0.030	1.60	0.65
8	0.050	0.154	0.008	0.020	2060	340	0.560	0.020	1.60	0.65

[a]Symmetric microemulsions were studied at constant $\phi = 0.500$ and $\varepsilon = 0.001$ for different PEO-*b*-PAlkGEs and polymer mass fractions δ within the overall amphiphilic mixture, with the surfactant and copolymer volume fractions ϕ_C and ϕ_D, respectively. Further listed are the fitting parameters of the extended *TS* model: the scattering vector q_{max} and the intensity I_{max} that define the peak (position) of the SANS curve of the bicontinuously structured microemulsion, the intensity I_0 at $q = 0$, the incoherent background scattering intensity $I_{incoh.}$, and the fraction of double scattering f and the additional broadening x. For the sake of completeness, the transmission values of the respective SANS measurements are listed, too.

8. Determination of the End-to-End Distances (Ree) of the Homopolymers

SANS experiments were performed for three homopolymers to determine their end-to-end distances R_{ee} in the respective solvent. The SANS measurements were performed for the hydrophilic homopolymer PEO in D_2O, for the hydrophobic BnO-P(C_{12}GE)$_{14}$ in deuterated *n*-decane and for the larger BnO-P(C_{12}GE)$_{18}$ in deuterated *n*-decane as well as in deuterated *n*-octacosane. Note that the determination of the R_{ee} of the homopolymers was performed near the phase inversion temperature of the polymer-doped microemulsion systems of the type H_2O/NaCl – oil – C_iE_j (see $T(\gamma)$ sections within the manuscript). These measurements were performed Since the SANS investigations were performed at different SANS facilities and under different conditions, Table S4 summarizes the necessary information concerning the measurement conditions etc. whereas the obtained SANS curves are shown in Figure S24. The determined dependencies of the R_{ee} values on the molecular weight M_w of the respective polymer blocks are shown in Figure S25.

Table S4: SANS facilities and measurement conditions used for the investigation of the homopolymers PEO (M_w = 5290 g mol^{-1}), BnO-P(C_{12}GE)$_{14}$ and BnO-P(C_{12}GE)$_{18}$ within the specified solvents for the determination of their radius of gyration R_g and their end-to-end distances $R_{ee,w}$ or $R_{ee,o}$, respectively.[a,b,c]

Sample	SANS facility	T_{SANS}/° C	M_w/ g mol^{-1}	R_g/Å	$R_{ee,w}$/Å	$R_{ee,o}$/Å
PEO (5290 gmol^{-1}, 0.25wt% in D_2O)	MLZ	24.9	5290	26.6[b]	65.1	-
PEO (5290 gmol^{-1}, 0.25wt% in D_2O)	MLZ	60.3	5290	26.6[b]	65.1	-
BnO-P(C_{12}GE)$_{14}$ (0.5wt% in deut. *n*-decane)	NIST	22.1	3960	12.5[c]	-	30.6
BnO-P(C_{12}GE)$_{18}$ (0.5wt% in deut. *n*-decane)	NIST	28.9	4825	13.3[c]	-	32.6
BnO-P(C_{12}GE)$_{18}$ (1.0wt% in deut. *n*-octacosane)	NIST	67.0	4825	13.3[c]	-	32.6

[a] The homopolymer samples PEO (5290 g mol^{-1}), BnO-P(C_{12}GE)$_{14}$ and BnO-P(C_{12}GE)$_{18}$ were studied at different weight fractions (wt%) in the respective deuterated solvents. [b] The SANS data obtained for PEO was evaluated by using a two-correlation length model, taking into account a scattering contribution at low

q obtained from formed clusters.[6-8] The SANS data obtained for the PAlkGE homopolymers was evaluated by using the *Guinier* model for spherical structures.[9] Note that both mentioned models initially only provide information about the gyration radius R_g. The end-to-end distances $R_{ee,o}$ and $R_{ee,w}$ can be calculated afterwards from R_g by using the relation $R_{ee} = 6^{1/2} R_g$.[10] It is interesting to note that the determined R_g and therefore R_{ee} values for all homopolymers under investigation seem to be temperature-independent and solvent-independent. Further experiments are necessary to verify the observed independence of R_{ee} on temperature and solvent.

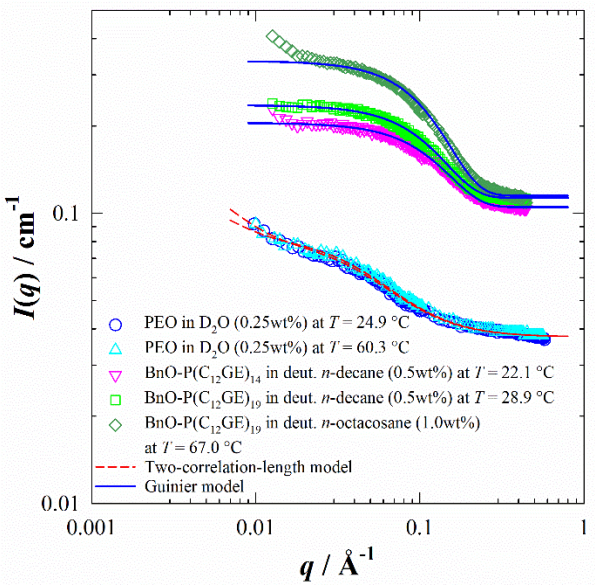

Figure S24. SANS curves obtained for the three homopolymers PEO (M_w = 5290 g mol^{-1}), BnO-P(C_{12}GE)$_{14}$ and BnO-P(C_{12}GE)$_{18}$ in the respective solvents. Scattering curves of PEO, in D_2O (0.25wt%), were fitted by using a two-correlation-length model displayed as a dashed red line, which takes into account the scattering contribution of occurring clusters at low q.[6-8] The hydrophobic homopolymers BnO-P(C_{12}GE)$_{14}$ and BnO-P(C_{12}GE)$_{18}$ were studied in deuterated *n*-decane (0.5wt%) and fitted using the Guinier model (blue solid lines).[9] The more hydrophobic BnO-P(C_{12}GE)$_{18}$ homopolymer was additionally investigated in deuterated *n*-octacosane (1.0wt%) and again fitted using the Guinier model.[9] Note that the shown scattering curves correspond to the data without the subtraction of the scattering contribution of the pure solvents and the incoherent scattering background $I_{incoh.}$, respectively.

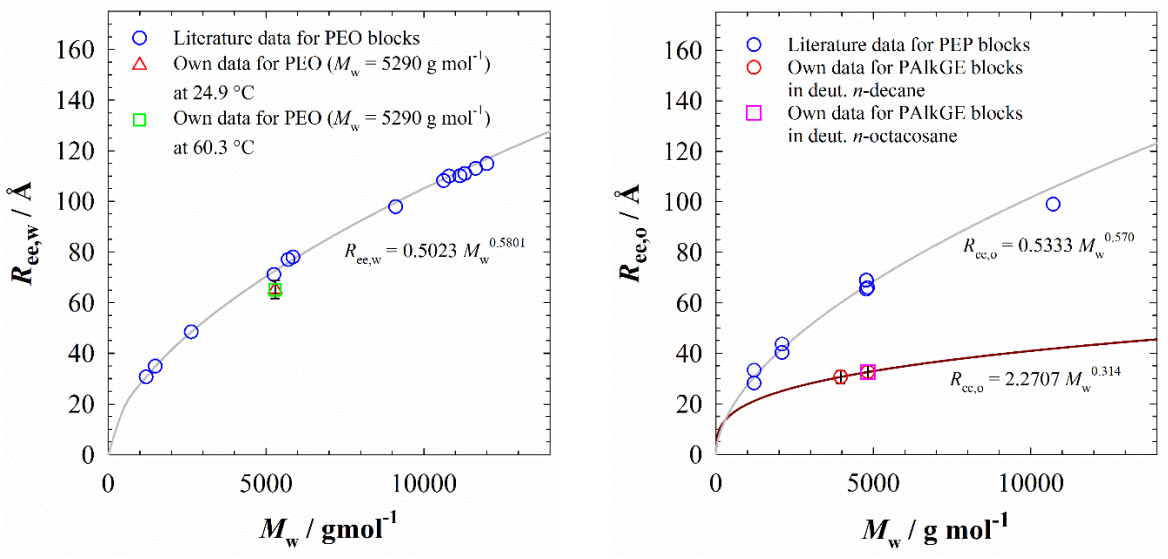

Figure S25. Trends of the end-to-end distance $R_{ee,w}$ (left) and $R_{ee,o}$ (right) as a function of molecular weight M_w for different types of homopolymers/polymer blocks. On the left, the $R_{ee,w}(M_w)$ dependency found for the hydrophilic PEO block within H_2O or D_2O is shown. Note that the theoretical values (taken from[10–13]) are all calculated from an equation derived by Kawaguchi et al. (see ref.[1]), which is based on light scattering experiments performed for varying molecular weights M_w of PEO in water to obtain the radius of gyration R_g of the PEO homopolymer. The red upward triangle represents the result we obtained from SANS investigations of PEO (M_w = 5290 g mol^{-1}) in D_2O at T = 24.9 °C, whereas the green square corresponds to the measurement performed at T = 60.3 °C. As can be seen, the temperature has a negligible effect upon the $R_{ee,w}$ of the PEO homopolymer and our value determined with SANS almost quantitatively agrees with the literature data calculated with the equation derived by Kawaguchi et al.. On the right, the $R_{ee,o}(M_w)$ dependency of the hydrophobic PAlkGE polymer blocks is shown. To the best of our knowledge, there are no comparable data on alkyl glycidyl ether polymers so far. We therefore show the values we obtained via SANS for the two homopolymers BnO-P(C_{12}GE)$_{14}$ and BnO-P(C_{12}GE)$_{18}$ (cf. Table S4), alongside literature data on PEP blocks in cyclohexane or benzene[10–12]. The red circles are displaying the results obtained for these two polymers in deuterated *n*-decane (BnO-P(C_{12}GE)$_{14}$ at T = 22.1 °C and BnO-P(C_{12}GE)$_{18}$ at T = 28.9 °C) whereas the pink square illustrates the result obtained for BnO-P(C_{12}GE)$_{18}$ in deuterated *n*-octacosane at T = 67.0°C. On the basis of this result it can be concluded, that using either *n*-decane or *n*-octacosane has no influence upon $R_{ee,o}$.

References

(1) Kawaguchi, S.; Imai, G.; Suzuki, J.; Miyahara, A.; Kitano, T.; Ito, K. Aqueous solution properties of oligo- and poly(ethylene oxide) by static light scattering and intrinsic viscosity. *Polymer* **1997**, *38*, 2885–2891.

(2) Teubner, M.; Strey, R. Origin of the scattering peak in microemulsions. *J. Chem. Phys.* **1987**, *87*, 3195–3200.

(3) Schelten, J.; Schmatz, W. Multiple-scattering treatment for small-angle scattering problems. *J. Appl. Crystallogr.* **1980**, *13*, 385–390.

(4) Silas, J. A.; Kaler, E. W. Effect of multiple scattering on SANS spectra from bicontinuous microemulsions. *J. Colloid Interface Sci.* **2003**, *257*, 291–298.

(5) Pieruschka, P.; Safran, S. A.; Marčelja, S. T. Comment on ‘‘Fluctuating interfaces in microemulsion and sponge phases’’. *Phys. Rev. E* **1995**, *52*, 1245–1247.

(6) Hammouda, B.; Ho, D.; Kline, S. SANS from Poly(ethylene oxide)/Water Systems. *Macromolecules* **2002**, *35*, 8578–8585.

(7) Hammouda, B.; Ho, D. L.; Kline, S. Insight into Clustering in Poly(ethylene oxide) Solutions. *Macromolecules* **2004**, *37*, 6932–6937.

(8) Hammouda, B.; Ho, D. L. Insight into chain dimensions in PEO/water solutions. *J. Polym. Sci. Part B: Polym. Phys.* **2007**, *45*, 2196–2200.

(9) Glatter, O.; Kratky, O. *Small angle X-ray scattering*, 2nd printing 36; Academic Press: London, 1982.

(10) Endo, H.; Mihailescu, M.; Monkenbusch, M.; Allgaier, J.; Gompper, G.; d. Richter; Jakobs, B.; Sottmann, T.; Strey, R.; Grillo, I. Effect of amphiphilic block copolymers on the structure and phase behavior of oil–water-surfactant mixtures. *J. Chem. Phys.* **2001**, *115*, 580–600.

(11) Byelov, D.; Frielinghaus, H.; Holderer, O.; Allgaier, J.; d. Richter. Microemulsion efficiency boosting and the complementary effect. 1. Structural properties. *Langmuir* **2004**, *20*, 10433–10443.

(12) Jakobs, B. *Amphiphile Blockcopolymere als Efficiency Booster für Tenside*, 1st ed.; Cuvillier Verlag: Göttingen, 2001.

(13) Tchekountieu Mboumi, L. J. *Technisch relevante amphiphile Blockcopolymere in Mikroemulsionen: Dissertation*, 2010.